AD-A164 505 BOOST CONTROL DESIGN FOR SPINNING MISSILE(U) NAVAL POSTGRADUATE SCHOOL MONTEREY CA R L PARK DEC 85 1/2

UNCLASSIFIED F/G 16/4.2 NL

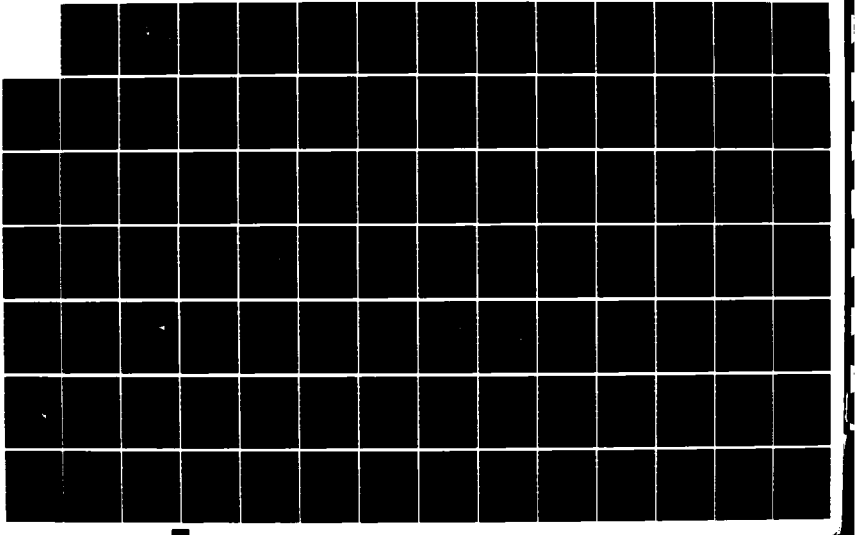

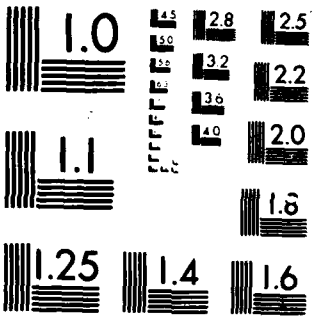

(2)

NAVAL POSTGRADUATE SCHOOL
Monterey, California

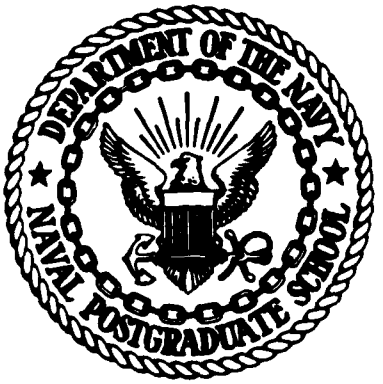

THESIS

BOOST CONTROL DESIGN
FOR
SPINNING MISSILE

by

Richard L. Park, Jr.

December 1985

Thesis Advisor: R. D. Strum

Approved for public release; distribution is unlimited.

AD-A164 525

SECURITY CLASSIFICATION OF THIS PAGE

REPORT DOCUMENTATION PAGE

1a. REPORT SECURITY CLASSIFICATION UNCLASSIFIED	1b. RESTRICTIVE MARKINGS
2a. SECURITY CLASSIFICATION AUTHORITY	3. DISTRIBUTION / AVAILABILITY OF REPORT Approved for public release; distribution is unlimited.
2b. DECLASSIFICATION / DOWNGRADING SCHEDULE	
4 PERFORMING ORGANIZATION REPORT NUMBER(S)	5. MONITORING ORGANIZATION REPORT NUMBER(S)
6a. NAME OF PERFORMING ORGANIZATION Naval Postgraduate School 6b. OFFICE SYMBOL (If applicable) 62	7a. NAME OF MONITORING ORGANIZATION Naval Postgraduate School
6c. ADDRESS (City, State, and ZIP Code) Monterey, California 93943-5100	7b. ADDRESS (City, State, and ZIP Code) Monterey, California 93943-5100
8a. NAME OF FUNDING / SPONSORING ORGANIZATION 8b. OFFICE SYMBOL (If applicable)	9. PROCUREMENT INSTRUMENT IDENTIFICATION NUMBER
8c. ADDRESS (City, State, and ZIP Code)	10. SOURCE OF FUNDING NUMBERS PROGRAM ELEMENT NO. / PROJECT NO. / TASK NO. / WORK UNIT ACCESSION NO.

11 TITLE (Include Security Classification)
Boost Control Design for Spinning Missile

12 PERSONAL AUTHOR(S)
Park, Richard L. Jr.

13a TYPE OF REPORT	13b TIME COVERED	14. DATE OF REPORT (Year, Month, Day)	15 PAGE COUNT
Master's Thesis	FROM _____ TO _____	1985 December	97

16 SUPPLEMENTARY NOTATION

17 COSATI CODES			18. SUBJECT TERMS (Continue on reverse if necessary and identify by block number)
FIELD	GROUP	SUB-GROUP	Spinning Missile; Thrust Vector Control

19 ABSTRACT (Continue on reverse if necessary and identify by block number)

A compensation scheme is presented for the pitch-yaw control system of a strategic missile which maintains stability and performance while the missile spins. The conventional missile control design for boost has uncoupled pitch, yaw and roll channels ideally suited for a non-rolling missile. The effect roll has on the conventional pitch-yaw controller is discussed and the development and simulation of a modified system is presented.

20 DISTRIBUTION / AVAILABILITY OF ABSTRACT ☒ UNCLASSIFIED/UNLIMITED ☐ SAME AS RPT ☐ DTIC USERS	21 ABSTRACT SECURITY CLASSIFICATION UNCLASSIFIED
22a NAME OF RESPONSIBLE INDIVIDUAL Prof R.D. Strum	22b TELEPHONE (Include Area Code) 408-646-2652 22c OFFICE SYMBOL 62St

DD FORM 1473, 84 MAR 83 APR edition may be used until exhausted
All other editions are obsolete

SECURITY CLASSIFICATION OF THIS PAGE

Approved for public release; distribution is unlimited.

Boost Control Design for Spinning Missile

by

Richard L. Park, Jr.
Captain, United States Marine Corps
B.M.E., Georgia Institute of Technology, 1980

Submitted in partial fulfillment of the requirements for the degree of

MASTER OF SCIENCE IN ELECTRICAL ENGINEERING

from the

NAVAL POSTGRADUATE SCHOOL
December 1985

Author: Richard L. Park Jr.
Richard L. Park, Jr.

Approved by: R.D. Strum
R.D. Strum, Thesis Advisor

D.E. Kirk
D.E. Kirk, Second Reader

Harriet B. Rigas, Chairman, Department of Electrical and Computer Engineering

J.N. Dyer
J.N. Dyer,
Dean of Science and Engineering

ABSTRACT

A compensation scheme is presented for the pitch-yaw control system of a strategic missile which maintains stability and performance while the missile spins. The conventional missile control design for boost has uncoupled pitch, yaw and roll channels ideally suited for a non-rolling missile. The effect roll has on the conventional pitch-yaw controller is discussed and the development and simulation of a modified system is presented.

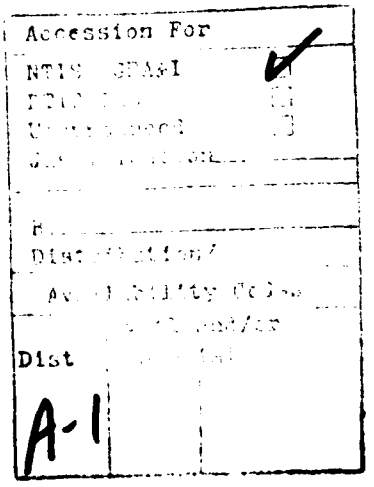

TABLE OF CONTENTS

I. INTRODUCTION

Future ballistic missiles may need the ability to spin during boost ascent through the atmosphere as a countermeasure against first-generation continuous-duty laser threats. Since the conventional missile control design has uncoupled pitch, yaw and roll channels, some performance and even system stability may be lost in rolling the missile. This study evaluates the performance of a conventional pitch-yaw controller in the presence of spin. A compensation scheme is then proposed to restore system performance.

The block diagram of a submarine-launched ballistic missile's pitch-yaw control system is used as the design vehicle for this study. Since the physical parameters of this system are classified, only the block diagram is used in the analysis and design process. All numerical values needed for analysis and simulation are borrowed from other systems or derived as needed.

The study is conducted as follows. First, the basic laws of motion and thrust vector control are introduced. Together, these sets of equations define the flight dynamics of the missile and the method for controlling the missile. The pitch-yaw controller for the non-rolling missile is then designed and simulated. This system has uncoupled channels for pitch and yaw control which become coupled when the missile is rolled. Next, the missile is forced to roll and the effect cross-coupling has on the system's performance is analyzed. A compensation scheme is then proposed to restore the system's performance. Analysis and design are carried out using classical and modern controls analysis and simulation results are presented.

A. MISSILE DYNAMICS AND THRUST VECTOR CONTROL

1. Notation and Reference Axis System

The reference axis system used to define vector quantities, dimensions and angles of interest is shown in Fig. 1-1. The axis system is fixed within the missile body with its origin at the missile's center of gravity. The orthogonal axes, x, y and z, will also be referred to as the roll, pitch and yaw axes, respectively. Fig. 1-1 indicates that the right-hand rule is used to determine the positive direction for rotational vector quantities.

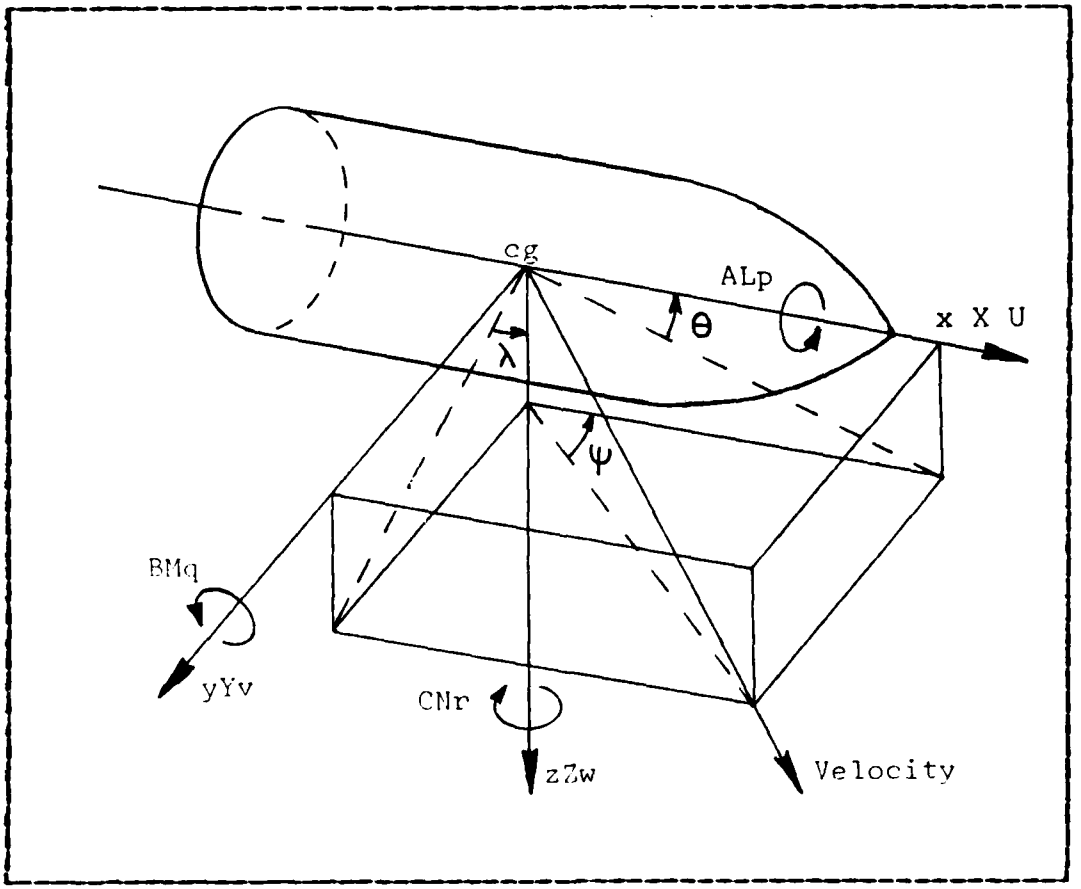

Fig. 1-1 Reference Axis System

Table 1-1 lists the symbols used to refer to key parameters and quantities of interest. Other symbols will be defined as they arise. The moments of inertia about the center of gravity (cg) are defined as:

$$A = \sum \delta m \ (y^2+z^2) \tag{1.1}$$

$$B = \sum \delta m \ (z^2+x^2) \tag{1.2}$$

$$C = \sum \delta m \ (x^2+y^2) \tag{1.3}$$

The products of inertia are defined as:

$$D = \sum (\delta m) \ yz \tag{1.4}$$

$$E = \sum (\delta m) \ xz \tag{1.5}$$

$$F = \sum (\delta m) \ xy \tag{1.6}$$

Where $\Sigma \delta m$ symbolizes the sum of differential mass elements which make up the missile body.

TABLE 1-1

NOTATION DEFINITIONS

	Roll Axis x	Pitch Axis y	Yaw Axis z
Angle of incidence	λ	θ	ψ
Angular rate	p	q	r
Component of missile velocity along axis	U	v	w
Component of force on missile along axis	X	Y	Z
Moments acting on missile about axis	L	M	N
Moments of inertia about each axis	A	B	C
Products of inertia	D	E	F

2. Euler's Equations of Motion

The equations of motion for a body with six degrees of freedom and a mass, m, are summarized below. A dot ($\dot{}$) over any symbol refers to the time rate of change, d/dt, of the quantity indicated. [Ref. 1]

$$m(\dot{U} + qw - rv) = X \tag{1.7}$$

$$m(\dot{v} + rU - pw) = Y \tag{1.8}$$

$$m(\dot{w} - qU + pv) = Z \tag{1.9}$$

$$A\dot{p} - (B-C)qr + D(r^2-q^2) - E(pq+\dot{r}) + F(rp-\dot{q}) = L \quad (1.10)$$

$$B\dot{q} - (C-A)rp + E(p^2-r^2) - F(qr+\dot{p}) + D(pq-\dot{r}) = M \quad (1.11)$$

$$C\dot{r} - (A-B)pq + F(q^2-p^2) - D(rp+\dot{q}) + E(qr-\dot{p}) = N \quad (1.12)$$

The first three equations above are force equations and the second three are moment equations. In particular, Eqs. (1.11) and (1.12) are those from which pitch and yaw angular accelerations are found. Note that the second term in each of these equations constitutes a cross-coupling term between the two channels which is proportional to the roll rate. This cross-coupling effect is eliminated in the conventional pitch-yaw controller design by preventing roll and thus setting the roll rate, p, equal to zero.

Assuming that the missile body is approximately rigid leads to the conclusion that the products of inertia are equal to zero. Thus Eqs. (1.11) and (1.12) are reduced to:

$$B\dot{q} - (C-A)rp = M \quad (1.13)$$

$$C\dot{r} - (A-B)pq = N \quad (1.14)$$

3. Thrust Vector Control

The only means used to control the flight of the missile under study is to deflect the exhaust nozzle as shown in two dimensions in Fig. 1-2. Deflecting the exhaust nozzle causes the driving force of the rocket motor to be pointed in a direction other than along the missile's longitudinal axis. This action creates force components perpendicular to the roll axis which do not act through the missile's center of gravity. The resulting moments are about the y- and z-axes and cause the missile to pitch and yaw. The moments about the center of gravity caused by the deflected thrust vector are:

$$M = (T_z)\, l_c \tag{1.15}$$

$$N = (T_y)\, l_c \tag{1.16}$$

Where l_c is the length from the missile's center of gravity to the point of application of the thrust (exhaust nozzle) and T_y and T_z are the lateral thrust components parallel to the y-axis and z-axis. If d_θ and d_ψ are the angles of nozzle deflection in the pitch and yaw planes, then the perpendicular thrust components are related to the total rocket motor thrust by the following equations:

$$T_y = T \cdot \sin(d_\psi) \tag{1.17}$$

$$T_z = T \cdot \sin(d_\theta) \tag{1.18}$$

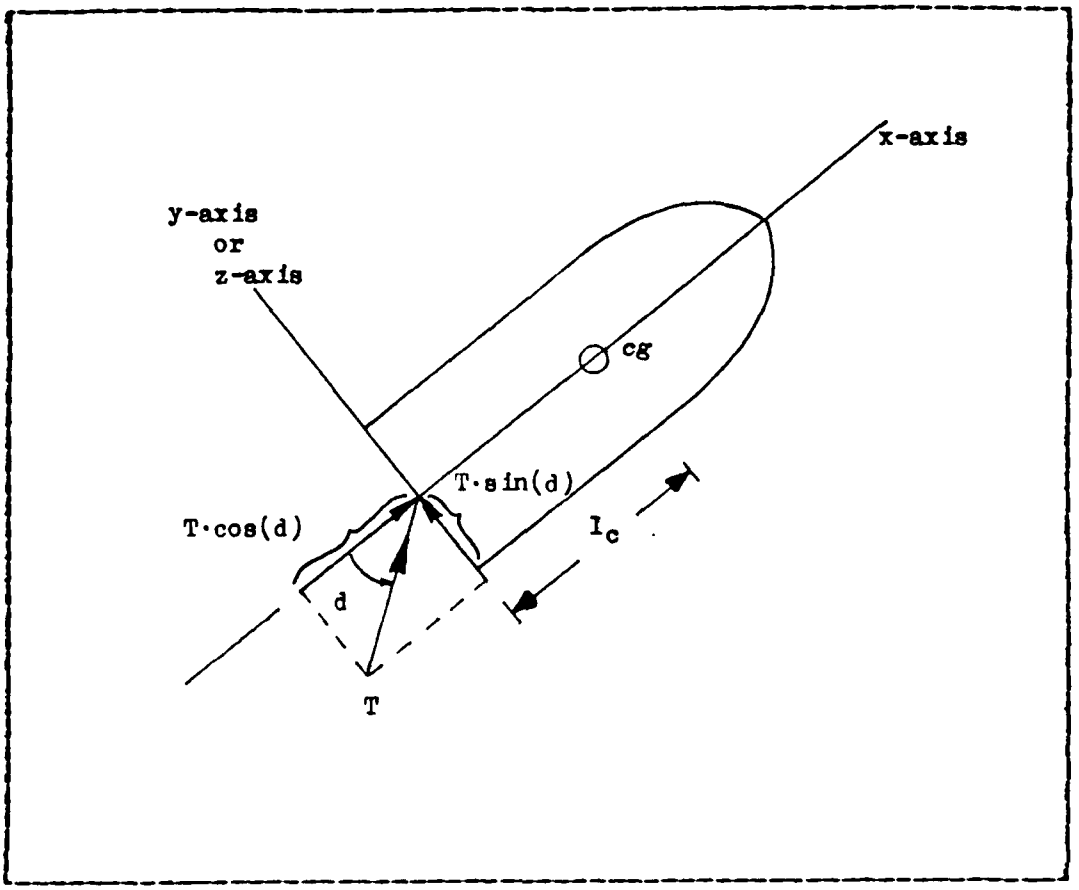

Fig. 1-2 Thrust Vector Control

Assuming that the maximum angle of nozzle deflection is small, as it must be for any physical system of this type, permits further simplification of Eqs. (1.15) and (1.16) to the linear Eqs. (1.21) and (1.22).

$$\sin(d_\theta) \cong d_\theta \tag{1.19}$$

$$\sin(d_\psi) \cong d_\psi \tag{1.20}$$

$$M = T \cdot d_\theta \cdot l_c \tag{1.21}$$

$$N = T \cdot d_\psi \cdot l_c \tag{1.22}$$

Equations (1.21) and (1.22) give the moments in pitch and yaw caused by the rocket motor. Combining these two equations with the general rotational motion equations in pitch and yaw, Eqs. (1.13) and (1.14), permits formulation of the general differential equations for pitch and yaw.

$$T \cdot d_\theta \cdot l_c = B\dot{q} - (C-A)rp \tag{1.23}$$

$$T \cdot d_\psi \cdot l_c = C\dot{r} - (A-B)pq \tag{1.24}$$

Solving for the angular acceleration components gives:

$$\dot{q} = (1/B)[T \cdot d_\theta \cdot l_c + (C-A)rp] \tag{1.25}$$

$$\dot{r} = (1/C)[T \cdot d_\psi \cdot l_c + (A-B)pq] \tag{1.26}$$

Equations (1.25) and (1.26) point out the cross-coupling effect that the roll rate, p, has on the system. For instance, if the roll rate is set equal to zero the equations for pitch and yaw are completely uncoupled.

$$\dot{q} = (1/B)T \cdot d_\theta \cdot l_c \tag{1.27}$$

$$\dot{r} = (1/C)T \cdot d_\psi \cdot l_c \tag{1.28}$$

Figure 1-3 depicts the rolling pitch-yaw system just described in block diagram form and highlights the cross-coupling terms introduced by roll. The classical missile control system design approach assumed that the roll rate was small and went to great lengths to ensure this was true. Making the assumption that the roll rate is negligible allows the system designer to separate the pitch and yaw channels and deal with them independently. This study will analyze the effect cross-coupling has on stability and performance and formulate a compensation scheme for the cross-coupled system.

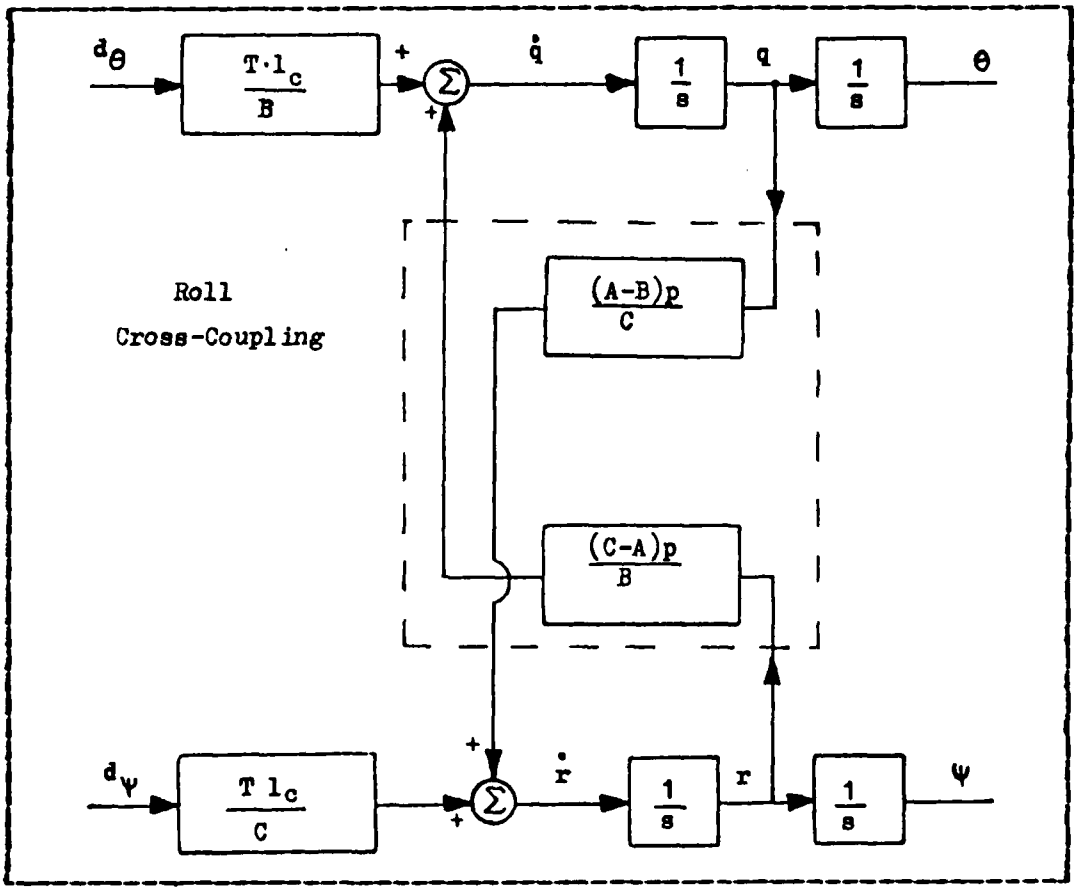

Fig. 1-3 Thrust Vector Control Dynamics

II. DEVELOPMENT OF THE NON-ROLLING MISSILE

The strategic missile whose pitch-yaw control system will be used as the design vehicle for this study. The block diagram of the system's pitch-yaw control system (without roll) is shown in Fig. 2-1. Since the physical parameters of this missile are classified, only the block diagram will be used. All system constants and physical parameter values which are used for analysis and simulation will be taken from other systems or derived as needed.

The missile is a three-stage booster rocket. Flight of the missile is controlled by vectoring the exhaust thrust as described in the preceding section. Based upon predetermined flight trajectories and measured or estimated parameters during flight, the guidance computer generates pitch and yaw commands and transmits these to the pitch-yaw controller [Ref. 2]. The algorithm which the guidance computer uses to generate the pitch and yaw commands will not be addressed. Only the response of the pitch-yaw controller to a general set of commands will be considered.

Table 2-1 lists the physical parameter values used at the various stages for design and simulation. These parameters bear no resemblance to those of the Trident II missile but serve only to provide actual numbers for the variables so that simulation could be done. The parameters listed in Table 2-1 were actually taken from the Saturn V Rocket; also a three-stage booster rocket. The moments of inertia listed in Table 2-1 were obtained from the other parameters by assuming that each stage has approximately the same inertial characteristics as a uniform right-circular cylinder.

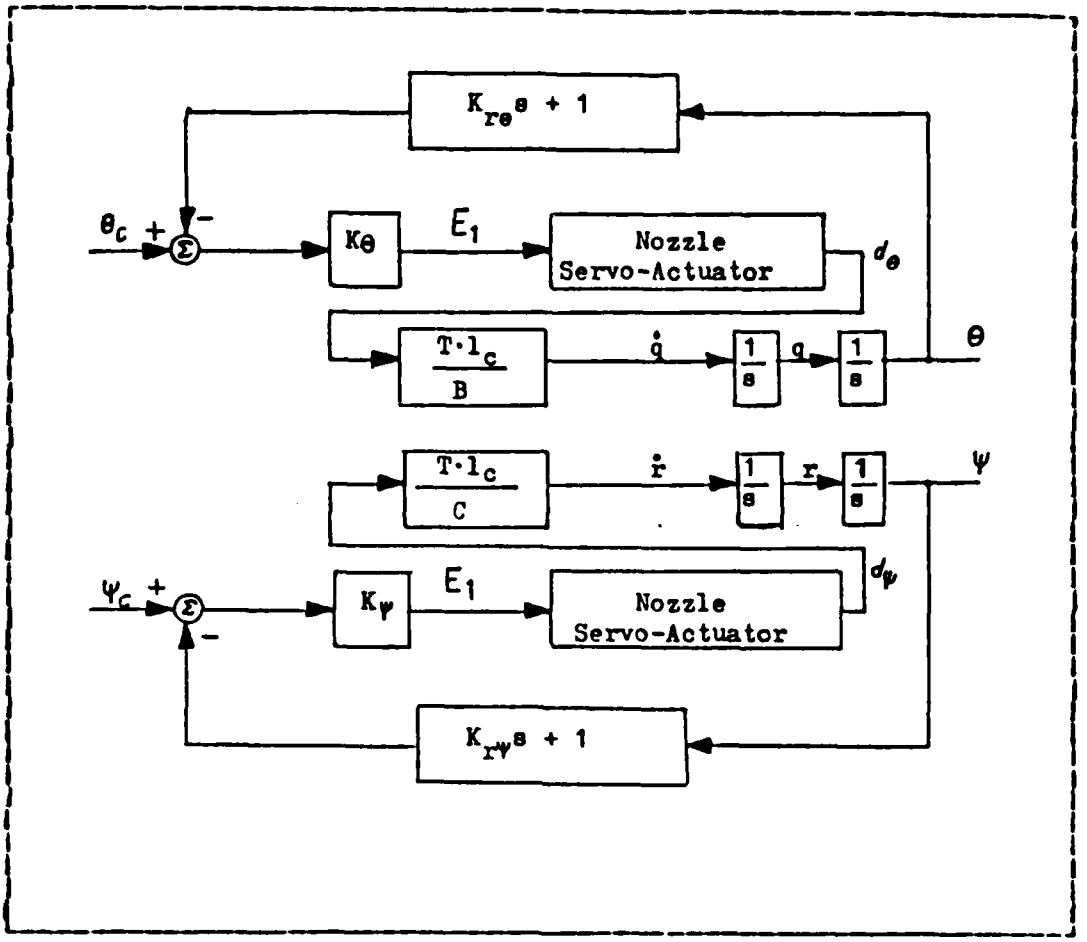

Fig. 2-1 Non-Rolling Pitch-Yaw Control System

Figure 2-1 shows the schematic block diagram of the system used to control pitch and yaw in the missile. Since the missile does not spin, the pitch and yaw channels are uncoupled. The system consists of a servo-actuator used to deflect the exhaust nozzle, the missile dynamics and sensors which feed back angular velocity and position. The deflectable exhaust nozzle saturates at a maximum deflection of ± five degrees. In this analog system all gains are constant throughout operation.

TABLE 2-1

PHYSICAL PARAMETER SPECIFICATIONS

		1st Stage	2nd Stage	3rd Stage
Initial Mass	slugs	1.488×10^5	3.22×10^4	8.14×10^3
Mass Rate	slug/sec	930	81.49	14.75
Thrust	lb_f	7.496×10^6	1.125×10^6	2.249×10^5
Length	ft	133	130	100
Burn Time	sec	150	359	479
Moment of Inertia about Pitch Axis	$slug\text{-}ft^2$	m(1542.1)	m(1476.4)	m(858.3)
Moment of Inertia about Yaw Axis	$slug\text{-}ft^2$	m(1542.1)	m(1476.4)	m(858.3)
Moment of Inertia about Roll Axis	$slug\text{-}ft^2$	m(136.1)	m(136.1)	m(50.0)

A. DESIGN OF THE SERVO-ACTUATOR

The transfer function of the servo-actuator which deflects the exhaust nozzle of the missile is given in Eq. (2.1). The task is to select numerical values for the parameters, a, b and f, such that the servo-actuator has acceptable performance characteristics. Again, the parameter values will be selected without regard to those used on the actual missile.

$$\frac{d_\theta(s)}{E_1(s)} = \frac{ab^2}{(s + a)(s^2 + 2fbs + b^2)} \qquad (2.1)$$

It is desired that the actuator's performance resemble that of a well damped second-order system with minimum overshoot and a short settling time in response to step inputs. These performance characteristics need to be more stringent than those imposed on the entire system so that the actuator does not become a limiting element when the entire system is considered later. The design specifications used for the actuator are summarized as follows.

1. Pole Locations

In order to ensure that this third-order system behaves essentially as a second-order system, the real pole must have a magnitude significantly greater than the real part of the complex roots of the second-order term, e.g.

$$a > 10fb \qquad (2.2)$$

2. Damping

In order to make the dominant complex pair of poles exhibit good damping, the value of f must approach one.

$$1 \geq f > 0.8 \qquad (2.3)$$

3. Settling Time

In order to keep the actuator from limiting the settling time of the entire system, the servo's settling time must be significantly shorter than that of the pitch-yaw controller. If the desired settling time of the entire system is to be approximately ten seconds and the actuator's settling time is 3% of the system's, then the actuator's settling time will be selected according to the relationship below.

$$t_{\text{settling servo}} \leq 0.03\ t_{\text{settling system}} \tag{2.4}$$

4. Peak Overshoot

The peak overshoot of the servo-actuator must be small. Otherwise, it may have an appreciable effect on the overall system's peak overshoot.

$$M(\text{servo}) - 1 < 1\% \tag{2.5}$$

Where M(servo) is the peak overshoot of the actuator.

Equation (2.5) permits selection of the appropriate damping ratio, f. If the system is assumed to exhibit second-order characteristics, then Eq. (2.6) can be solved for the damping ratio.

$$M(\text{servo}) - 1 = \exp\left[\frac{-\pi f}{\sqrt{1-f}}\right] < 0.01 \tag{2.6}$$

Solving for the damping ratio, f, yields the following.

$$f > \sqrt{\frac{[\ln(0.01)]^2}{\pi^2 + [\ln(0.01)]^2}} = 0.826 \tag{2.7}$$

So, a damping ratio of 0.9 will be used. This selection also satisfies Eq. (2.3).

The specification of Eq. (2.4), combined with the above choice of damping ratio, can be used to select the natural frequency of the second-order term.

$$t_{\text{settling servo}} = \left[\frac{4}{fb}\right] < 0.3 \text{ sec} \qquad (2.8)$$

Solving for the natural frequency leads to a selection of b equal to 15.

$$b > 14.8 \text{ rad/sec} \qquad (2.9)$$

Equation (2.2), combined with the above choices of damping ratio and natural frequency, leads to a selection of the real pole, a, equal to 150.

$$a > 10fb = 135 \qquad (2.10)$$

The root locus of the system's characteristic equation, obtained by varying the real pole, a, is shown in Fig. 2-2. Highlighted are the root locations for the above choice of parameter values. As shown in Fig. 2-2, all the roots are well into the left half of the s-plane, a large phase margin exists for the second-order complex pole pair and the second-order pair is far enough to the right of the single real pole to achieve dominance. Figure 2-3 shows the open-loop frequency response of the actuator and makes the large phase margin more evident. Figure 2-4, the closed-loop frequency response, points out the limitation of the actuator to follow input signals of frequency greater than about 10 radians/second. Figure 2-5 shows the step response of the system and as indicated, it meets the design specifications. Note that although the simulation shown in Fig. 2-5 is that of a full step of unit magnitude, the nozzle actuator saturates at a maximum angle of deflection of 0.0873 radians (5 degrees).

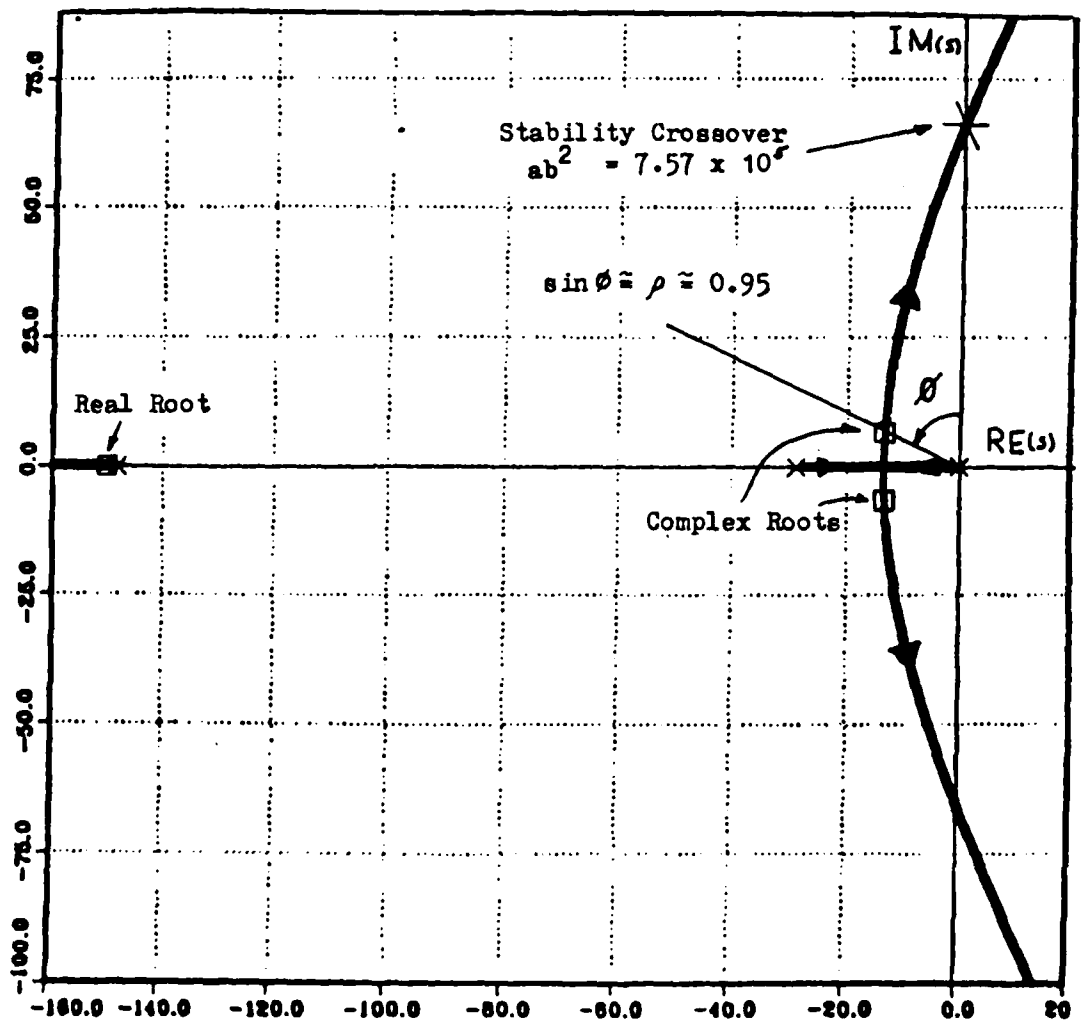

Fig. 2-2 Servo-Actuator Root Locus Plot

Figure 2-2 shows that the magnitude of the real pole is far greater than the real part of the complex pair and, therefore, will have little effect on the system's performance. Also, the dominant second-order pair is well damped with approximately a 72-degree phase margin and an effective damping ratio of 0.95. The system is stable as long as the term, ab^2, remains less than 7.57×10^5.

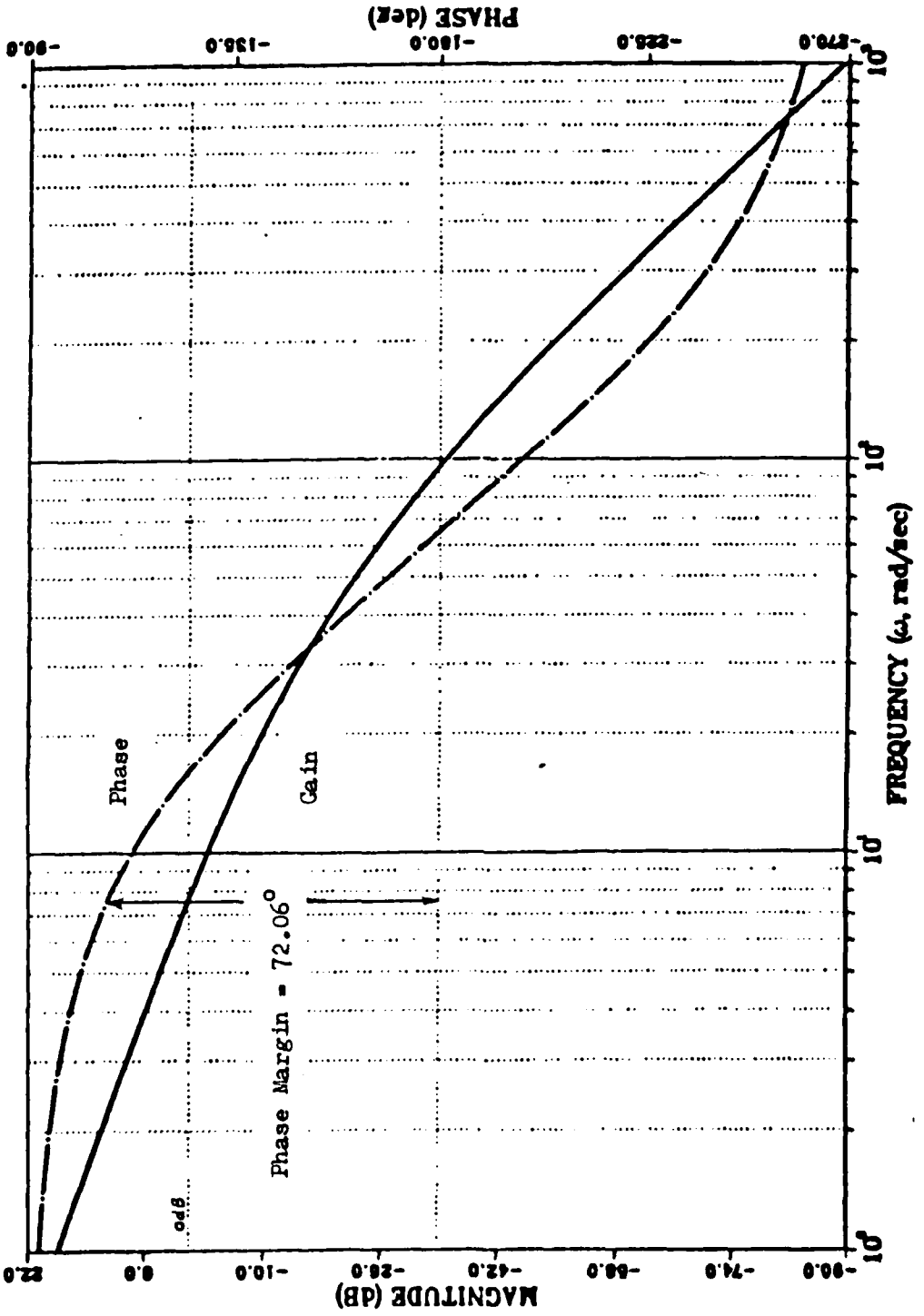

Fig. 2-3 Servo-Actuator Open-Loop Frequency Response

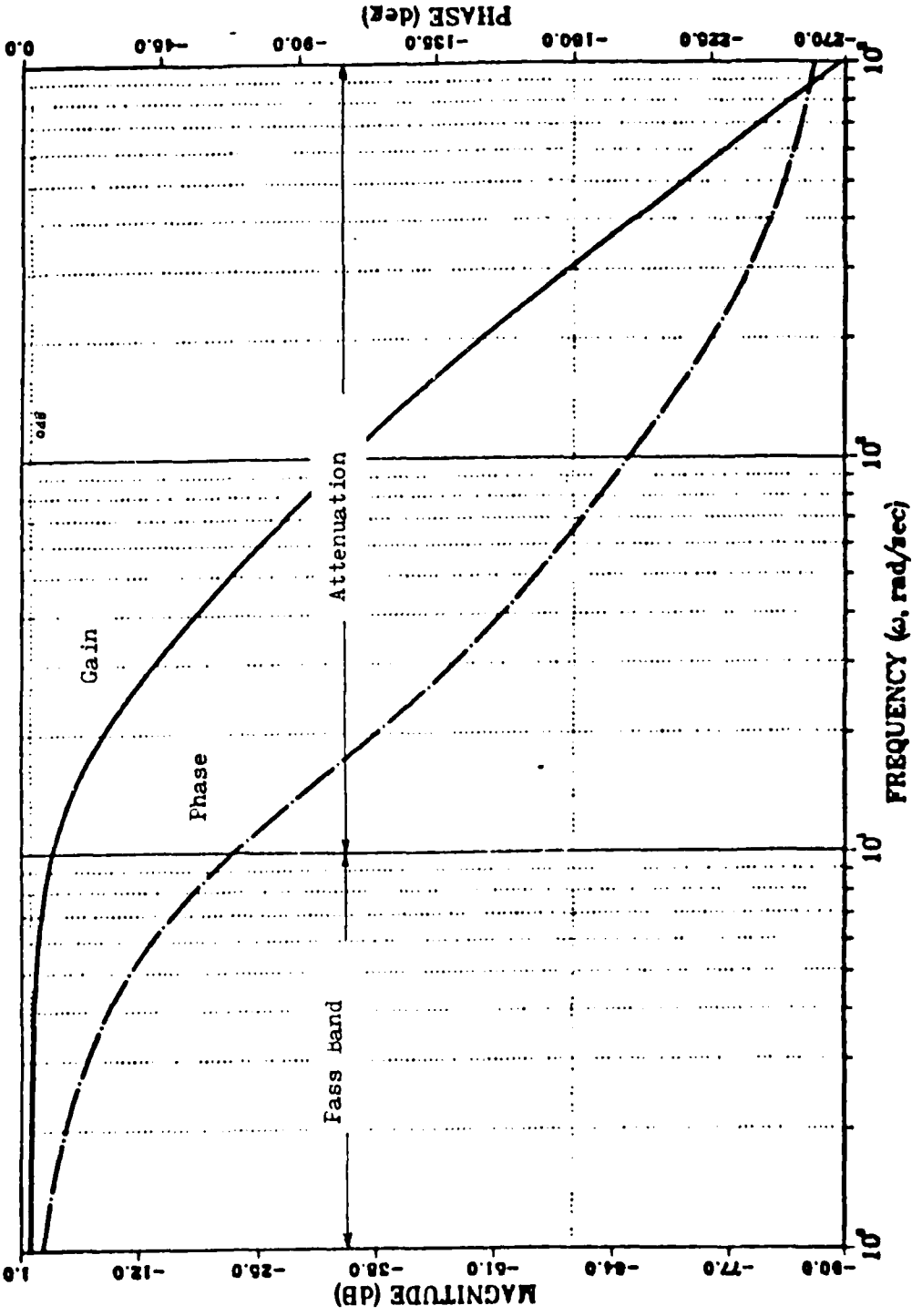

Fig. 2-4 Servo-Actuator Closed-Loop Frequency Response

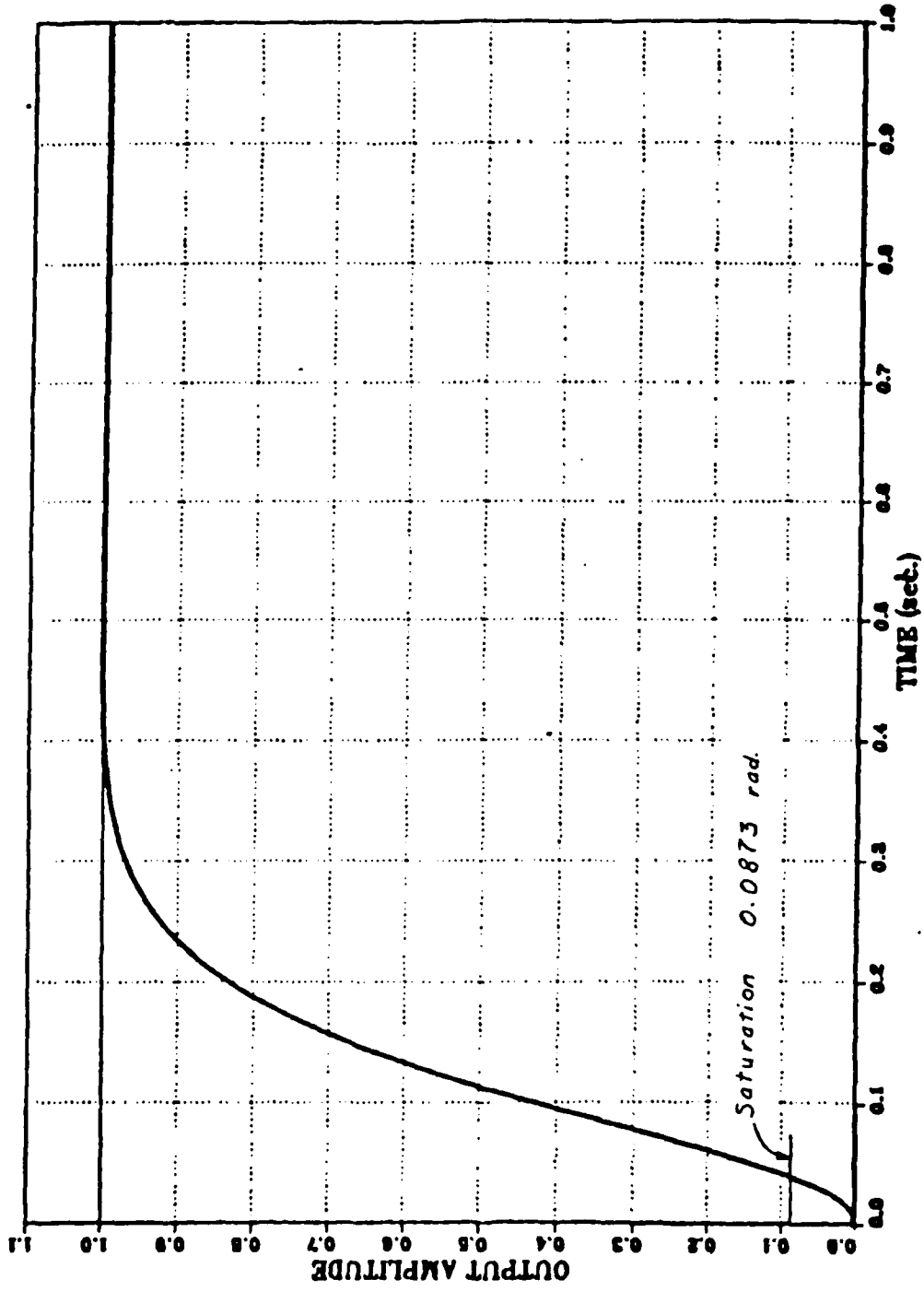

Fig. 2-5 Servo-Actuator Step Response

B. DESIGN OF THE PITCH-YAW CONTROLLER

The block diagram of the pitch-yaw control system is shown in Fig. 2-1. Since the pitch and yaw channels are identical and decoupled only one of them need be considered. The parameters $K_{r\theta}$ ($K_{r\psi}$) and K_{θ} (K_{ψ}) will be selected so that the system will exhibit minimal overshoot to step inputs and have a settling time less than ten seconds. The one-channel system to be considered is shown in Fig. 2-6.

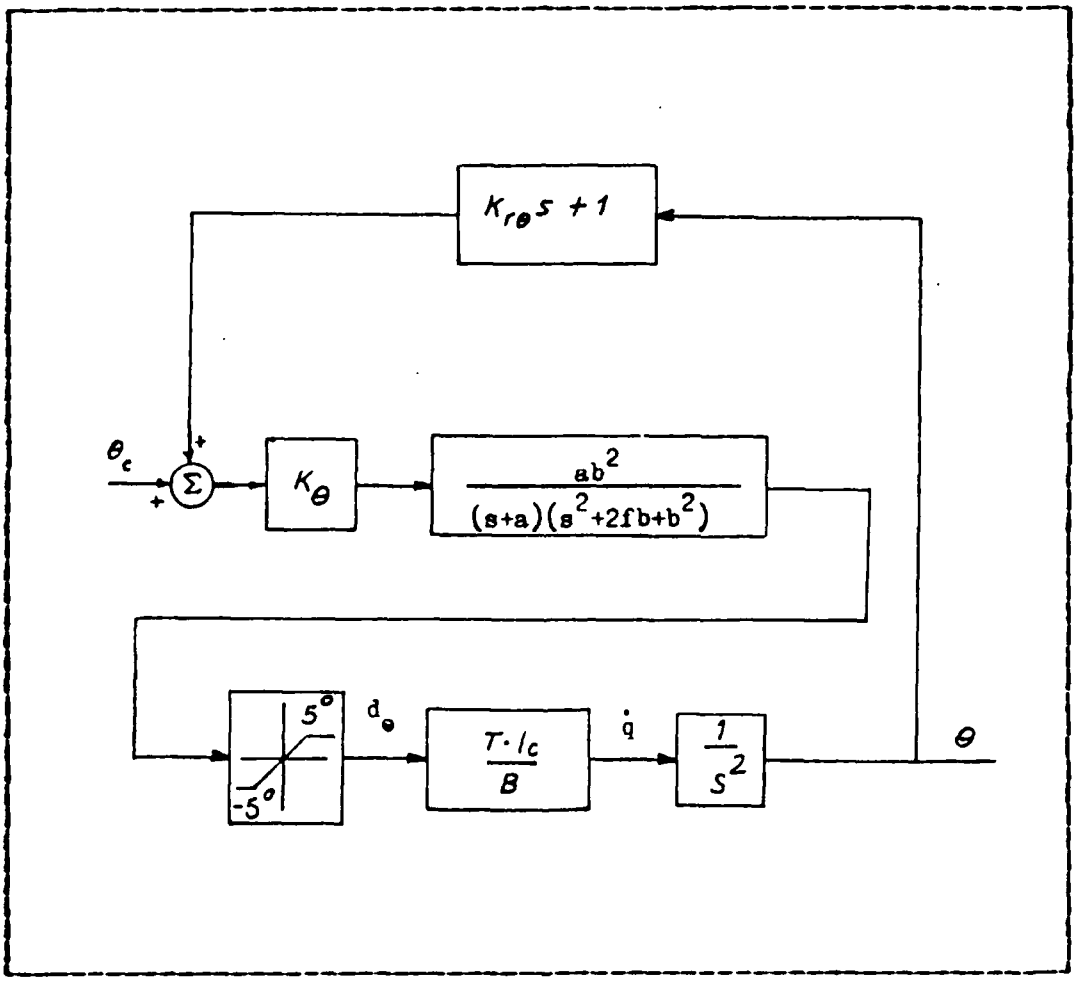

Fig. 2-6 Pitch or Yaw Channel Block Diagram

In order to begin the analysis, it is necessary to temporarily ignore the nonlinear saturation of the servo-actuator. The linearized transfer function for the pitch-yaw control system then becomes that of Eq. (2.11).

$$\frac{\theta(s)}{\theta c(s)} = \frac{K_\theta ab^2 Tl_c/B}{s^5 + s^4(a+2fb) + s^3(b^2+2fba) + s^2(ab^2) + s(K_{re}K_\theta ab^2 Tl_c/B) + K_\theta ab^2 Tl_c/B} \quad (2.11)$$

The denominator of Eq. (2.11), when set equal to zero, defines the system's characteristic equation. The characteristic equation may be partitioned as follows. Define a new variable, J.

$$J = ab^2 K_\theta (Tl_c/B) \quad (2.12)$$

The characteristic equation now becomes;

$$s^5 + s^4(a+2fb) + s^3(b^2+2fba) + s^2(ab^2) + s(K_{re}J) + J = 0 \quad (2.13)$$

Rearranging yields the partitioned form shown below.

$$\frac{K_{re}s + 1}{s^5 + s^4(a+2fb) + s^3(b^2+2fba) + s^2(ab^2)} = \frac{-1}{J} \quad (2.14)$$

Equation (2.14) is in the form for root locus analysis where J is treated as the open-loop gain and the left side of the equality as the open-loop transfer function. Varying K_{re} and J together sweeps out a region in the s-plane into which the roots of the characteristic equation can be located. These "root relocation zones" are shown in Fig. 2-7. [Ref. 3]

Figure 2-7 was made by varying J and K_{re} in Eq. (2.14) and plotting the root locations. For example, if $K_{re} = 0$ then Eq. (2.14) contains five finite poles and five zeros at infinity. The root locus will follow the path indicated in

Fig. 2-7 (as J increases). Note that the real pole at -150 is not shown in Fig. 2-7. As K_{re} is increased incrementally from zero towards infinity and the same procedure is used, i.e., plot the root locus over a large (positive) range of J, then a family of root loci will be swept out. The cross-hatched area in Fig. 2-7 is the area enlosed by the root loci for J and K_{re} varying from 0 to ∞.

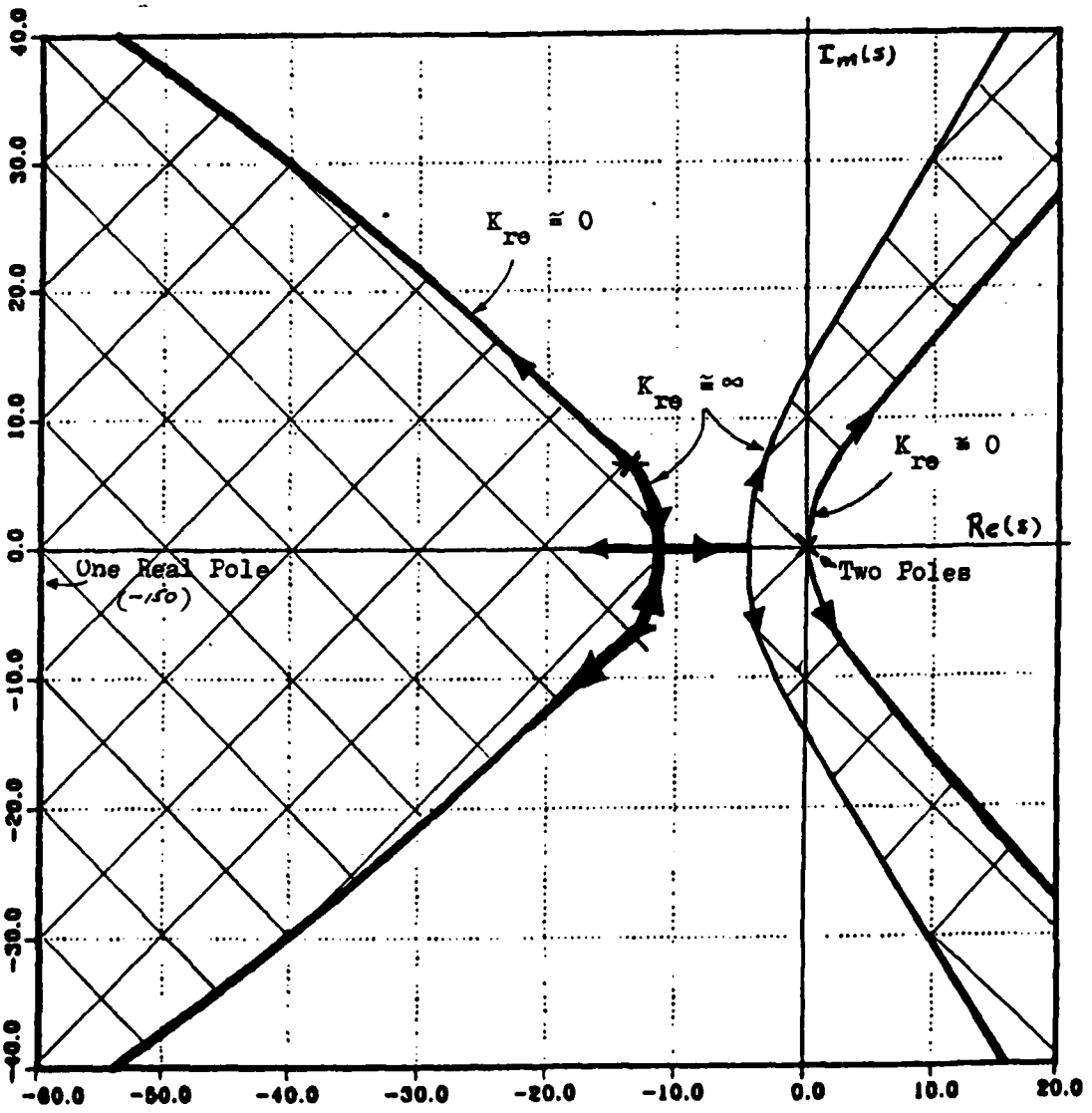

Fig. 2-7 Root Relocation Zones of Pitch-Yaw Controller

Figure 2-7 indicates that the system is unstable, with two roots in the right half-plane, for values of K_{re} less than or equal to zero. The values of K_{re} and J are estimated as 0.8 and 1.57 X 10^5, respectively. This selection locates the characteristic equation roots as shown in Fig. 2-8. The open-loop gain, K_e, was found, from the definition of J, to range between the values shown below.

1st Stage	2nd Stage	3rd Stage
1.071-0.07	1.51-0.14	1.45-0.19

Exact solutions for K_e and K_{re} were not obtained analytically since the system contains a nonlinear saturation effect which was ignored in constructing the root locus. Also, K_e is a function of system parameters which change continuously during flight and dramatically at booster stage separations. To fine tune the selection of K_e and K_{re}, simulation studies were conducted using DSL/360 during each of the three booster stages of operation. The results of the simulations, for various values of K_{re}, are shown in Figs. 2-9, 2-10 and 2-11, where θ is given as a function time.

The simulations illustrated that the gain, K_e, has little effect on the system's performance. This is because it is "upstream" from the saturated nozzle actuator and, as such, can only shorten the time required for the actuator to reach maximum deflection. Since this time is already small compared to the system's response, K_e has negligible effect. To simplify the problem, K_e was set equal to one. The velocity feedback gain K_{re} has a pronounced effect on both the overshoot and the settling time of the system. From the simulations, K_{re} was selected to be 1.5. This choice ensures the specified settling time of ten seconds during all stages and results in overshoot only during stages one and two, where it is less than ten percent.

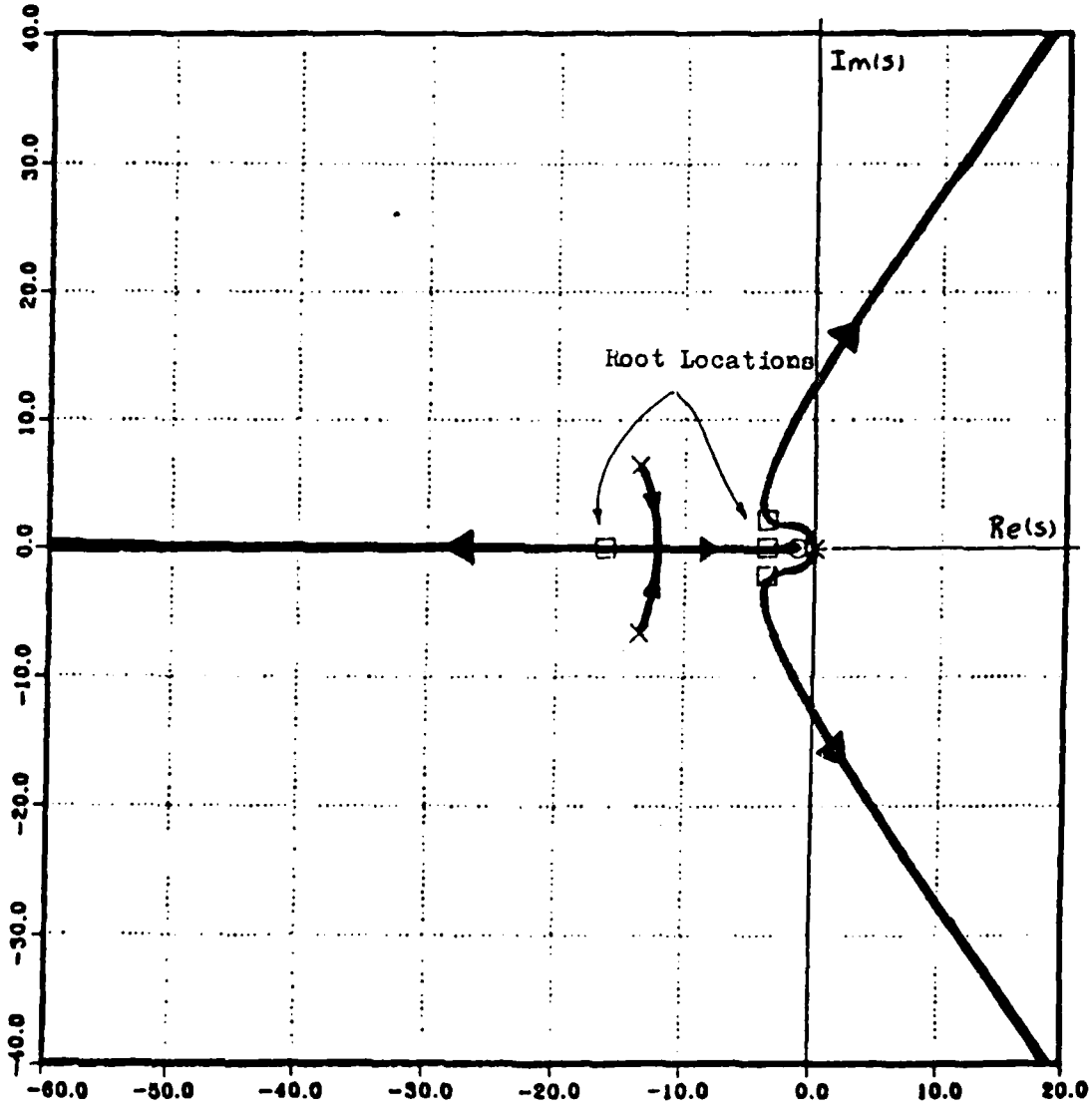

Fig. 2-8 Rcot Selection of Partitioned Equation

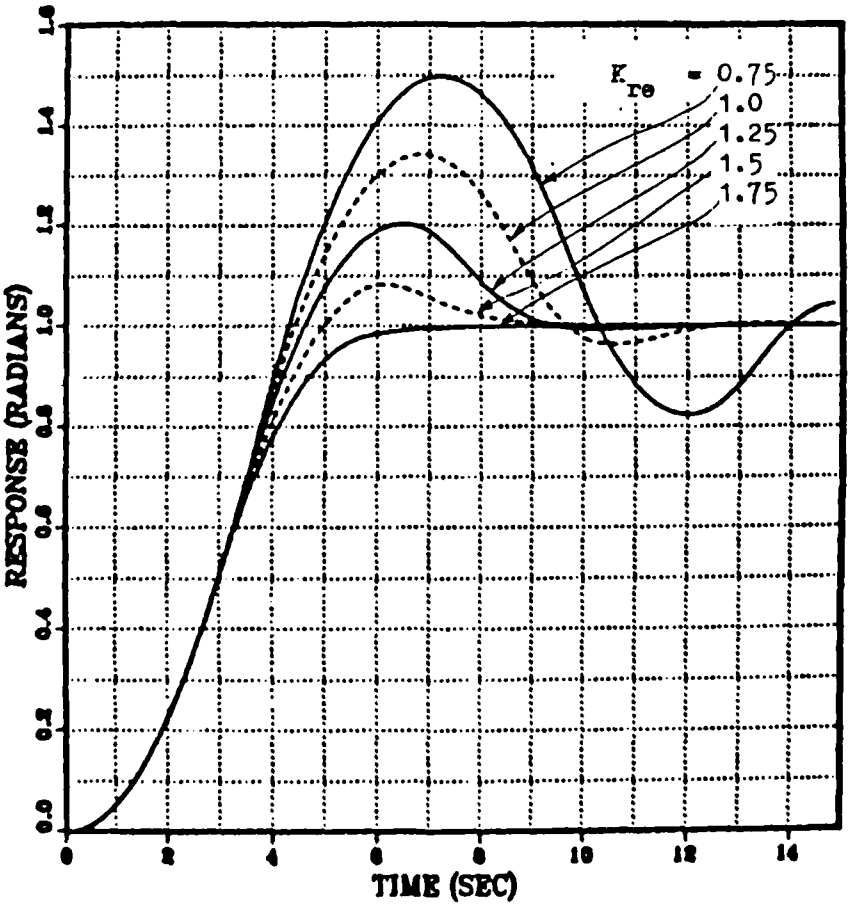

Fig. 2-9 First Stage Simulation of Pitch-Yaw Controller

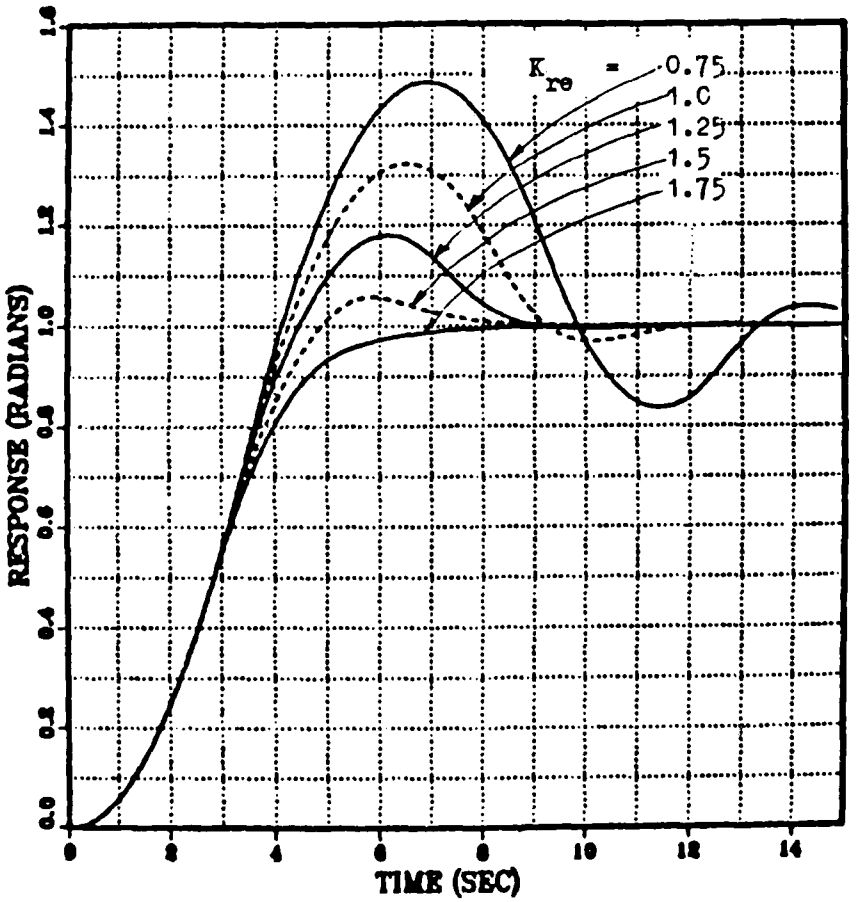

Fig. 2-10 Second Stage Simulation of Pitch-Yaw Controller

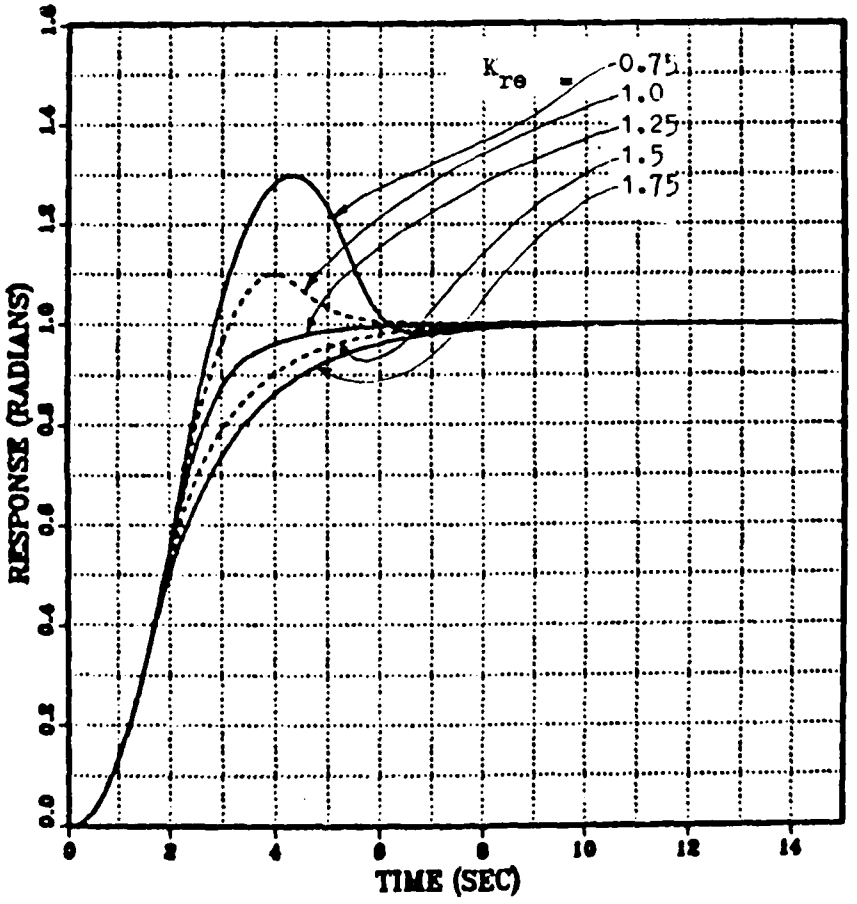

Fig. 2-11 Third Stage Simulation of Pitch-Yaw Controller

III. EFFECT OF ROLL

When the non-rolling pitch-yaw control system just designed is forced to roll, the system becomes cross-coupled as shown in Fig. 3-1. The mechanism which creates and maintains the rolling motion will not be considered. It is assumed that a control system outside the pitch-yaw controller and independent of the main thrust motor maintains an approximately constant roll rate, p. Furthermore, it is assumed that the roll rate can be measured during flight or estimated from measured parameters with reasonable accuracy. The purpose of this section is to analyze the effect roll has on the previously non-rolling pitch-yaw controller.

The Laplace transformations of the linearized non-rolling system's governing differential equations can be written as two separate equations; one for the pitch channel and one for the yaw channel.

$$s^2\theta + GK_{r\theta}s\theta + G\theta = G\theta_c \tag{3.1}$$

$$s^2\psi + HK_{r\psi}s\psi + H\psi = H\psi_c \tag{3.2}$$

Where G and H are defined as:

$$G = K_\theta(Tl_c/B)\left[\frac{ab^2}{(s+a)(s^2+2fbs+b^2)}\right] \tag{3.3}$$

$$H = K_\psi(Tl_c/C)\left[\frac{ab^2}{(s+a)(s^2+2fbs+b^2)}\right] \tag{3.4}$$

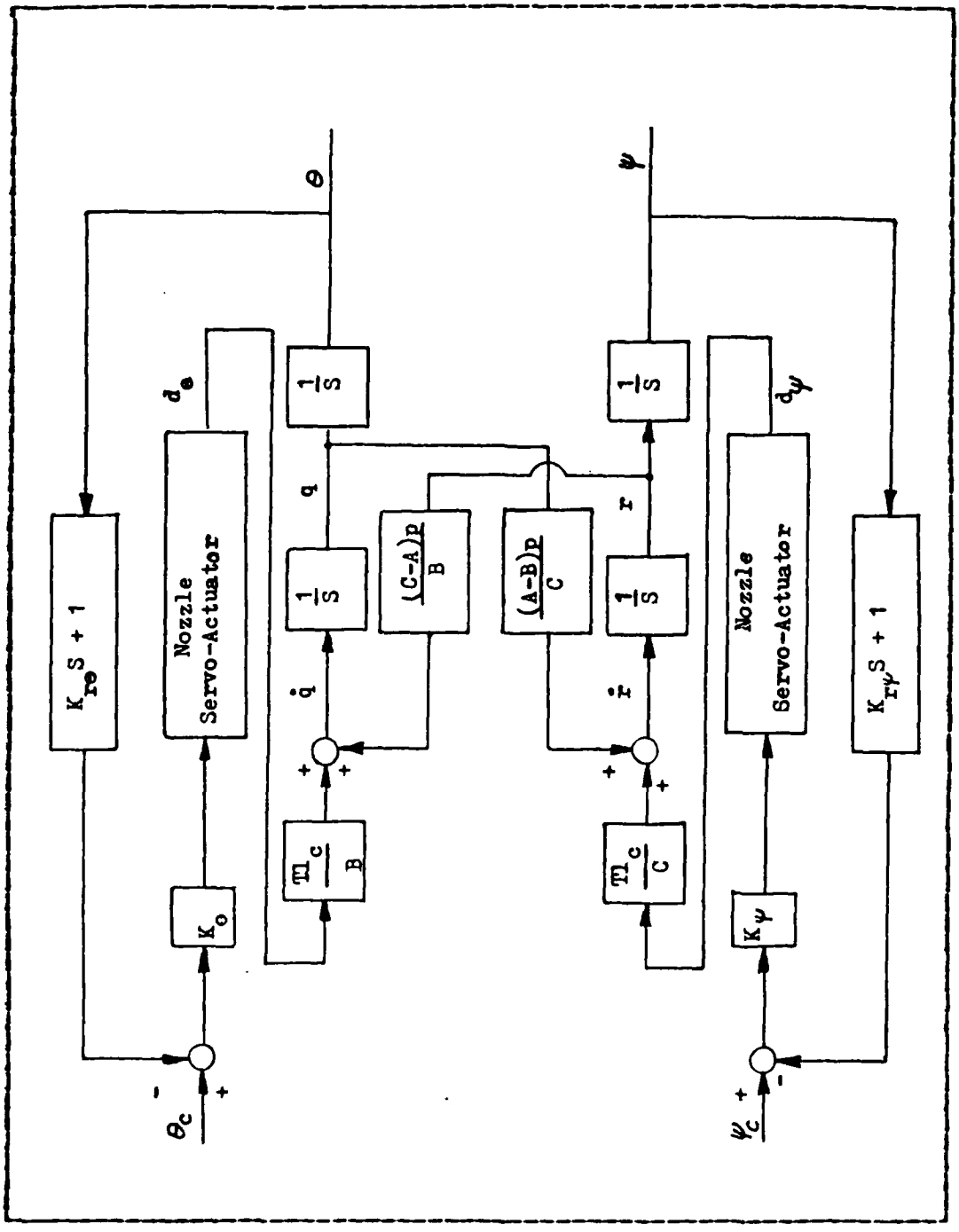

Fig. 3-1 Rolling Pitch-Yaw Controller Block Diagram

Equations (3.1) and (3.2) can be rearranged and put into matrix form as shown in Eq. (3.5). Note that the equation has only diagonal non-zero elements and is, therefore, uncoupled.

$$\begin{bmatrix} s^2+GK_{r\theta}s+G & 0 \\ 0 & s^2+HK_{r\psi}s+H \end{bmatrix} \begin{bmatrix} \theta \\ \psi \end{bmatrix} = \begin{bmatrix} G & 0 \\ 0 & H \end{bmatrix} \begin{bmatrix} \theta_c \\ \psi_c \end{bmatrix} \qquad (3.5)$$

Rolling the missile leads to the addition of cross-coupling terms between the equations governing pitch and yaw response. The transformed differential equations governing the responses of the rolling system are:

$$s^2\theta + GK_{r\theta}\, s\theta + G\theta + Qs\psi = G\theta_c \qquad (3.6)$$

$$s^2\psi + HK_{r\psi}\, s\psi + H\psi + Rs\theta = H\psi_c \qquad (3.7)$$

Where G and H are defined in Eqs. (3.3) and (3.4) and Q and R are defined in Eqs. (3.8) and (3.9).

$$Q = (A - C)\,p/B \qquad (3.8)$$

$$R = (B - A)\,p/C \qquad (3.9)$$

Rearranging Eqs. (3.6) and (3.7) into matrix form as before leads to the coupled form:

$$\begin{bmatrix} s^2+GK_{r\theta}\, s+G & Qs \\ Rs & s^2+HK_{r\psi}\, s+H \end{bmatrix} \begin{bmatrix} \theta \\ \psi \end{bmatrix} = \begin{bmatrix} G & 0 \\ 0 & H \end{bmatrix} \begin{bmatrix} \theta_c \\ \psi_c \end{bmatrix} \qquad (3.10)$$

Equation (3.10) shows that the introduction of roll has affected the transfer functions which determine the input-to-output relationships of the system in two ways. First,

it has changed the direct path transfer functions of pitch-to-pitch and yaw-to-yaw command-to-output. Second, roll has introduced pitch-to-yaw and yaw-to-pitch command-to-output transfer functions which were zero before the missile was forced to roll. The effect that these changes have on the system's stability and performance will be examined next.

A. EFFECT OF ROLL ON SYSTEM STABILITY

As pointed out, the rolling system is governed by four transfer functions (2 inputs x 2 outputs). Consider only the pitch-to-pitch input-to-output transfer function, i.e., hold the yaw-command input equal to zero and ignore the yaw output. Under these conditions, the block diagram of the system may be rearranged as shown in Fig. 3-2. The transfer function obtained from the diagram is given in Eq. (3.11). As indicated, the pitch response of the system is influenced by a variety of system parameters, as it was before the missile was rolled. Now, however, the root locations of the system are also affected by the roll rate.

$$\frac{\theta(s)}{\theta_c(s)} = \frac{N_5 s^5 + N_4 s^4 + N_3 s^3 + N_2 s^2 + N_1 s + N_0}{s^{10} + D_9 s^9 + D_8 s^8 + D_7 s^7 + D_6 s^6 + D_5 s^5 + D_4 s^4 + D_3 s^3 + D_2 s^2 + D_1 s + D_0} \qquad (3.11)$$

where;

$N_5 = (ab^2/B)Tl_c K_\theta$

$N_4 = (ab^2/B)Tl_c K_\theta (a + 2fb)$

$N_3 = (ab^2/B)Tl_c K_\theta (b^2 + 2fba)$

$N_2 = (ab^2/B)Tl_c K_\theta (ab^2)$

$N_1 = (ab^2/B)Tl_c K_\theta (K_{r\psi} K_\psi ab^2 Tl_c / C)$

$N_0 = (ab^2/B)Tl_c K_\theta (K_\psi ab^2 Tl_c / C)$

$D_9 = 2(a + 2fb)$

$$D_8 = 2(b^2+2fba) + [(A-B)(A-C)p^2/CB] + (a+2fb)^2 = D_{81} + D_{82}p^2$$

$$D_7 = 2ab^2 + 2(a+2fb)(b^2+2fba+[(A-B)(A-C)p^2/CB]) = D_{71} + D_{72}p^2$$

$$D_6 = (b^2+2fba)(b^2+2fba + 2[(A-B)(A-C)p^2/CB]) + (ab^2Tl_c)[(K_{r\psi}K_\psi/C)+(K_{r\theta}K_\theta/B)] + (a+2ab)(2ab^2) + [(A-B)(A-C)p^2/CB](a+2fb)^2 = D_{61} + D_{62}p^2$$

$$D_5 = (ab^2Tl_c)[(K_\theta/B)+(K_\psi/C)] + 2[(A-B)(A-C)p^2/CB](ab^2) + 2(b^2+2fba)(ab^2) + 2[(A-B)(A-C)p^2/CB](b^2+2fba)(a+2fb) + (a+2fb)(ab^2Tl_c)[(K_{r\psi}K_\psi/C)+(K_{r\theta}K_\theta/B)] = D_{51} + D_{52}p^2$$

$$D_4 = (ab^2Tl_c)[(K_\psi/C)+(K_\theta/B)](a+2fb) + 2[(A-B)(A-C)p^2/CB](a+2fb)(ab^2) + [(K_{r\psi}K_\psi/C)+(K_{r\theta}K_\theta/B)](ab^2Tl_c)(b^2+2fba) + [(A-B)(A-C)p^2/CB](b^2+2fba)^2 + (ab^2)^2 = D_{41} + D_{42}p^2$$

$$D_3 = [(K_\psi/C)+(K_\theta/B)](ab^2Tl_c)(b^2+2fba) + 2[(A-B)(A-C)p^2/CB](ab^2)(b^2+2fba) + [(K_{r\psi}K_\psi/C) + (K_{r\theta}K_\theta/B)]((ab^2Tl_c)ab^2) = D_{31} + D_{32}p^2$$

$$D_2 = [(K_\psi/C)+(K_\theta/B)](ab^2)(ab^2Tl_c) + [(A-B)(A-C)p^2/CB](ab^2)^2 + (K_{r\psi}K_\psi K_{r\theta}K_\theta/BC)(Tl_c ab^2)^2 = D_{21} + D_{22}p^2$$

$$D_1 = K_\theta(ab^2Tl_c/CB)^2K_{r\psi}K_\psi + K_{r\theta}K_\theta(ab^2Tl_c/CB)^2K_\psi$$

$$D_0 = [(K_\psi K_\theta)(ab^2Tl_c)^2]/CB$$

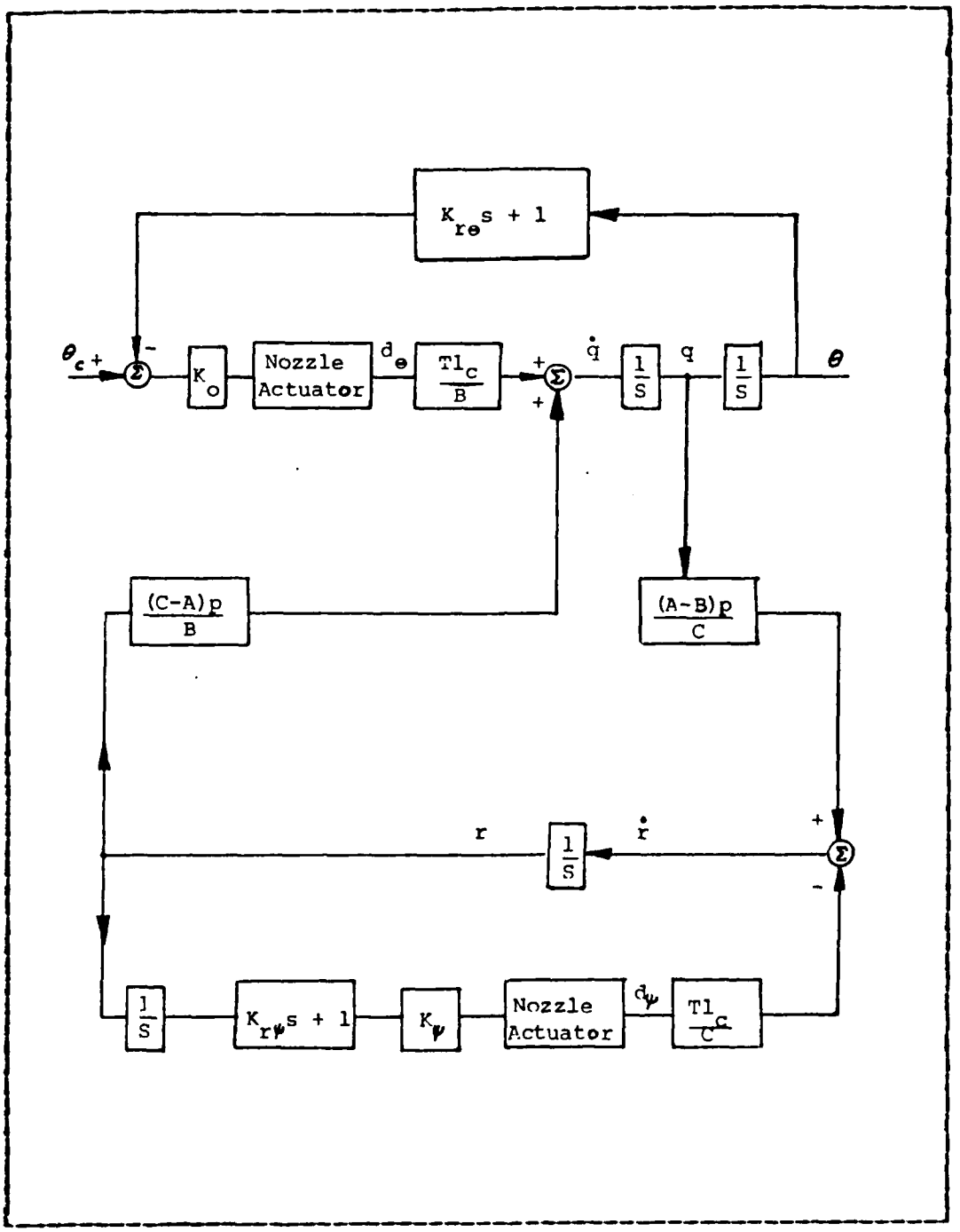

Fig. 3-2 Rolling System Rearranged with Yaw Suppressed

The denominator of Eq. (3.11), when set equal to zero, defines the characteristic equation of the system. Examination of Eq. (3.12) (in which Eq. (3.11) defines the coefficients) shows that as the roll rate is increased from zero, the roots of the characteristic equation will move as a function of the squared roll rate. For analysis, the region of operation will be restricted to the beginning and end of each booster stage. At these instants, the characteristic equation is as given in Eq. (3.12) with numerical values for the coefficients given in Table 3-1. The end of stage three is not considered because the missile is no longer performing powered flight at the end of the final stage.

$$s^{10} + D_9 s^9 + (D_{81} + D_{82} p^2) s^8 + (D_{71} + D_{72} p^2) s^7 \qquad (3.12)$$
$$+ (D_{61} + D_{62} p^2) s^6 + (D_{51} + D_{52} p^2) s^5 + (D_{41} + D_{42} p^2) s^4$$
$$+ (D_{31} + D_{32} p^2) s^3 + (D_{21} + D_{22} p^2) s^2 + D_1 s + D_0 = 0$$

The "migration" of the system's roots as the roll rate increases from zero is shown in Figs. 3-3 through 3-12. Figure 3-4, for example, shows that two roots of the system move into the right-half plane at a roll rate of approximately 12.2 radians/second. Since the linearized characteristic equation was used to construct the root loci shown in Figs. 3-3 through 3-12, the precise value of roll rate which causes instability cannot be determined from the figures. What the figures point out is the general migration of two system roots into the right-half plane in all phases of operation as the roll rate is increased.

TABLE 3-1

CHARACTERISTIC EQUATION COEFFICIENTS

	1st Stage		2nd Stage		3rd Stage
	Beginning	End	Beginning	End	Beginning
D_9	354.0	354.0	354.0	354.0	354.0
D_{81}	39,879.0	39,879.0	39,879.0	39,879.0	39,879.0
D_{82}	0.9755	0.9755	0.9401	0.9401	0.8869
D_{71}	1.5809×10^6	1.5809×10^6	1.5809×10^6	1.5809×10^6	1.5809×10^6
D_{72}	345.33	345.33	332.80	332.80	313.96
D_{61}	3.0355×10^7	3.0725×10^7	3.0368×10^7	3.0751×10^7	3.0549×10^7
D_{62}	38,902.0	38,902.0	37,490.0	37,490.0	35,368.7
D_{51}	3.1199×10^8	3.7781×10^8	3.1434×10^8	3.8236×10^8	3.4650×10^8
D_{52}	1.542×10^6	1.542×10^6	1.486×10^6	1.486×10^6	1.402×10^6
D_{41}	1.7182×10^9	3.3458×10^9	1.7764×10^9	3.4584×10^9	2.571×10^9
D_{42}	2.9483×10^7	2.9483×10^7	2.8413×10^7	2.8413×10^7	2.6805×10^7
D_{31}	4.8252×10^9	1.8385×10^{10}	5.310×10^9	1.9324×10^{10}	1.1929×10^{10}
D_{32}	2.815×10^8	2.815×10^8	2.7128×10^8	2.7128×10^8	2.5593×10^8
D_{21}	7.311×10^9	8.2761×10^{10}	8.5265×10^9	8.1567×10^{10}	3.389×10^{10}
D_{22}	1.11×10^9	1.11×10^9	1.0708×10^9	1.0708×10^9	1.0102×10^9
D_1	5.794×10^9	9.5278×10^{10}	7.0162×10^9	9.292×10^{10}	3.5410×10^{10}
D_0	1.931×10^9	3.176×10^{10}	2.3387×10^9	3.0972×10^{10}	1.1803×10^{10}

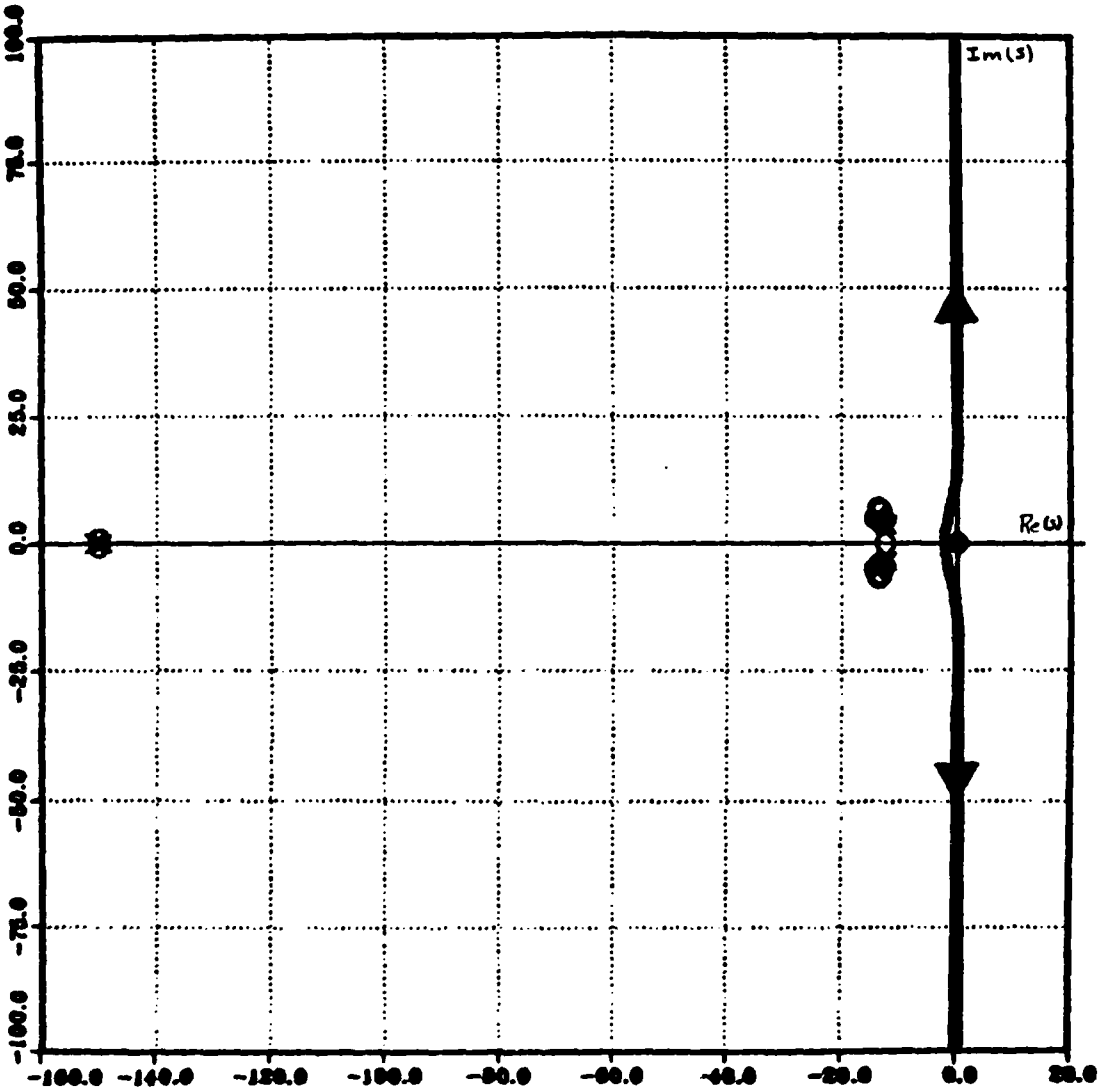

Fig. 3-3 Root Migration at Beginning of First Stage

Figures 3-3, 3-5, 3-7, 3-9 and 3-11 show how the roots of the characteristic equation of the rolling missile move as the roll rate is increased. A close-up view of the migration around the imaginary axis is shown in Figs. 3-4, 3-6, 3-8, 3-10 and 3-12.

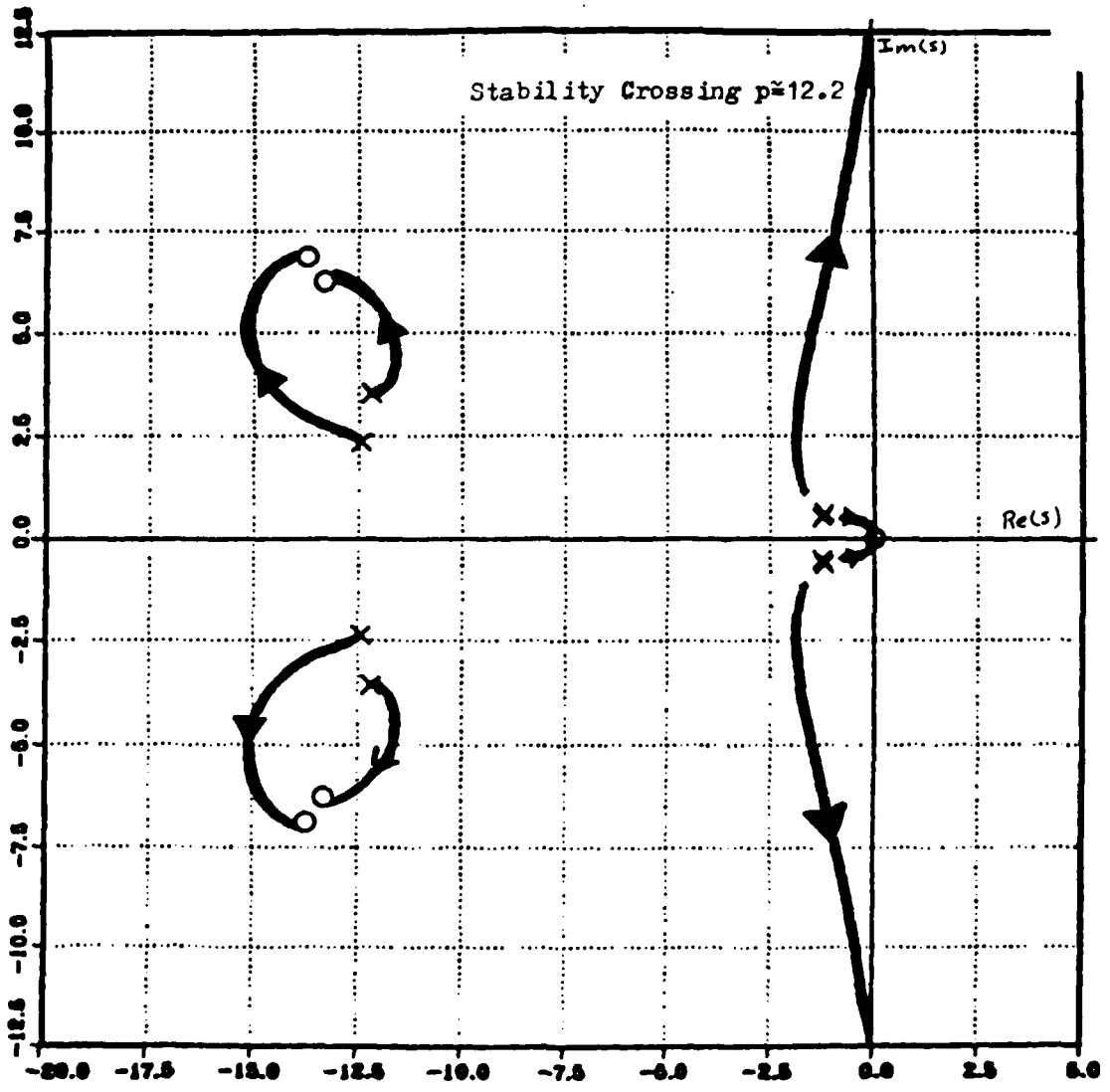

Fig. 3-4 Beginning of First Stage Root Migration Close-Up

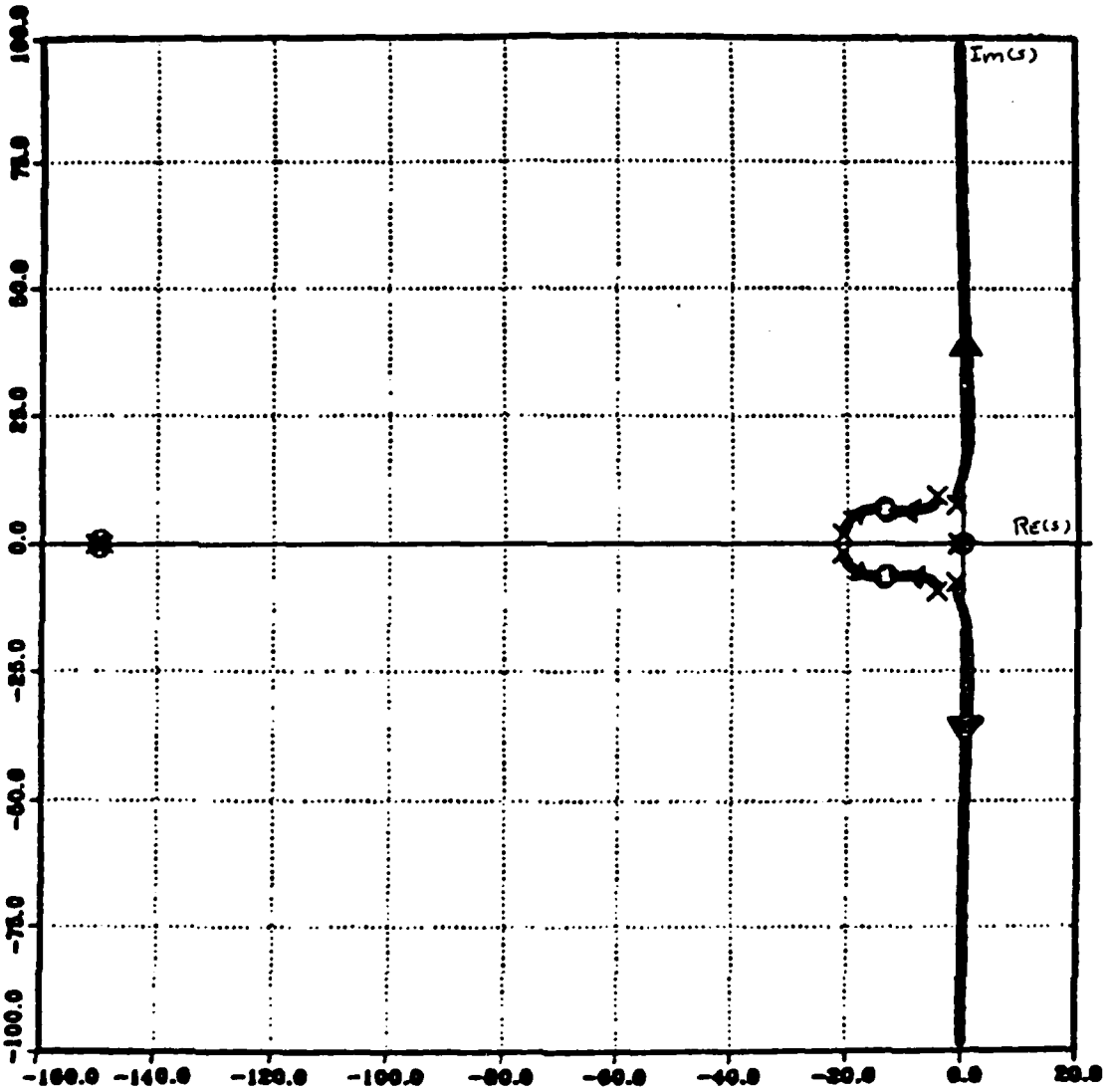

Fig. 3-5 Root Migration at End of the First Stage

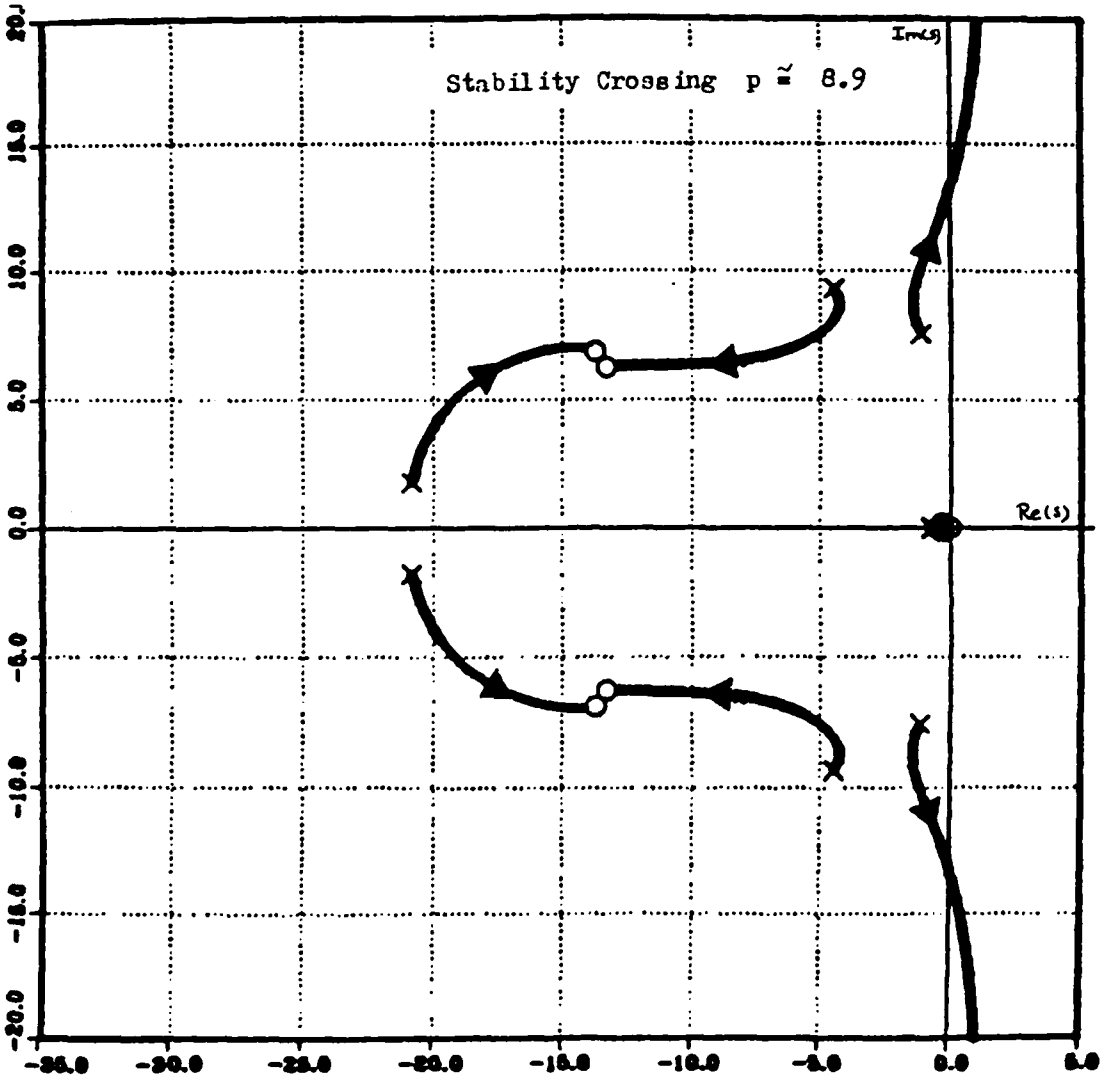

Fig. 3-6 End of the First Stage Root Migration Close-Up

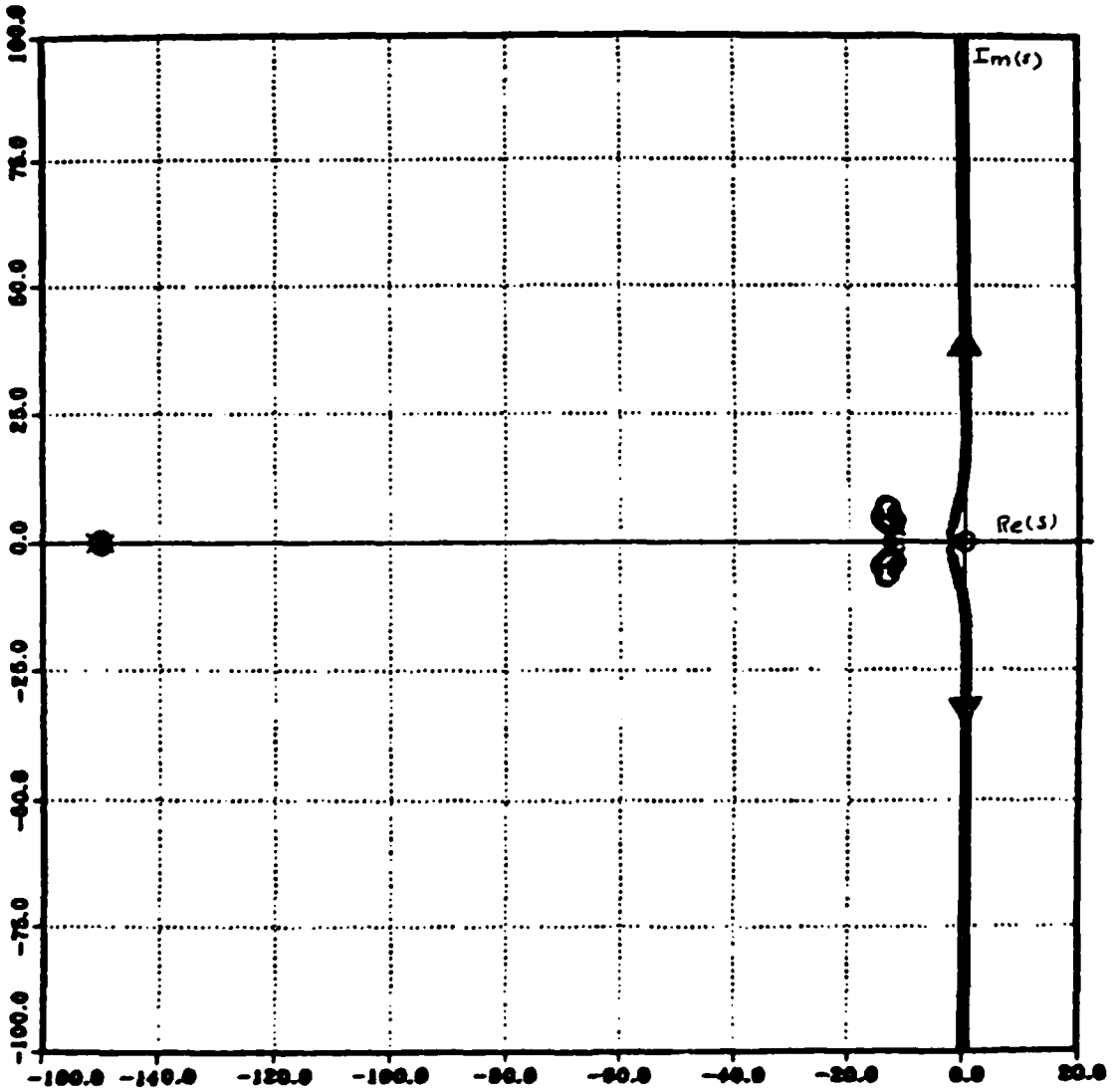

Fig. 3-7 Root Migration at Beginning of Second Stage

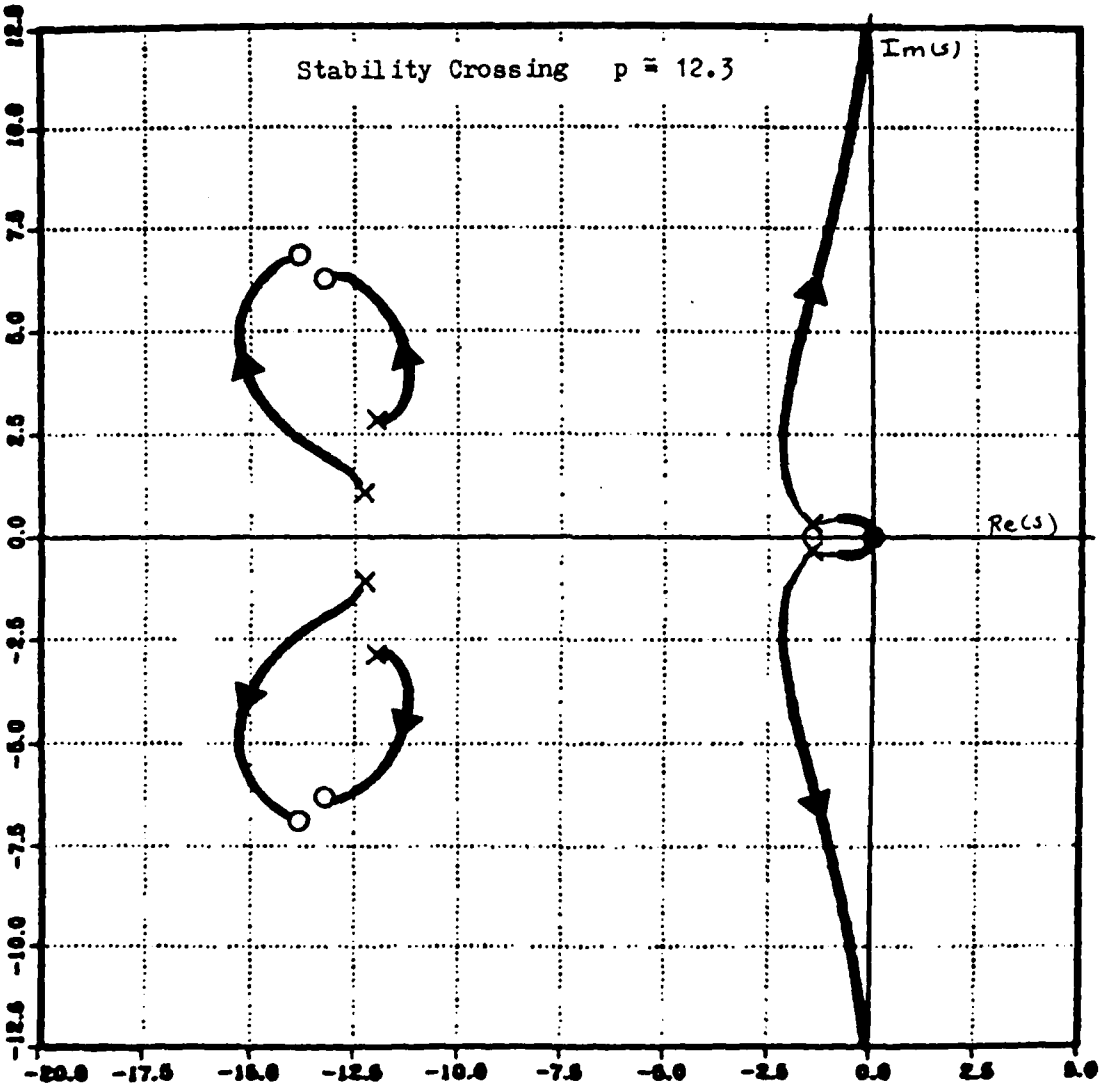

Fig. 3-8 Beginning of Second Stage Root Migration Close-Up

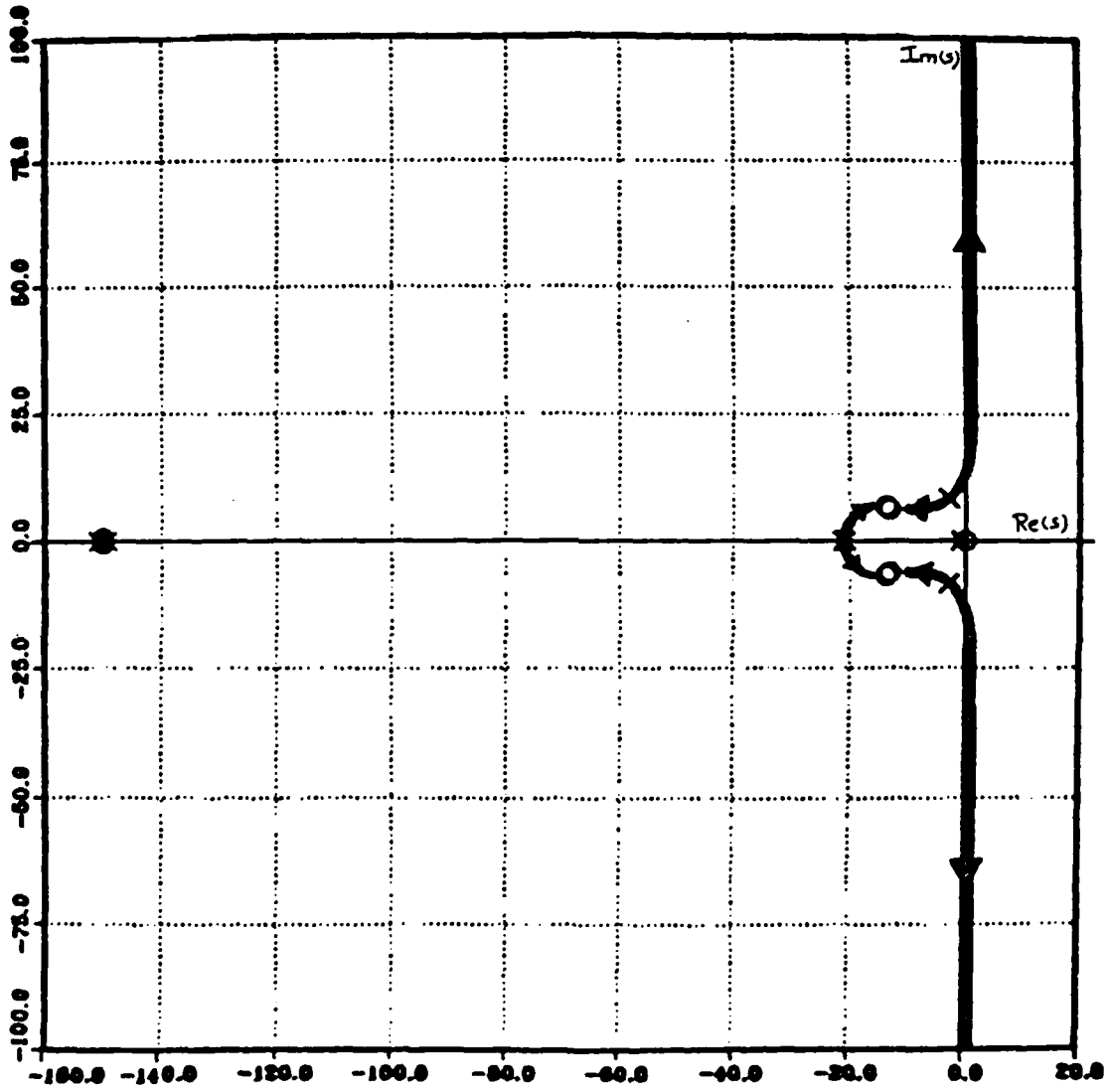

Fig. 3-9 Root Migration at End of the Second Stage

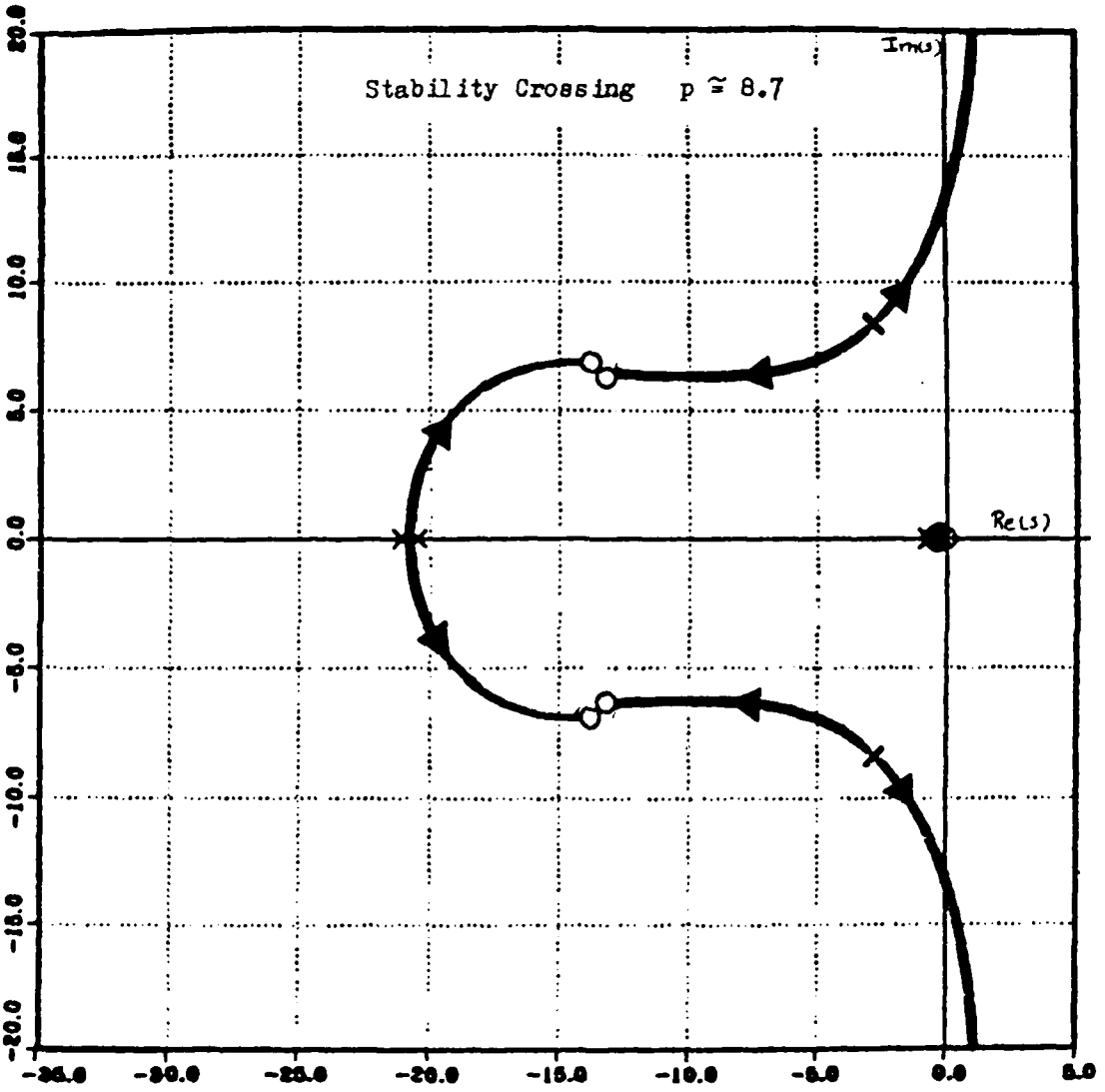

Fig. 3-10 End of the Second Stage Root Migration Close-Up

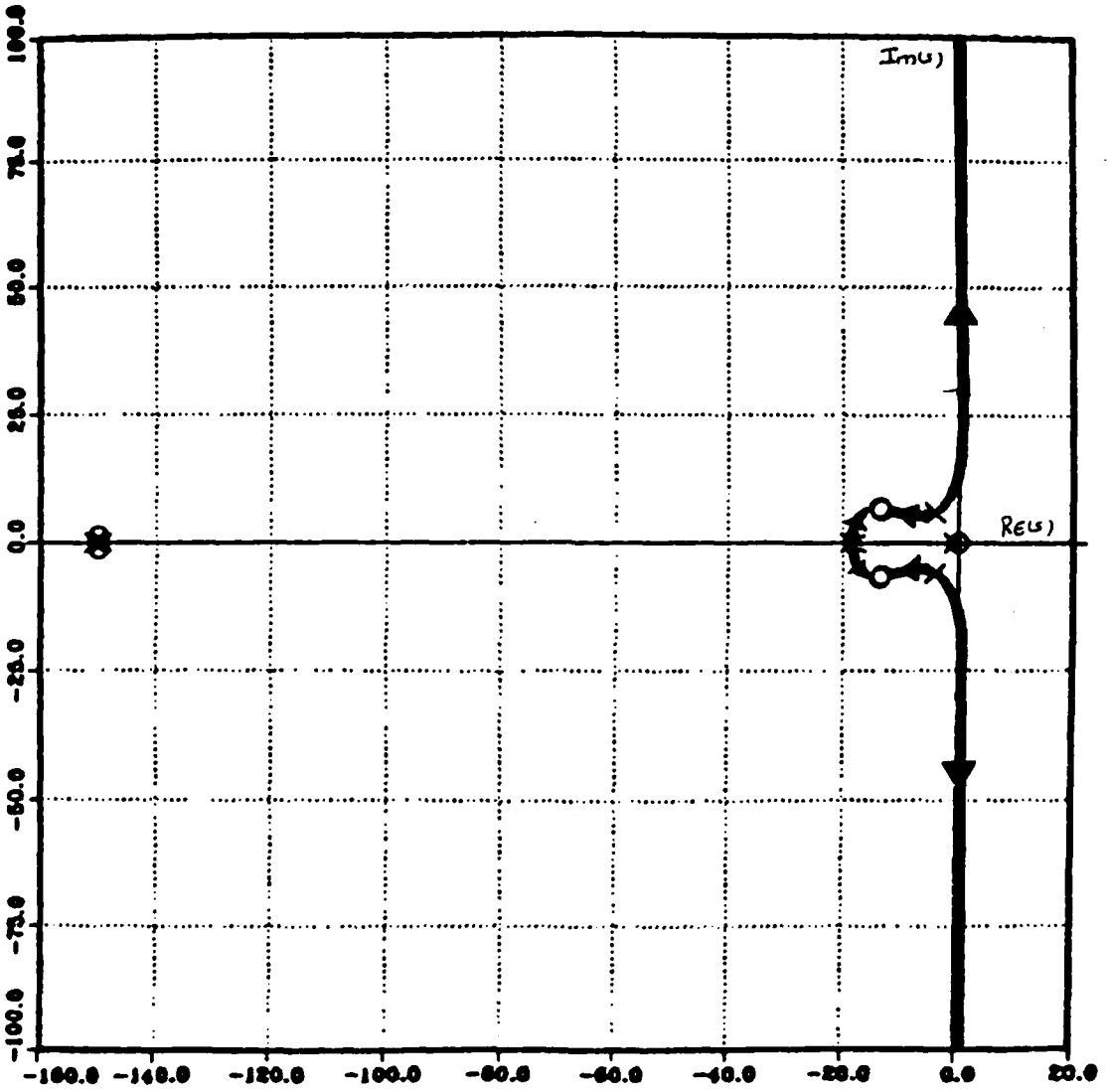

Fig. 3-11 Root Migration at Beginning of Third Stage

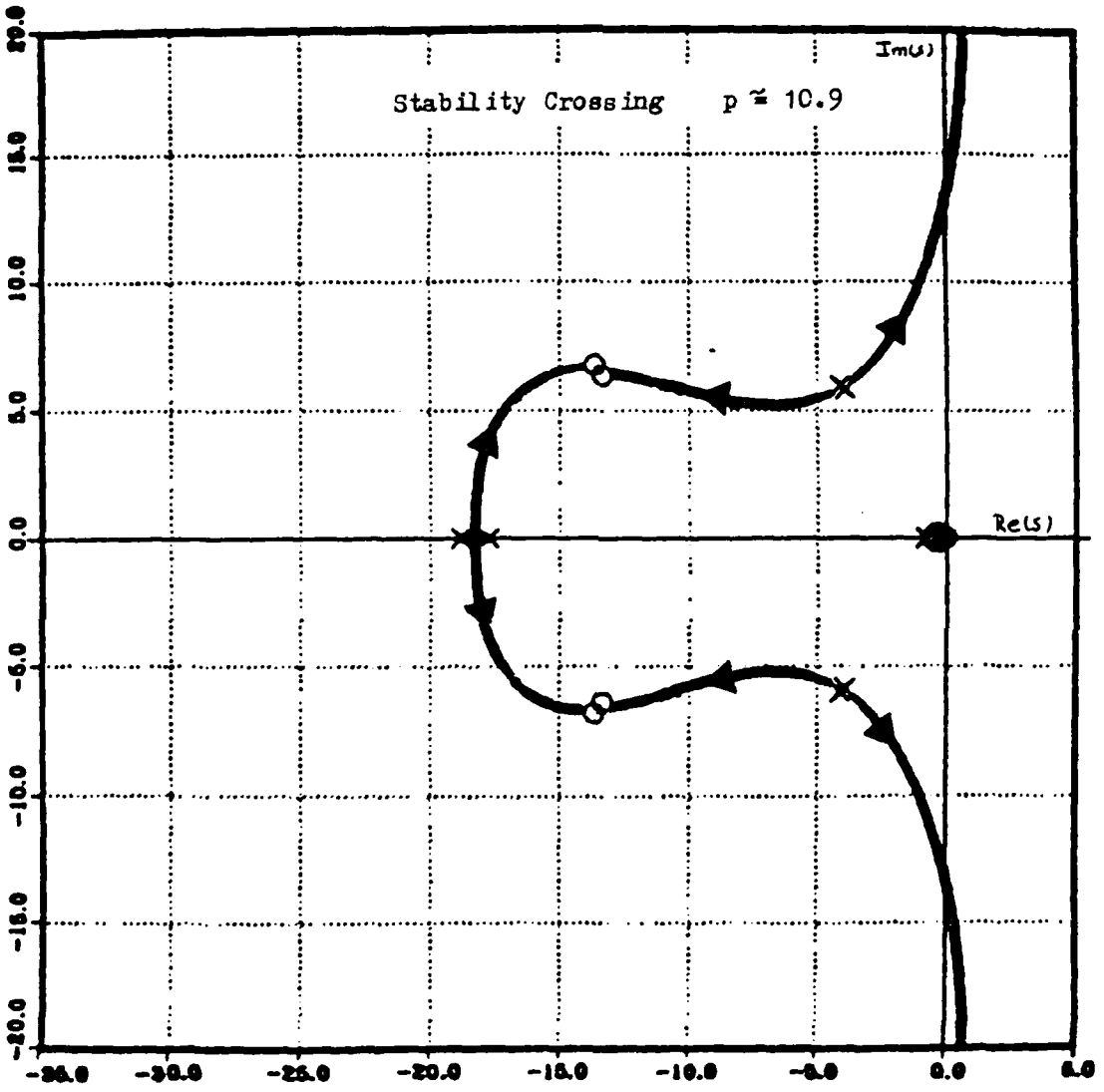

Fig. 3-12 Beginning of Third Stage Root Migration Close-Up

B. EFFECT OF ROLL ON SYSTEM PERFORMANCE

As shown, the introduction of roll into the pitch-yaw controller causes a migration of two system roots into the right-half of the s-plane. As the roots approach the imaginary axis (as the roll rate is increased) the system begins to show more transient oscillation due to the decreased damping ratio. The settling time of the system is also increased. Since the system contains the nonlinear saturation effect of the nozzle actuator and is of such high order (tenth), not much more than this qualitative observation was done analytically.

To study the effect of roll on system performance, a series of simulation studies was conducted with the saturation effect present. The simulation studies were performed by subjecting the system to three sets of step-input commands and constant roll rates. The first study consisted of giving the system a step-pitch input and a zero-yaw input and observing the transient response at six roll rates between 2.5 and 15 radians/second. The results of these simulations are plotted in Figs. 3-13 through 3-18. The second study involved subjecting the system to a zero-pitch input and a step-yaw input and conducting the same tests as the first study. The results of the second study are plotted in Figs. 3-19 through 3-24. Finally, the system was given both a step-pitch command and a step-yaw command and the tests were repeated. The responses of the system to the conditions of the third test are shown in Figs. 3-25 through 3-30. Unlike the non-rolling simulations which were run at separate booster stages (Figs. 2-9 through 2-11), the rolling simulations were run over several consecutive booster stages. This is because the settling time of the rolling missile system was often greater than the burn time of a single stage.

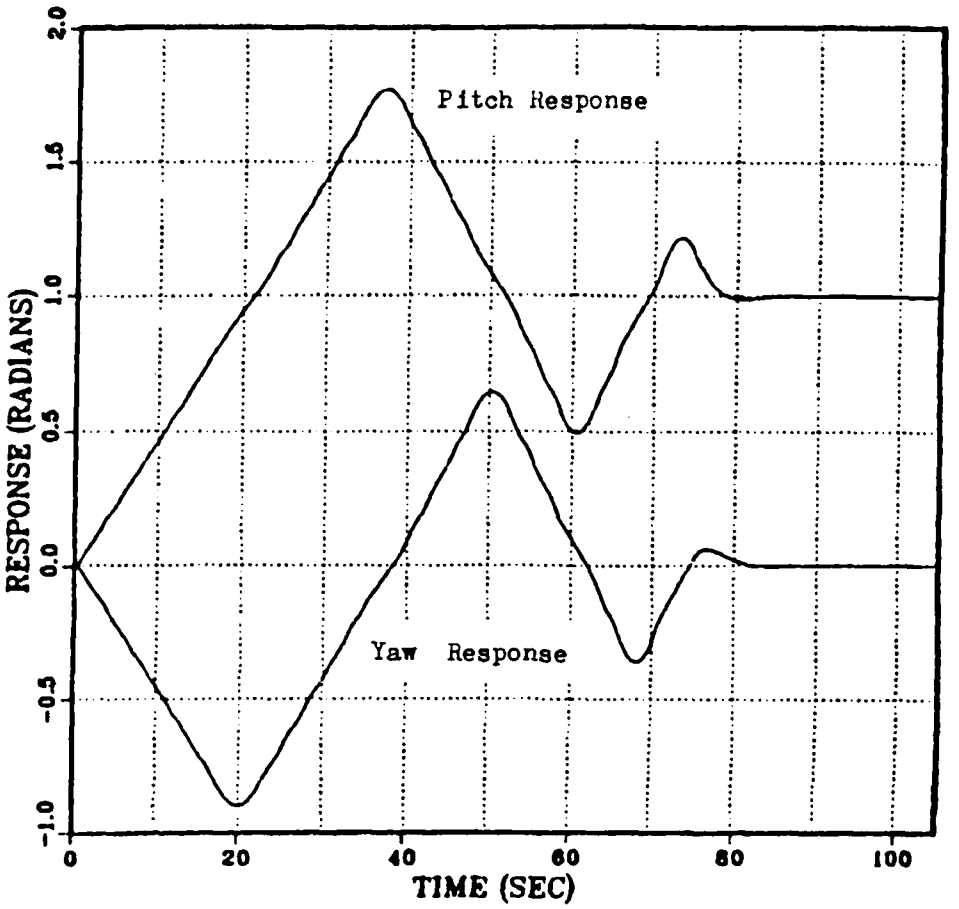

Fig. 3-13 Pitch-Step Response at Roll Rate of 2.5 rad/sec

Figures 3-13 through 3-18 show the system's pitch and yaw responses to a pitch-step input and a zero-yaw input at the specified roll rate. Note the dramatically increased overshoot, oscillation and settling time compared to the the non-rolling simulations, Figs. 2-9 through 2-11. Figure 3-18 shows shows the unstable response obtained at a roll rate equal of 15 rad/sec.

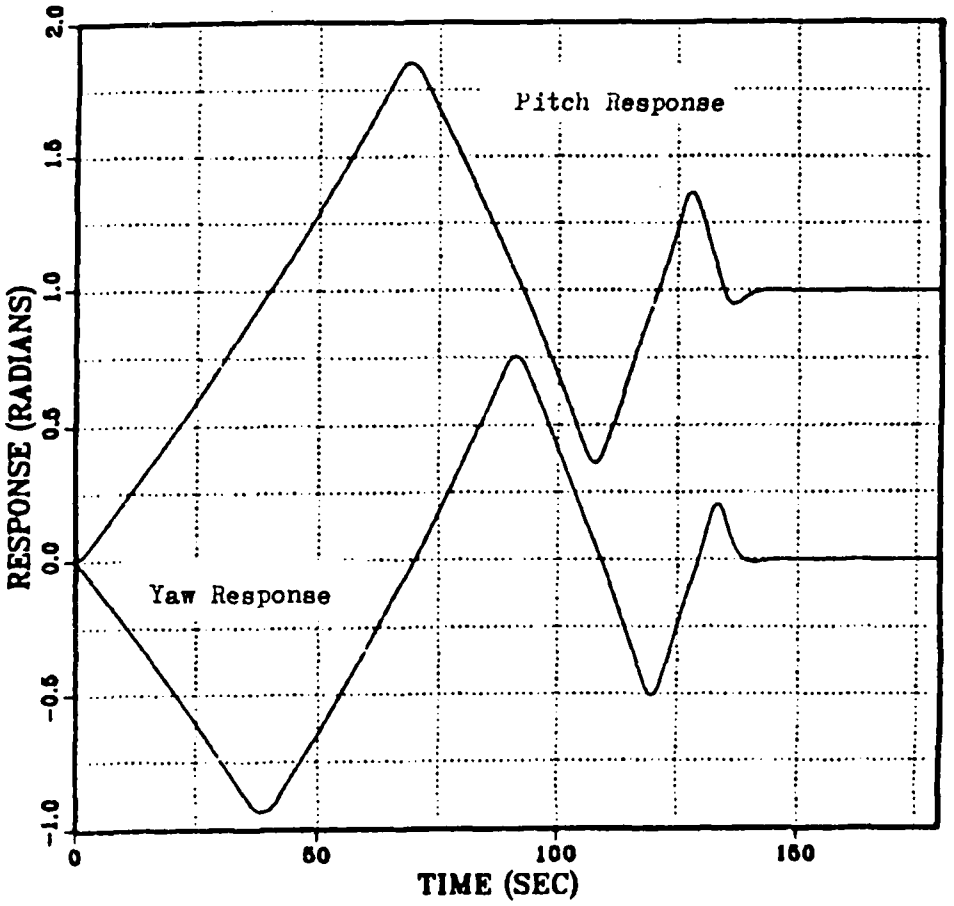

Fig. 3-14 Pitch-Step Response at Roll Rate of 5.0 rad/sec

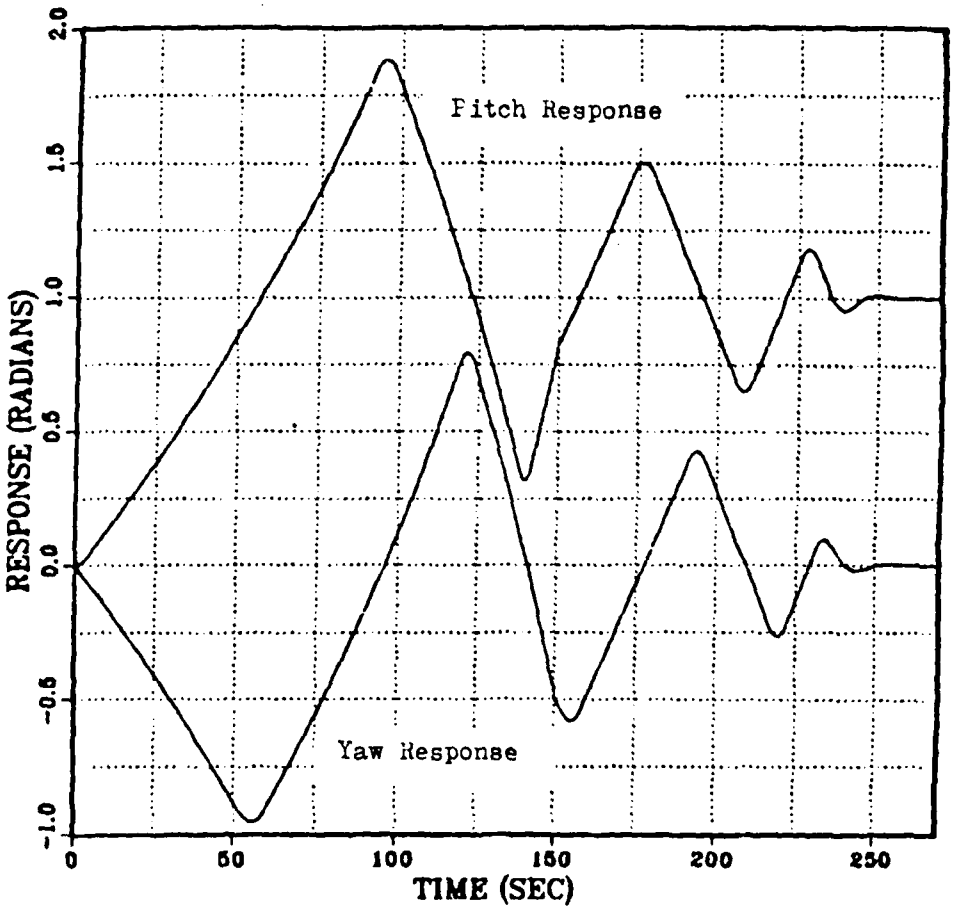

Fig. 3-15 Pitch-Step Response at Roll Rate of 7.5 rad/sec

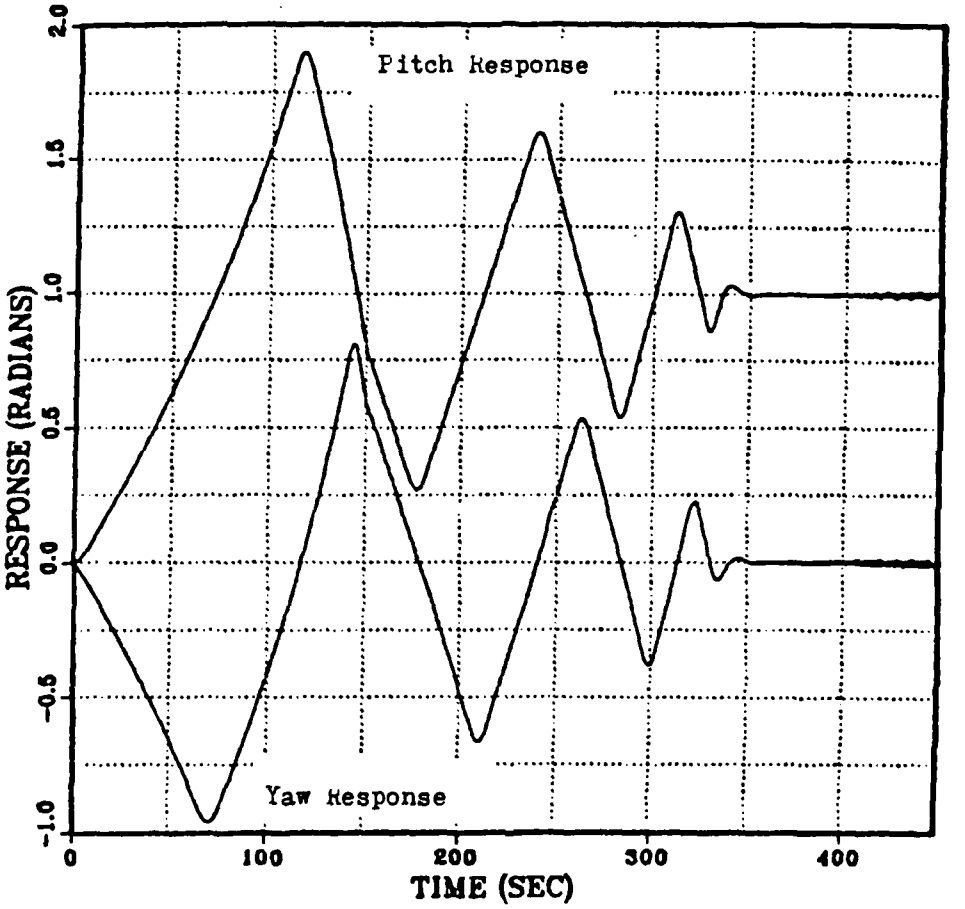

Fig. 3-16 Pitch-Step Response at Roll Rate of 10.0 rad/sec

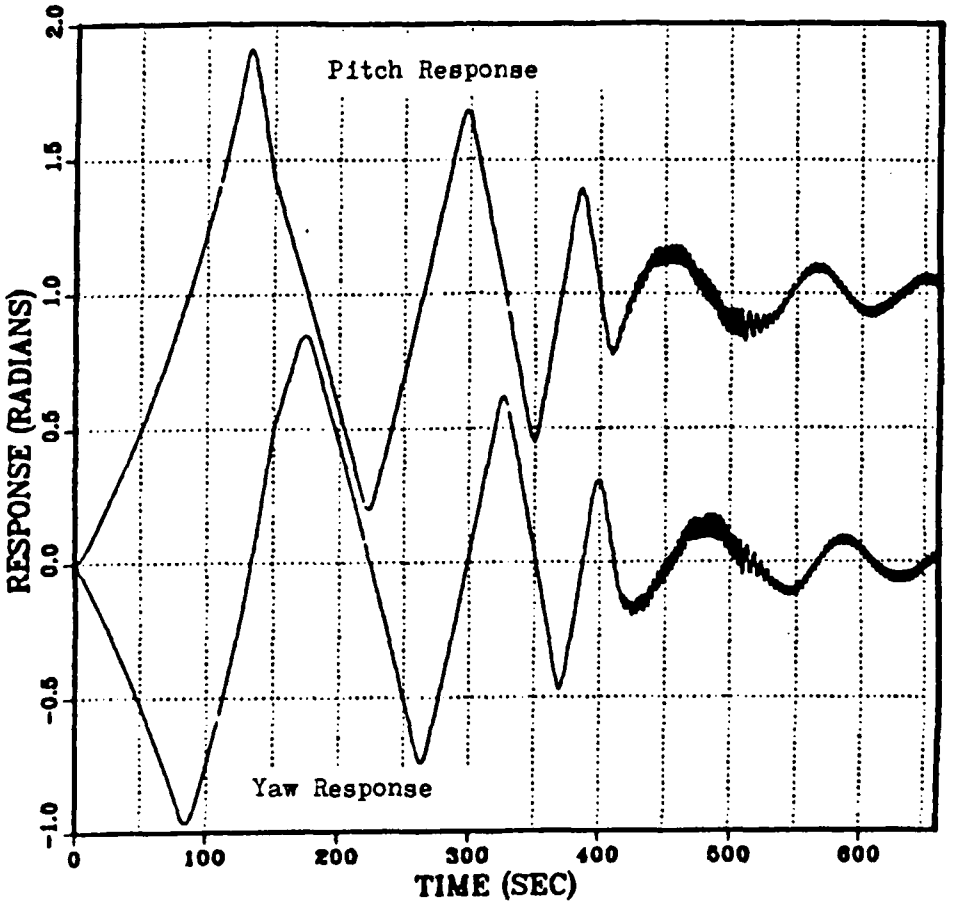

Fig. 3-17 Pitch-Step Response at Roll Rate of 12.5 rad/sec

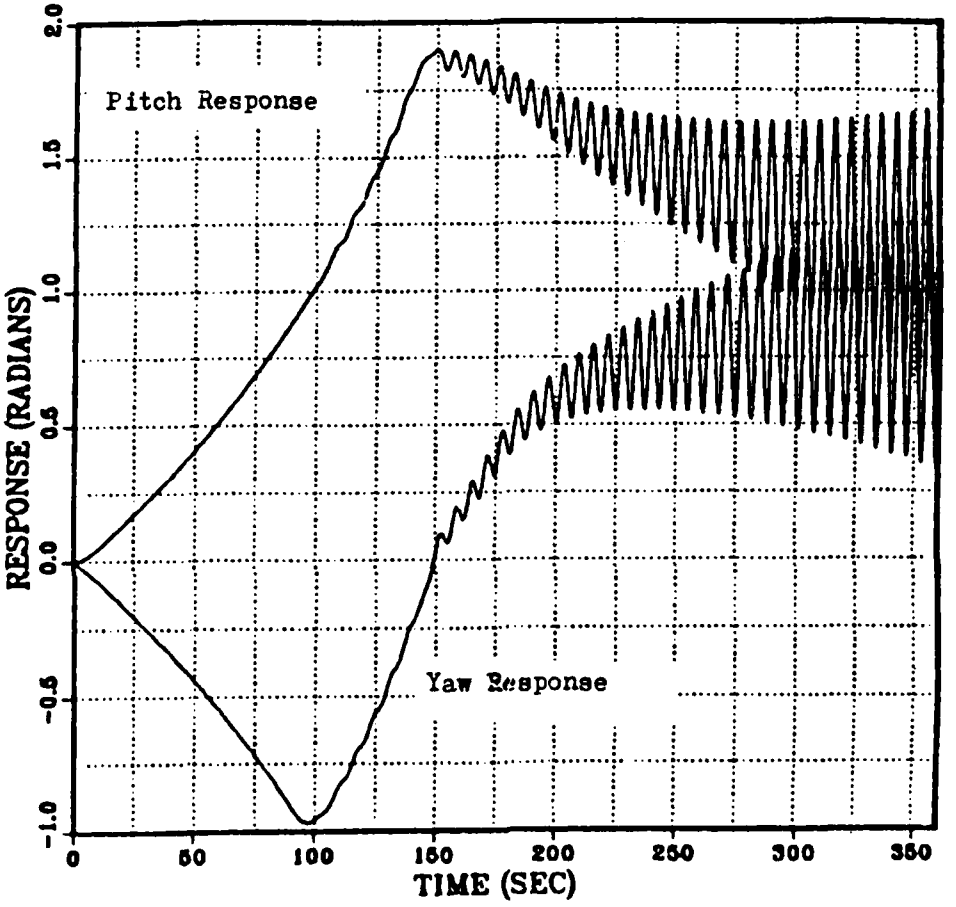

Fig. 3-18 Pitch-Step Response at Roll Rate of 15.0 rad/sec

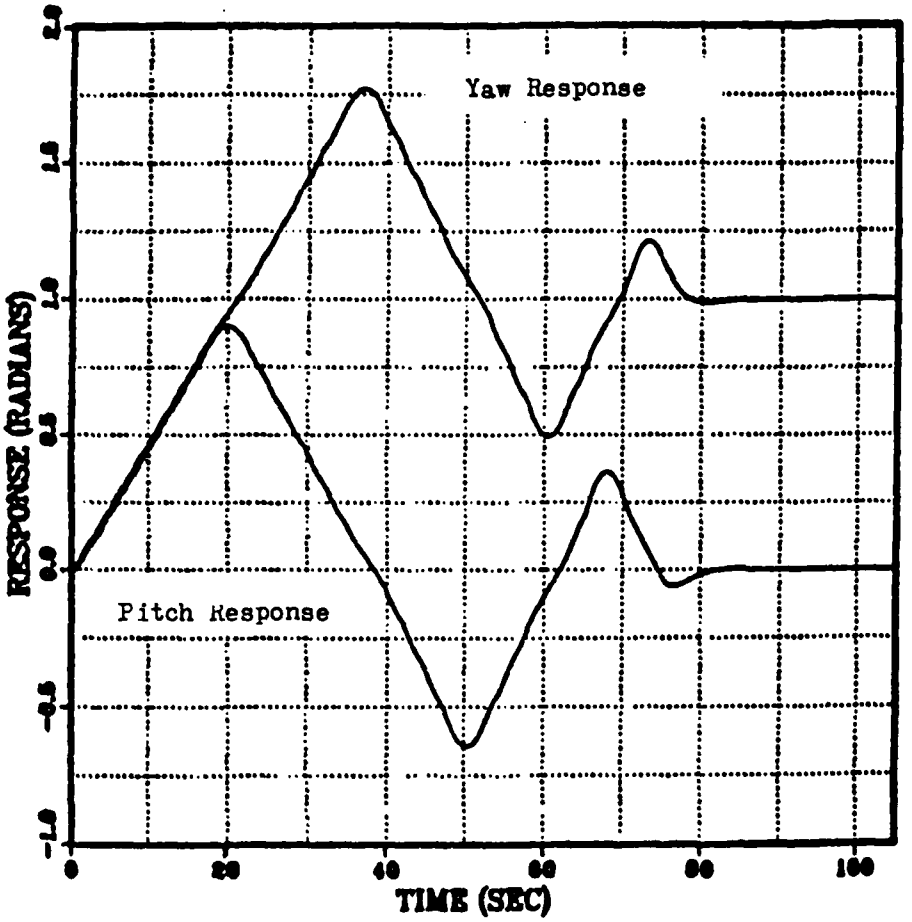

Fig. 3-19 Yaw-Step Response at Roll Rate of 2.5 rad/sec

Figures 3-19 through 3-24 show the system's pitch and yaw responses to a yaw-step input and a pitch-zero input at the specified roll rate. In these simulations, as in the previous ones, the overshoot and settling time are increased above that observed in the non-rolling simulations of Figs. 2-9 through 2-11. Figure 3-24 shows the unstable response at a roll rate of 15 rad/sec.

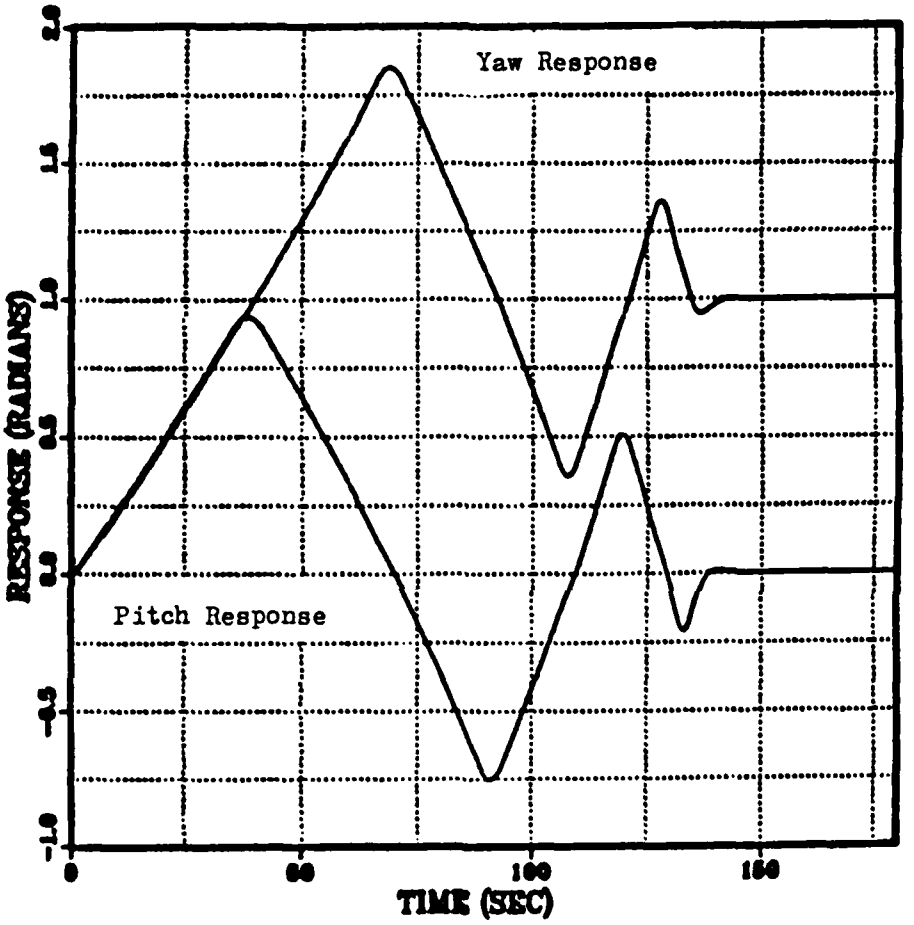

Fig. 3-20 Yaw-Step Response at Roll Rate of 5.0 rad/sec

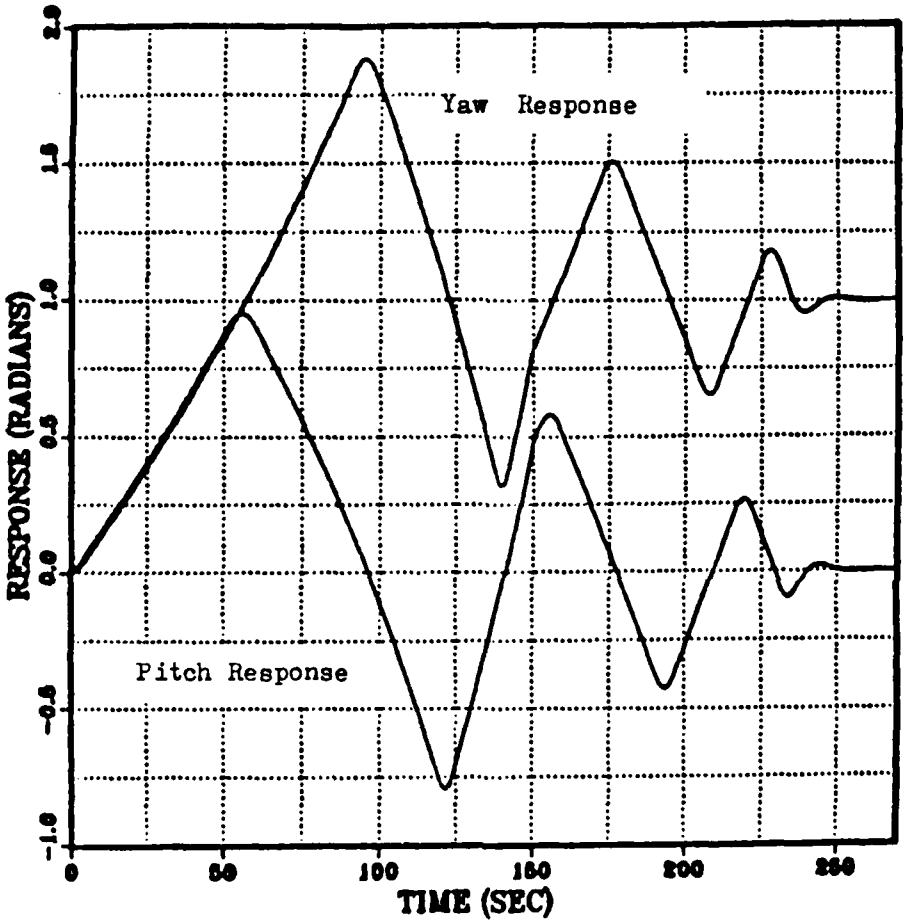

Fig. 3-21 Yaw-Step Response at Roll Rate of 7.5 rad/sec

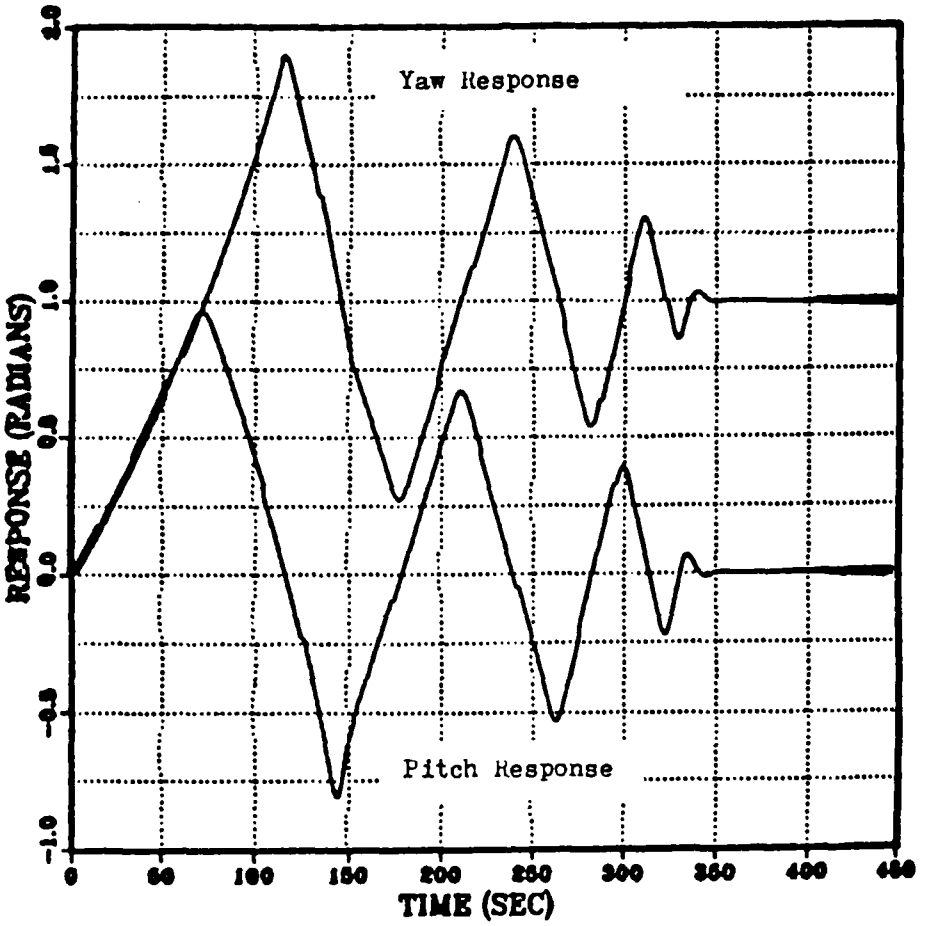

Fig. 3-22 Yaw-Step Response at Roll Rate of 10.0 rad/sec

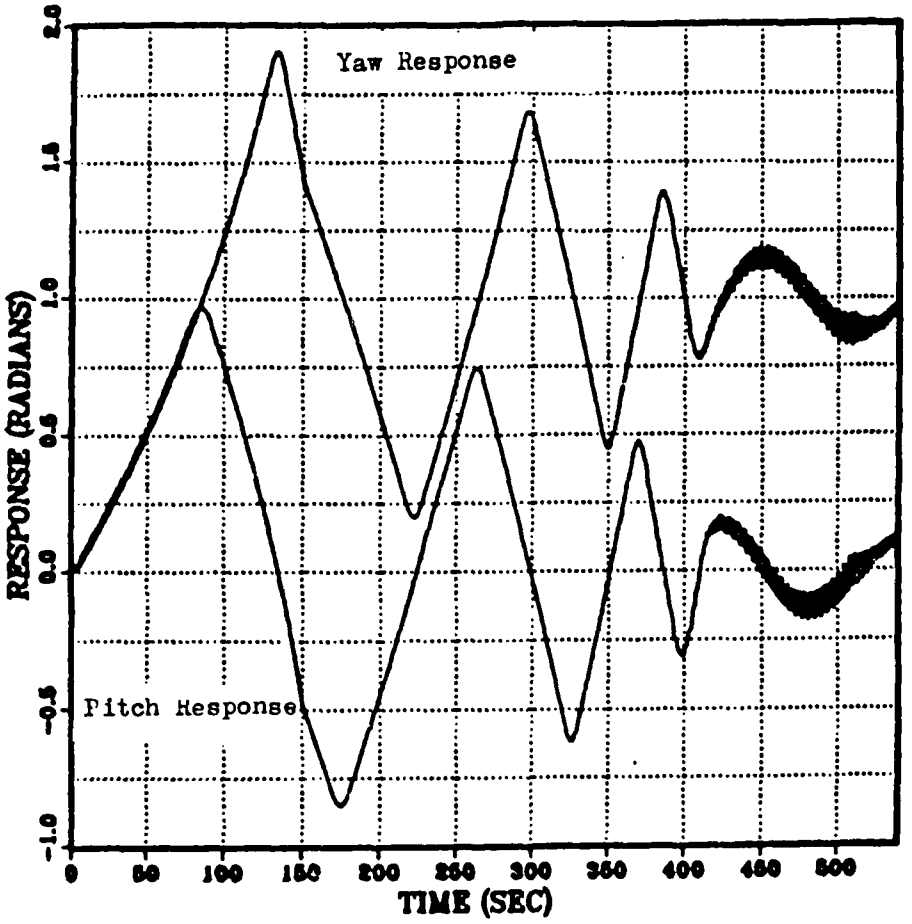

Fig. 3-23 Yaw-Step Response at Roll Rate of 12.5 rad/sec

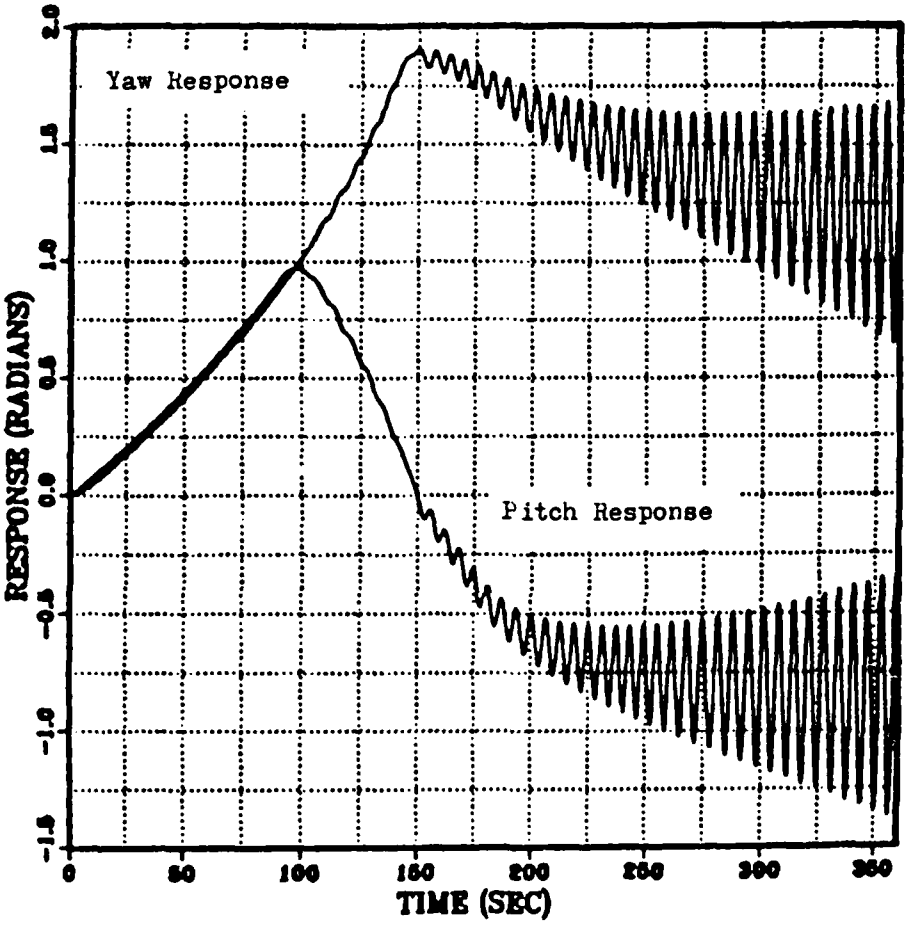

Fig. 3-24 Yaw-Step Response at Roll Rate of 15.0 rad/sec

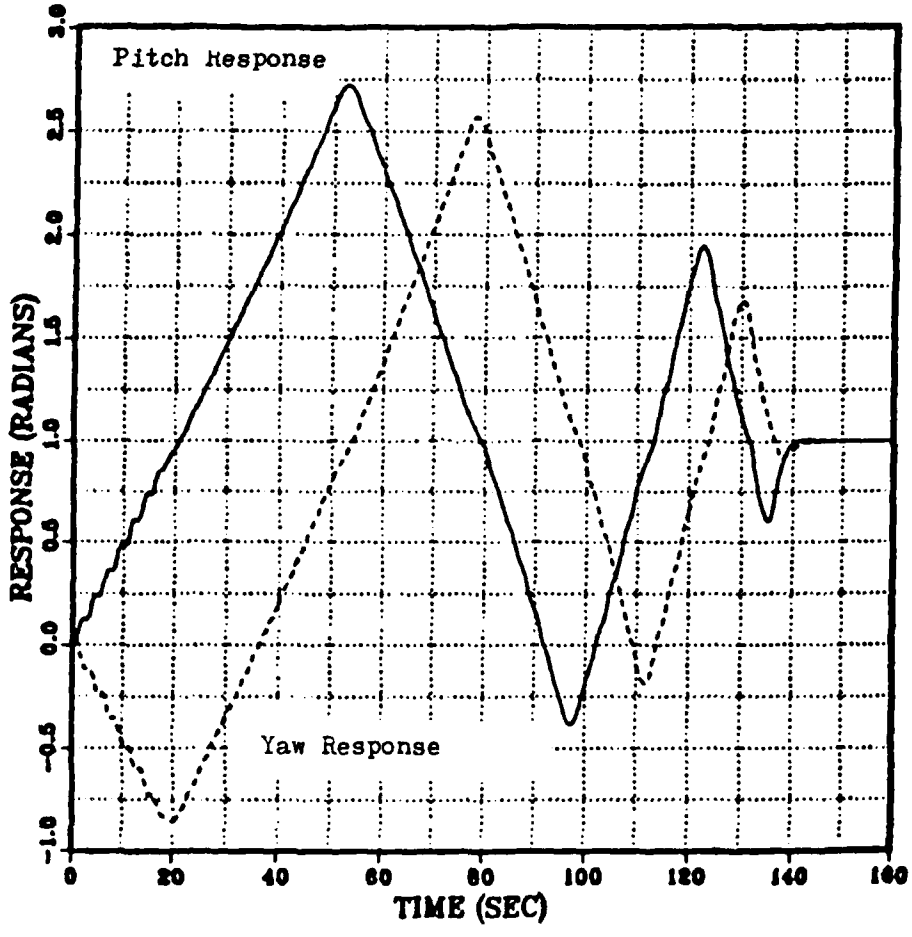

Fig. 3-25 Pitch- & Yaw-Step Response Roll Rate 2.5 rad/sec

Figures 3-25 through 3-30 show the system's pitch and yaw responses to pitch- and yaw-step inputs at the specified roll rate. Under these conditions, the under-damped oscillation observed in the two previous test is even more pronounced.

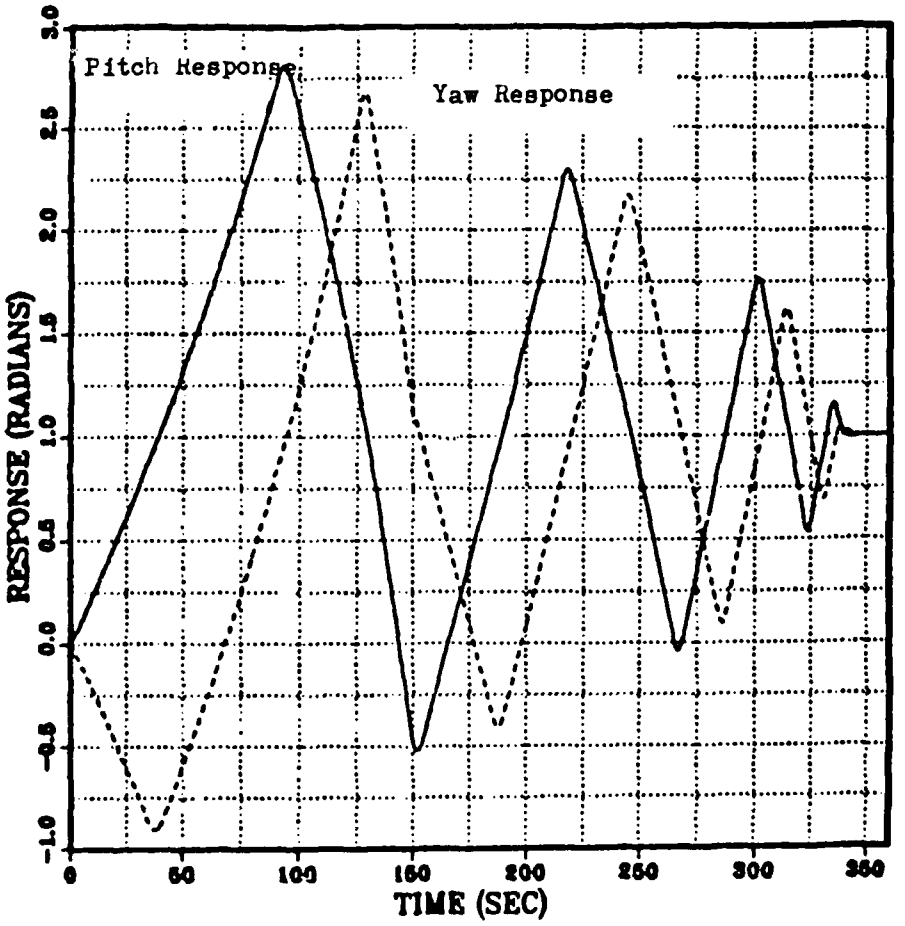

Fig. 3-26 Pitch- & Yaw-Step Response Roll Rate 5.0 rad/sec

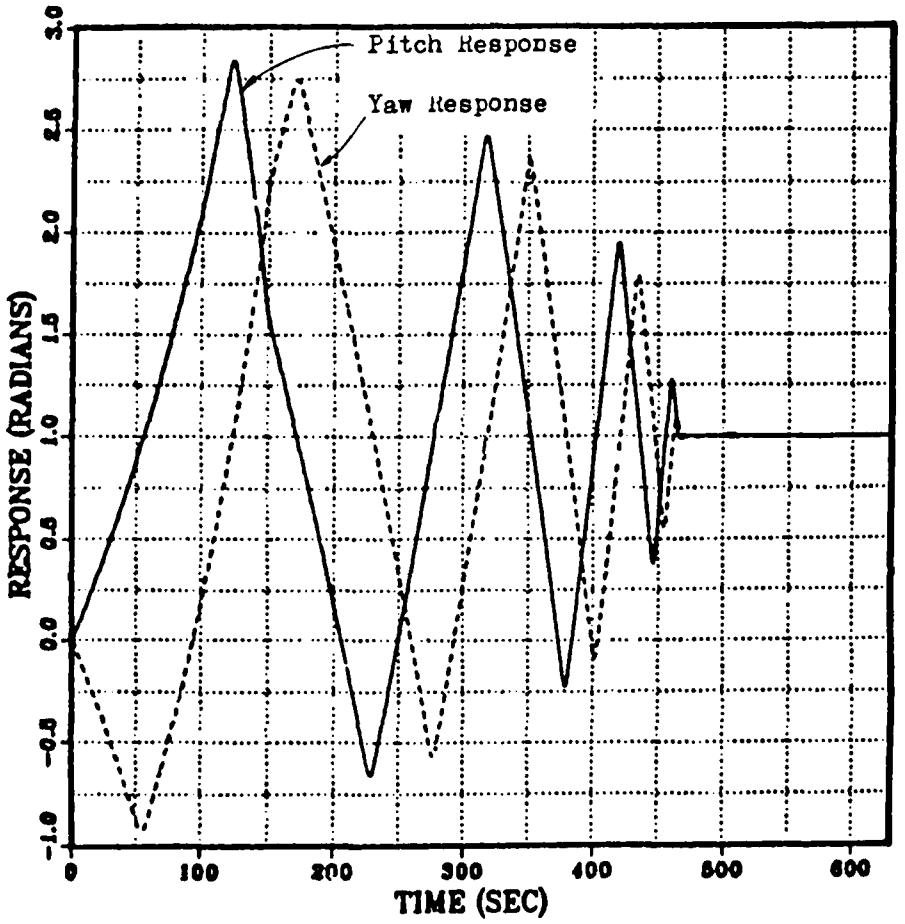

Fig. 3-27 Pitch- & Yaw-Step Response Roll Rate 7.5 rad/sec

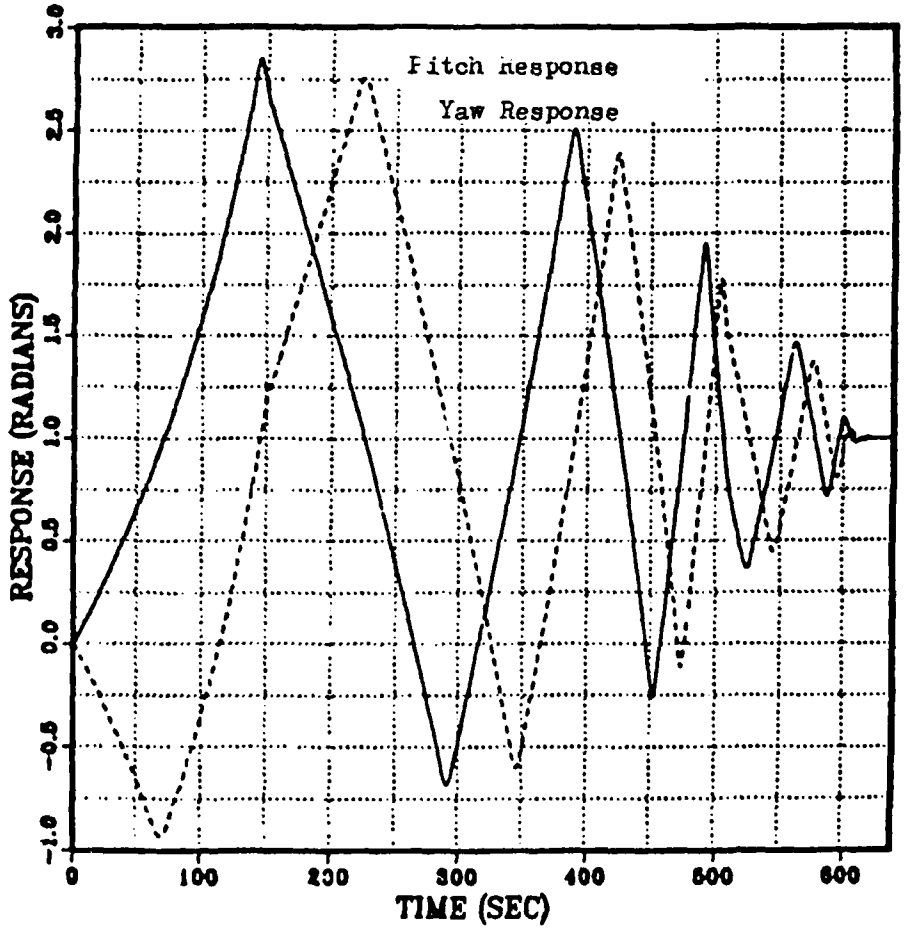

Fig. 3-28 Pitch- & Yaw-Step Response Roll Rate 10.0 rad/sec

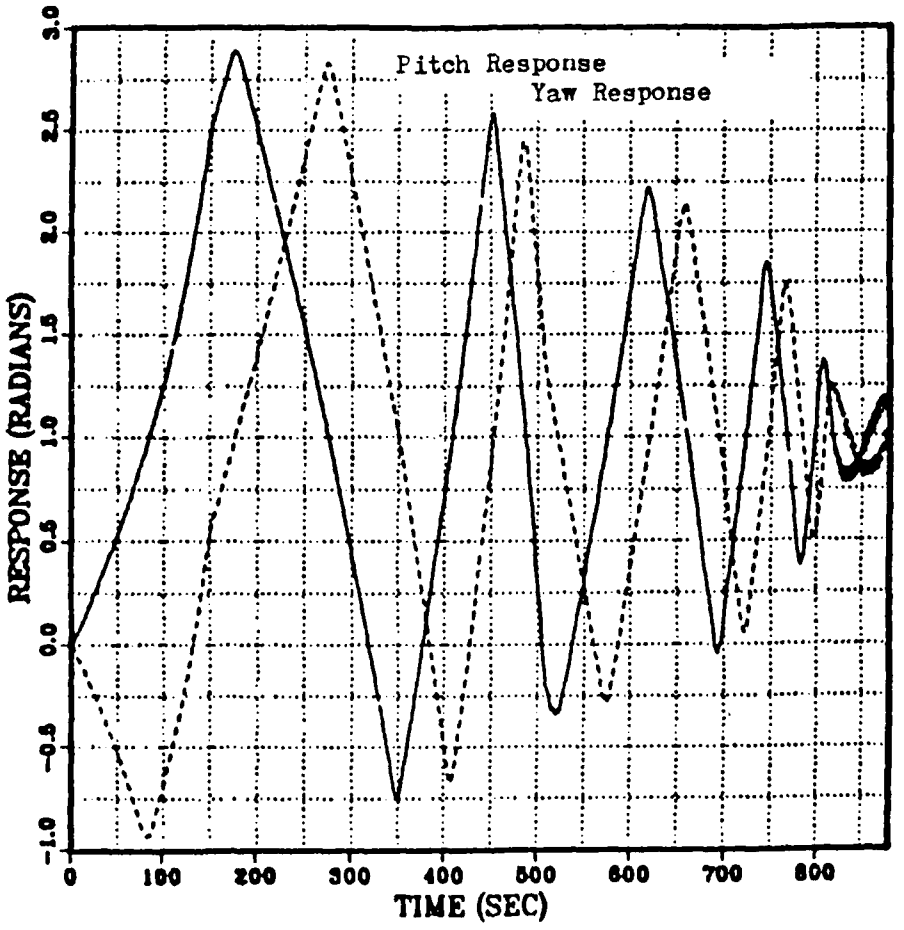

Fig. 3-29 Pitch- & Yaw-Step Response Roll Rate 12.5 rad/sec

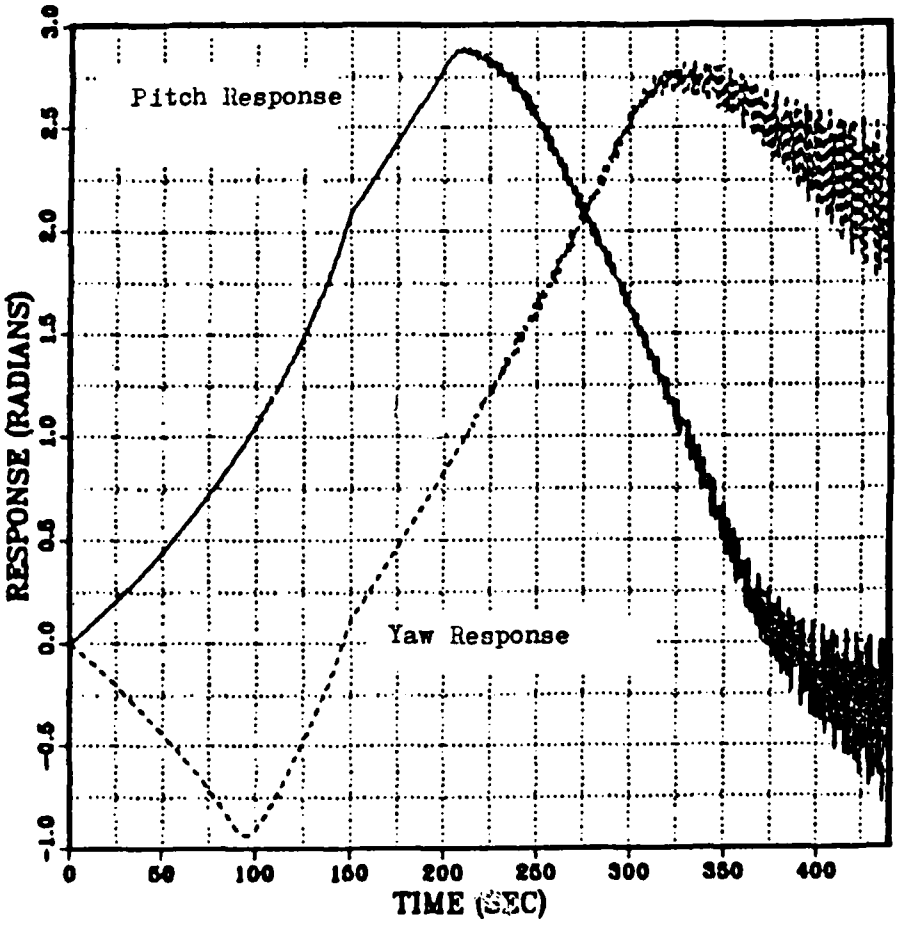

Fig. 3-30 Pitch- & Yaw-Step Response Roll Rate 15.0 rad/sec

The simulation studies showed that the system begins to reach instability at a roll rate of approximately 12 radians/second. However, at roll rates as low as 2.5 radians/second the system's performance has been severely degraded from the non-rolling case (Figs. 2-9 through 2-11). In all cases, the maximum peak overshoot is increased by a factor of at least five and the settling time by a factor of at least eight. The system's performance is approximately that of an under-damped oscillator. This response is caused by the two roots which have moved close to the imaginary axis as the roll rate was increased and are dominating the system's transient response. In the next section, a compensation scheme is proposed which increases the damping of the system and partially cancels the cross-coupling acceleration terms introduced by roll.

IV. COMPENSATION SCHEME

In the preceding chapter it was noted that rolling the missile had the effect of introducing cross-coupling terms into the pitch and yaw angular acceleration equations (Eqs. (3.6 and (3.7)). In order to completely restore the system's performance to its non-rolling condition, it is necessary to eliminate or cancel out the cross-coupling terms. Equation (3.10) can be rearranged into the form:

$$\begin{bmatrix} s^2 & Qs \\ Rs & s^2 \end{bmatrix} \begin{bmatrix} \theta \\ \Psi \end{bmatrix} = \begin{bmatrix} G(\theta_c - K_{r\theta} s\theta - \theta) \\ H(\Psi_c - K_{r\Psi} s - \Psi) \end{bmatrix} \qquad (4.1)$$

The left side of Eq. (4.1) contains the "dynamics" of the system. In other words, it gives the acceleration and velocity terms which determine the angular acceleration in the pitch and yaw channels. The only way to eliminate the cross-coupling terms directly would be to make changes to the left side of Eq. (4.1) which would cancel the terms, Qs and Rsθ. This would involve dramatic changes to the missile body, thrust vector control system and flight performance and, therefore, will not be attempted.

The right side of Eq. (4.1) constitutes the "electronics" of the system. It contains a sum of those terms which are added at the feedback junction then passed through the nozzle actuator. This side of the equation can be changed easily by altering the electronic network that makes up the feedback loop.

A. CROSS-CHANNEL FEEDBACK

Assume that the pitch rate and yaw rate can be accurately measured or estimated at any time during flight. Also, assume that the terms, G; H; Q and R, all functions of system parameters, can be measured or estimated accurately. Then, addition of the feedback terms of pitch-rate-to-yaw-input and yaw-rate-to-pitch-input permit cancellation of the cross-coupling terms. The block diagram realization of the proposed change is shown in Fig. 4-1. Equation (4.2) gives the compensated system's transformed differential equation in matrix form.

$$\begin{bmatrix} s^2 & Qs \\ Rs & s^2 \end{bmatrix} \begin{bmatrix} \theta \\ \psi \end{bmatrix} = \begin{bmatrix} G(\theta_c - K_{r\theta} s\theta - \theta + Qs\psi/G) \\ H(\psi_c - K_{r\psi} s\psi - \psi + Rs\theta/H) \end{bmatrix} \qquad (4.2)$$

Equation (4.2) can be reduced to Eq (4.3) by canceling the cross-coupling terms, Qs and RsQ, from both sides of the equation. Comparison of Eq. (4.3) with Eq. (3.5) shows that the transformed differential equation of the rolling system has been reduced to its original non-rolling form. Note that all that was done in this compensation scheme was to subtract the cross-coupling term from the command input to the nozzle actuator so than when it is added back on downstream the result will be no effective cross-channel terms into either control path.

$$\begin{bmatrix} s^2 & 0 \\ 0 & s^2 \end{bmatrix} \begin{bmatrix} \theta \\ \psi \end{bmatrix} = \begin{bmatrix} G(\theta c - K r\theta\, s\theta - \theta) \\ H(\psi c - K r\psi s\psi - \psi) \end{bmatrix} \qquad (4.3)$$

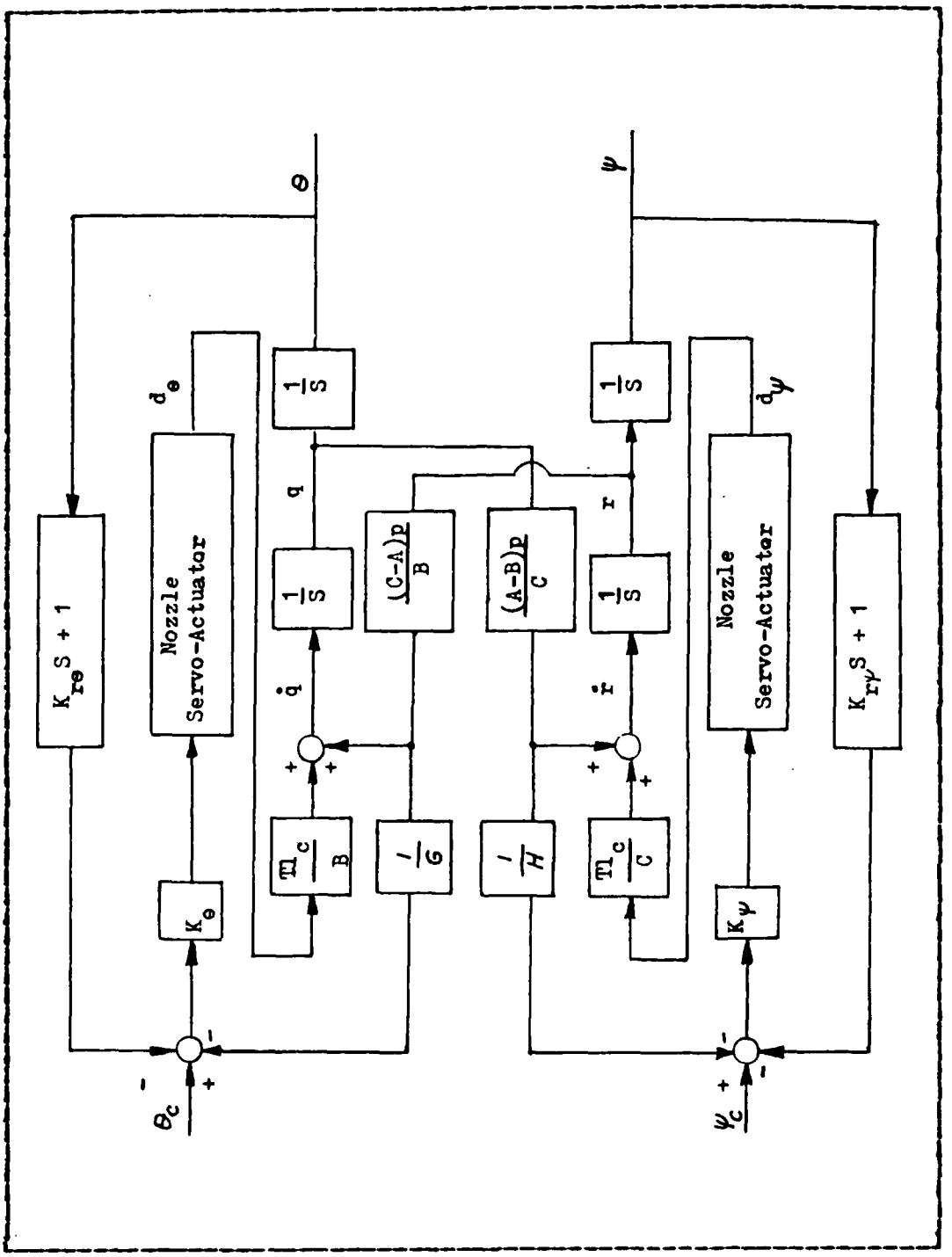

Fig. 4-1 Cross-Channel Feedback Compensation Scheme

Unfortunately, the problem is not as simple as Eq. (4.2) implies. The main problem is that the amount of control which can be used to force the system's response is limited by the maximum deflection angle of the exhaust nozzle. This nonlinear saturation of the actuator is not present in Eq. (4.2). Figure 4-2 summarizes the problem.

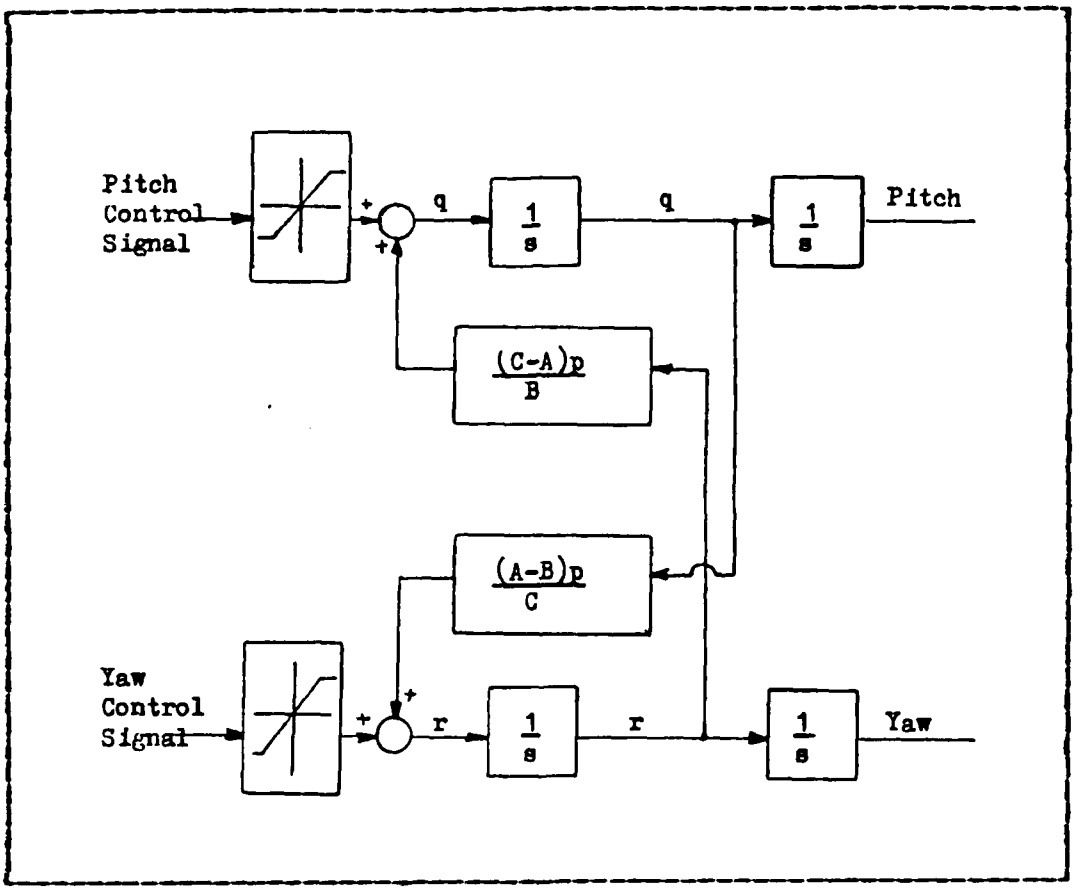

Fig. 4-2 Plant Dynamics and Control Input Limitations

Figure 4-2 shows that no matter what feedback scheme is employed to generate the pitch and yaw angular acceleration control signals, they are limited and, therefore, so is the

region of operation over which the performance of the system can be controlled and the degree of control possible.

Figure 4-3 shows the cross-coupling terms and the attempted cancellation of them by the cross-channel feedback terms under the compensation scheme just proposed. The simulation shown was performed during the first stage of operation with the system subject to a pitch-step command and a zero-yaw command. Note how the magnitude of the cross-channel feedback term is effectively saturated by the nozzle actuator and cannot follow the cross-coupling term outside a small region of operation. The simulation was made by subtracting the error term generated by the difference in command and feedback so that only the cross-channel feedback term is fed-through the nozzle actuator.

B. NONLINEAR FEEDBACK

Examination of Figs. 2-5, 2-9, 2-10 and 2-11 shows that the time the nozzle actuator takes to reach maximum deflection when given a large input command (>> maximum deflection) is insignificant (0.05 sec) when compared to the settling time of the entire pitch-yaw control system. Thus, the actuator is functioning almost like a switch in all regions of operation except near the command input (steady state). For example, Fig. 4-4 shows the nozzle deflection in the pitch plane during a simulation when the system was subject to a pitch-step input and a roll rate of 2.5 radians/second. The conclusion to be drawn from Fig. 4-4 is that since the amplitude of the effective control input to the plant cannot be increased above saturation, the only alternative is to "throw the switch" a little sooner.

The cross-channel feedback compensation scheme just proposed will cause a reduction in the effective servo command and result in earlier removal of the maximum nozzle deflection (turning off the switch). However, this approach can at best only follow the cross-coupling terms and can not "anticipate" the need to switch the deflection angle from

positive maximum to negative maximum. Another method to accomplish the objective of switching the nozzle earlier is to vary the velocity feedback gains, $K_{r\theta}$ and $K_{r\psi}$. Specifically, it is desired that the velocity feedback gains be low during the initial phases of operation when the error between command and position is large and increase as the system approaches the commanded value. This will result in the same basic system operation that was present before compensation (dominant complex-pair oscillation) but with low damping when the error is high and higher damping as the system approaches steady state.

The nonlinearity of the system prevents the use of most analytical tools which might be used to determine algorithms for $K_{r\theta}$ and $K_{r\psi}$. Instead, a trial and error approach was used based on the observations of the system's performance during earlier simulations and simulation studies performed specifically to determine appropriate parameters.

Assume that the algorithm for determining the velocity feedback gain consists of a constant which is reduced by an amount proportional to the error between command and position. This will result in low damping if the error is high and increased damping as the error decreases. For example, if V and W are constants, the pitch-channel velocity feedback gain can be determined from:

$$K_{r\theta} = V - W\left|\theta_c - \theta\right| \qquad (4.4)$$

Furthermore, the simulations shown in Figs. 3-13 through 3-30 indicated that the system becomes more underdamped (roots migrate toward the imaginary axis) as the roll rate is increased. So, the velocity feedback gains were made proportional to the roll rate. Normalizing the algorithm so that the relationship does not become zero if the roll rate is zero yields Eqs. (4.5) and (4.6).

$$K_{r\theta} = (V - W|\theta_c - \theta|)(1 + p) \tag{4.5}$$

$$K_r = (V - W|\psi_c - \psi|)(1 + p) \tag{4.6}$$

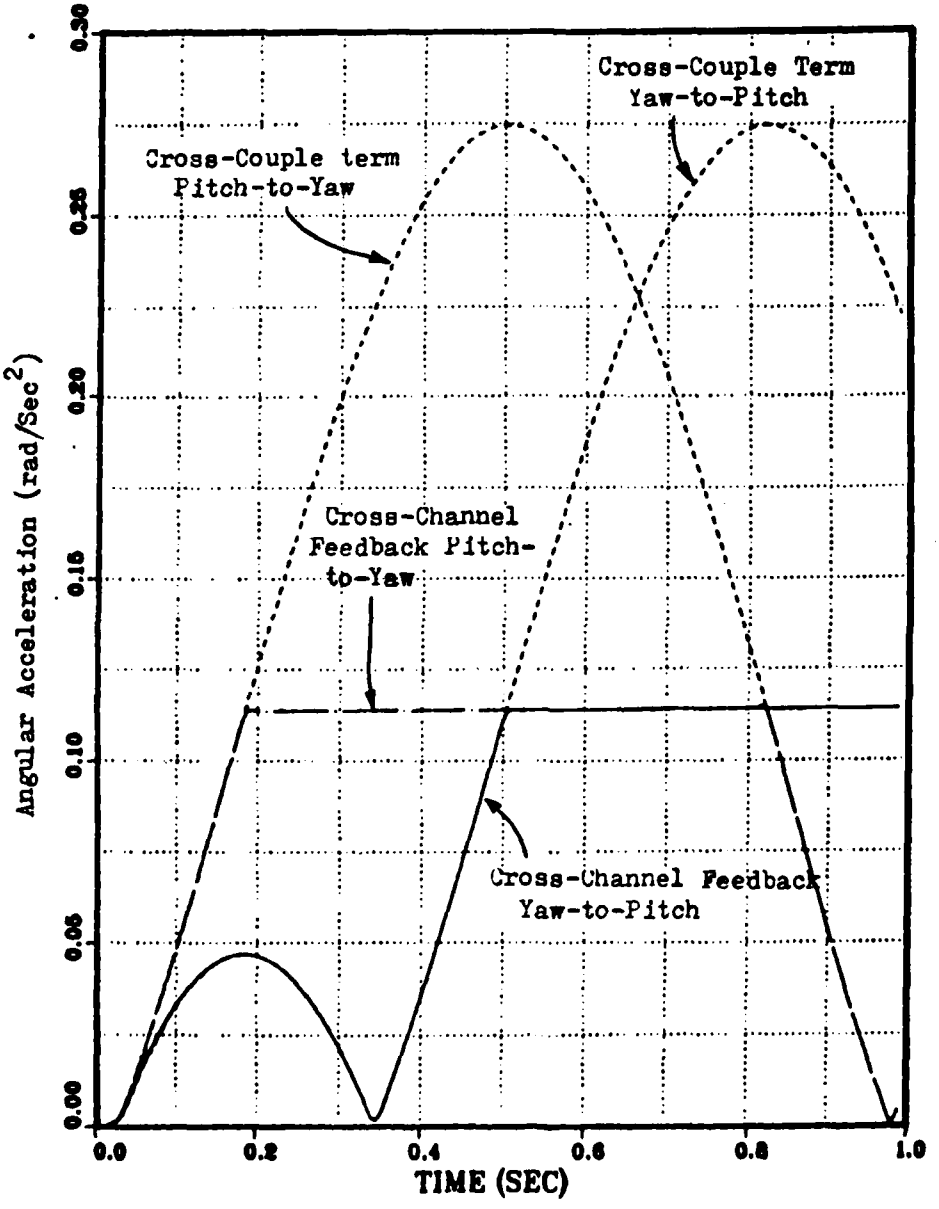

Fig. 4-3 Saturation of Cross-Channel Feedback

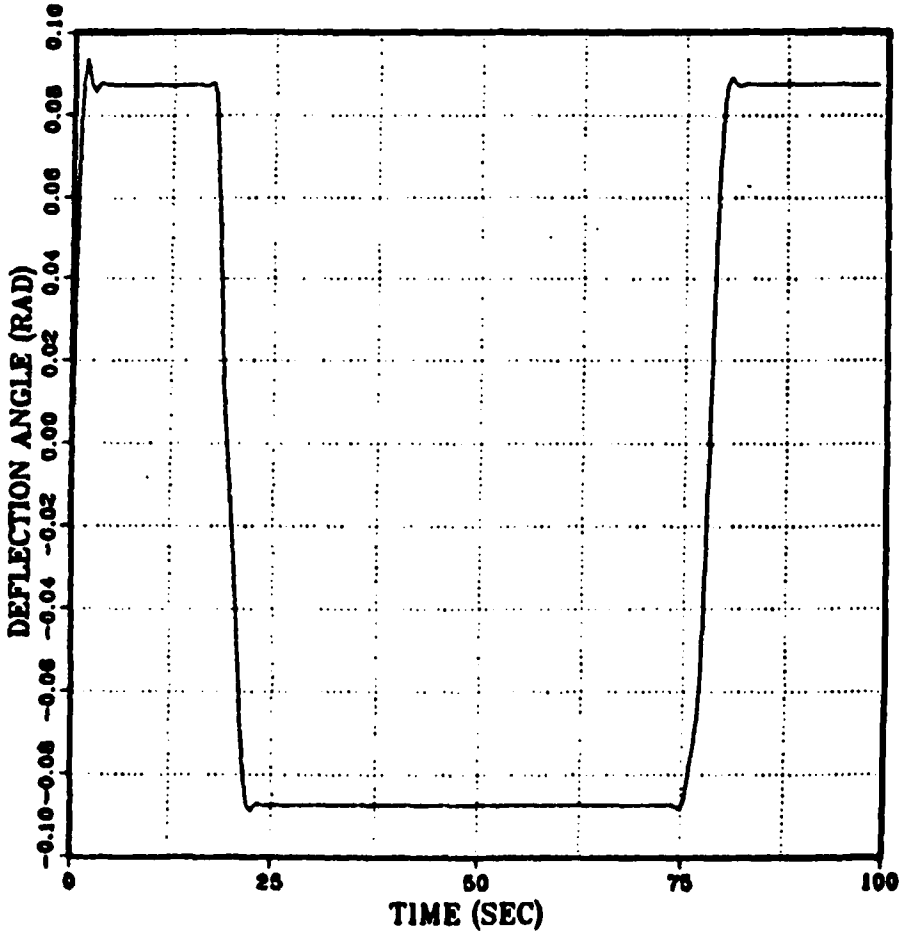

Fig. 4-4 Nozzle Deflection Angle Simulation

Figure 4-5 shows sample results of simulation studies which were conducted for various values of V and W and over various stages of operation and roll rates. The simulations showed that acceptable performance was obtained for V = 4 and W = 3.

Figures 4-6 through 4-14 show simulation results which were made by using the cross-channel feedback and variable velocity feedback gain compensation schemes together. For comparison, the uncompensated responses are also shown. The compensated simulation responses were obtained under the same operating conditions as those shown in Figs. 3-13 through 3-30.

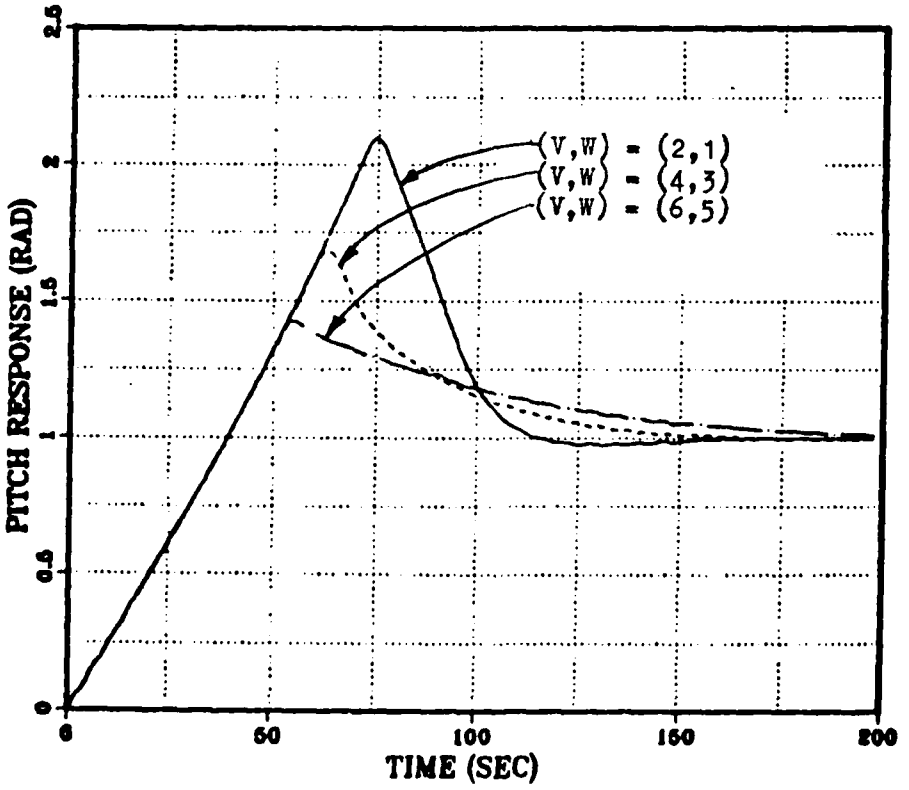

Fig. 4-5 Sample Algorithm Response Test Simulation

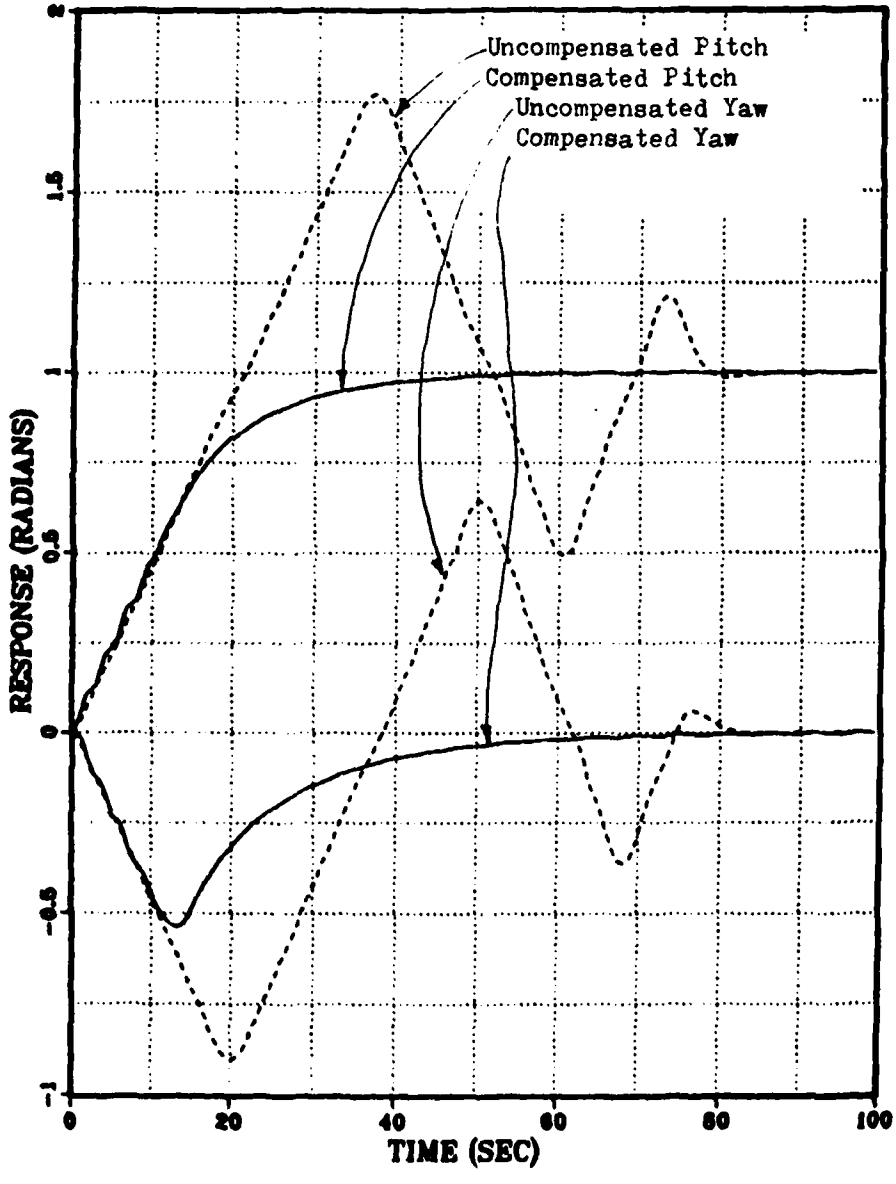

Fig. 4-6 Pitch-Step Response Roll Rate of 2.5 rad/sec

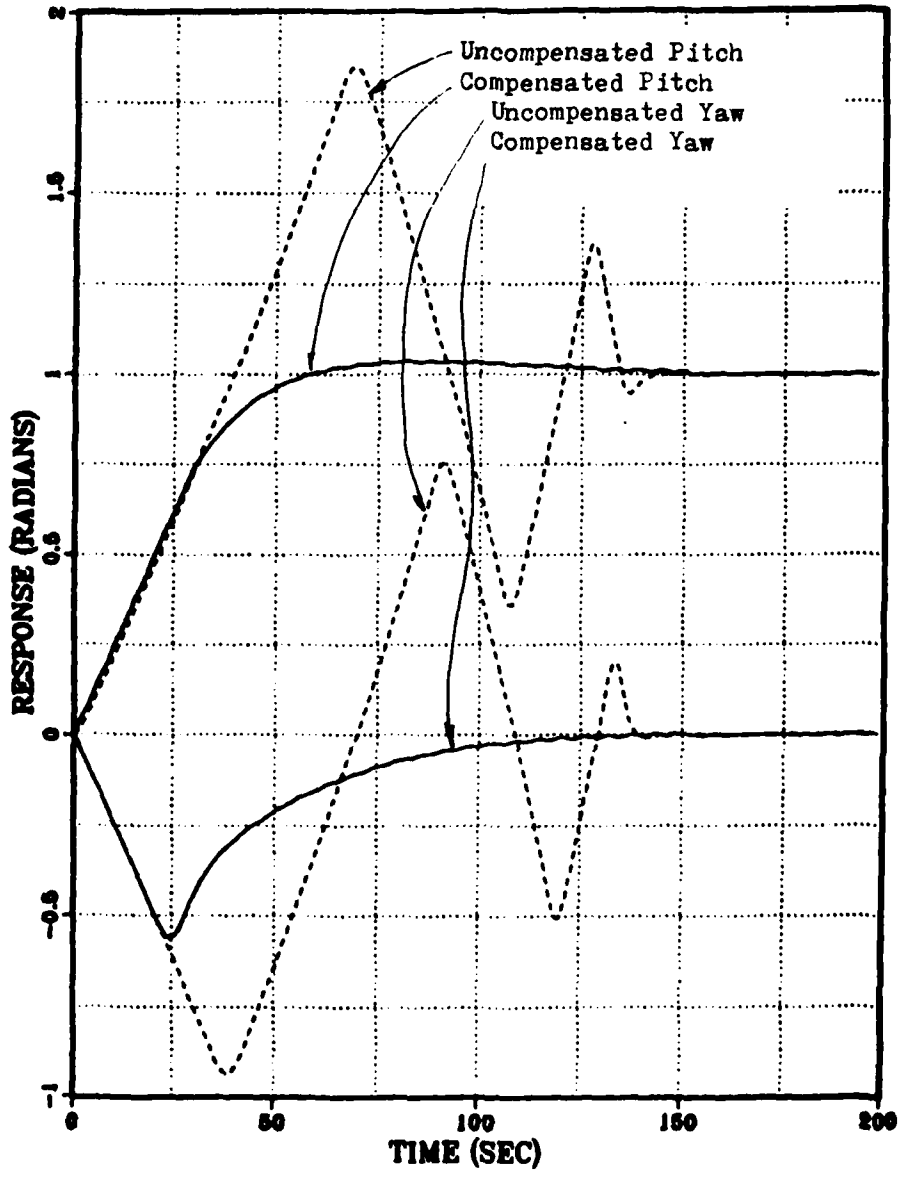

Fig. 4-7 Pitch-Step Response Roll Rate of 5.0 rad/sec

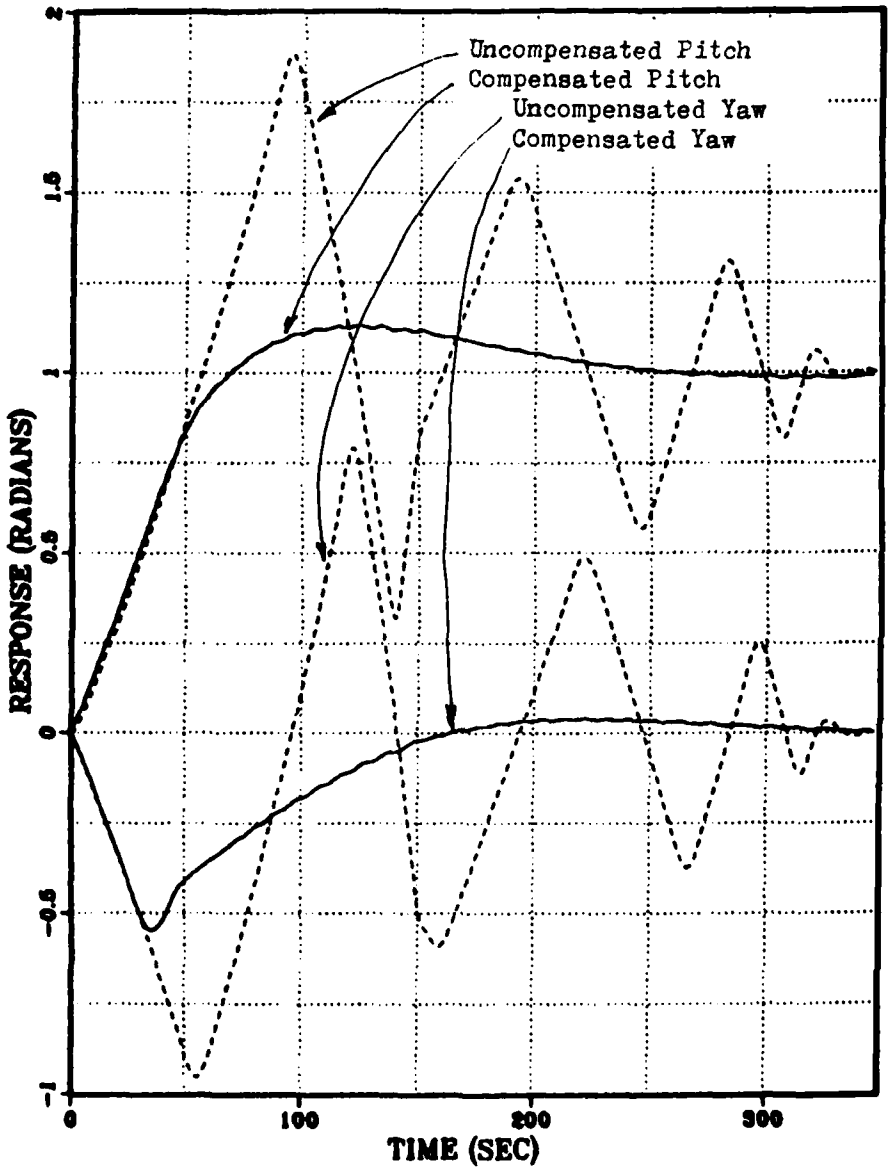

Fig. 4-8 Pitch-Step Response Roll Rate of 7.5 rad/sec

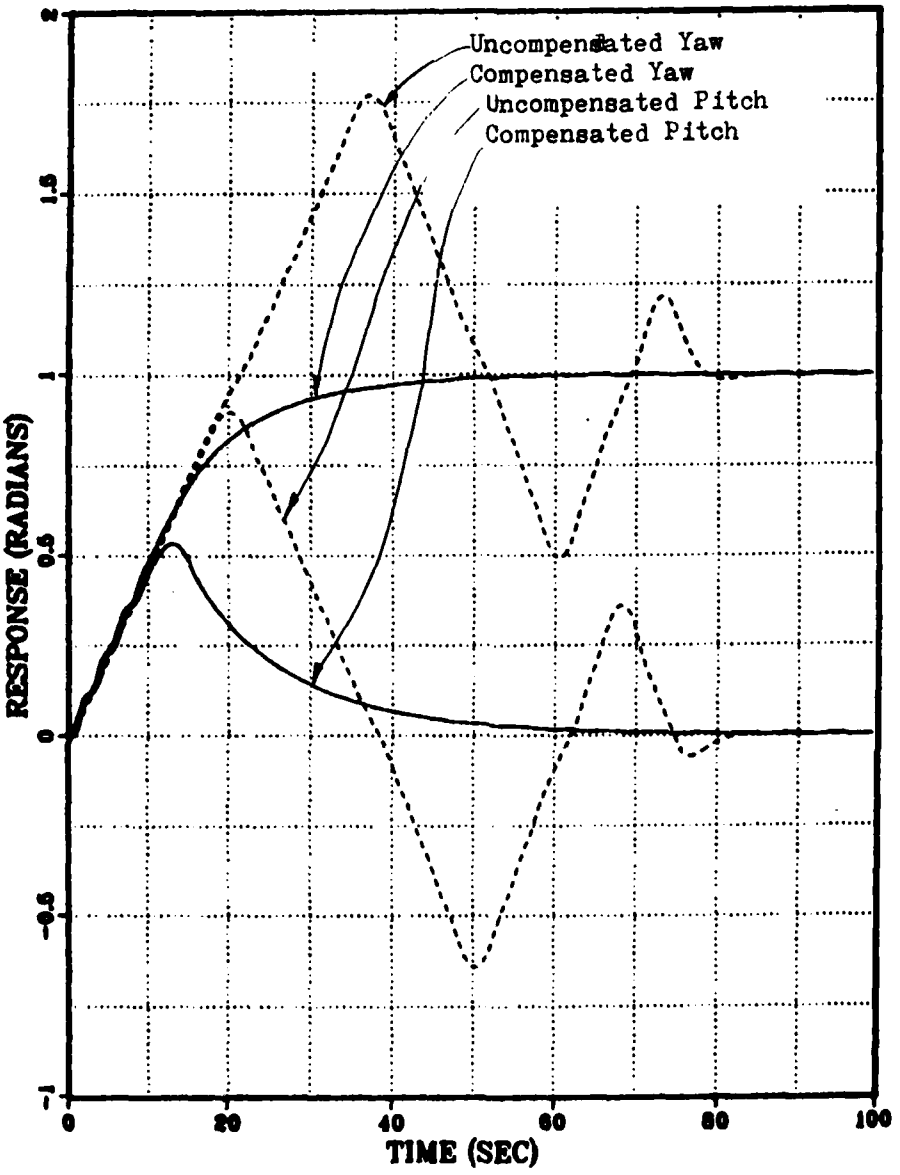

Fig. 4-9 Yaw-Step Response Roll Rate of 2.5 rad/sec

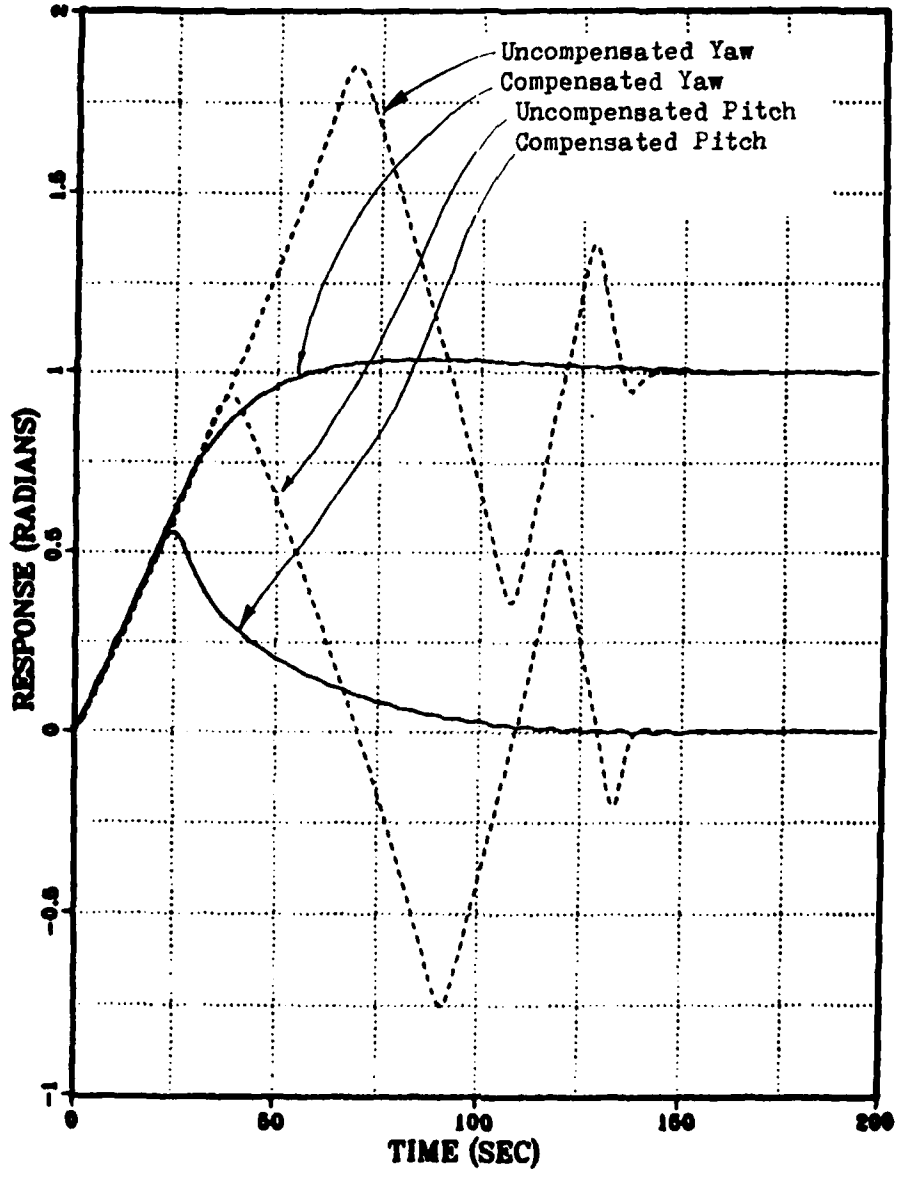

Fig. 4-10 Yaw-Step Response Roll Rate of 5.0 rad/sec

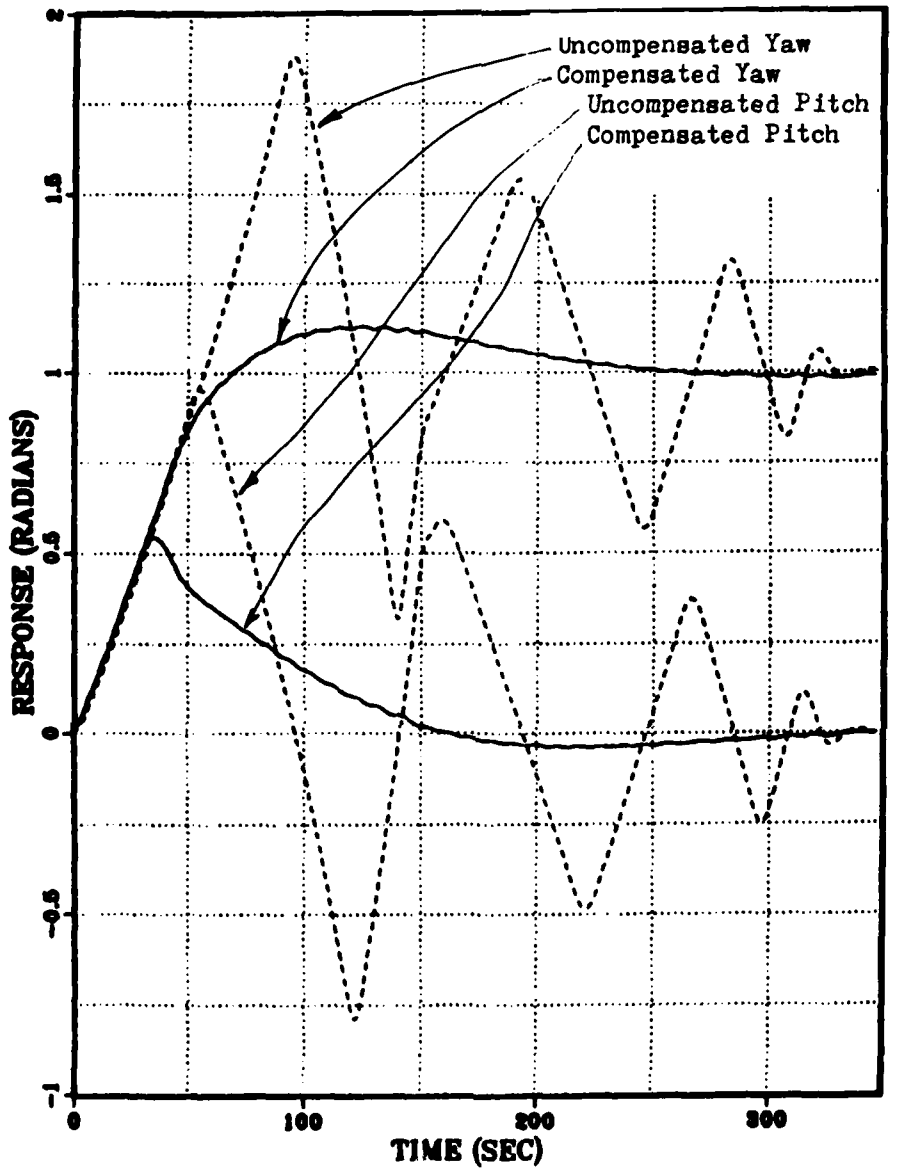

Fig. 4-11 Yaw-Step Response Roll Rate of 7.5 rad/sec

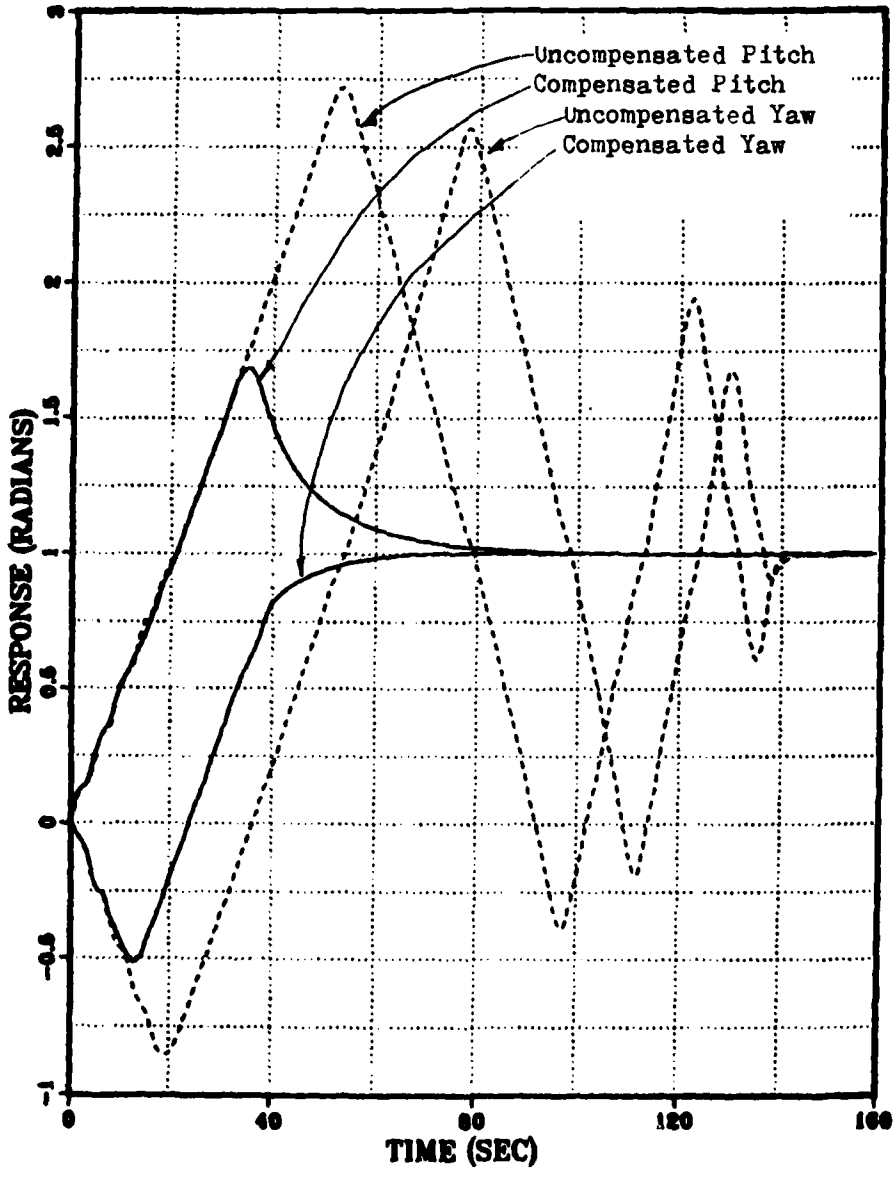

Fig. 4-12 Pitch- & Yaw-Step Response Roll Rate 2.5 rad/sec

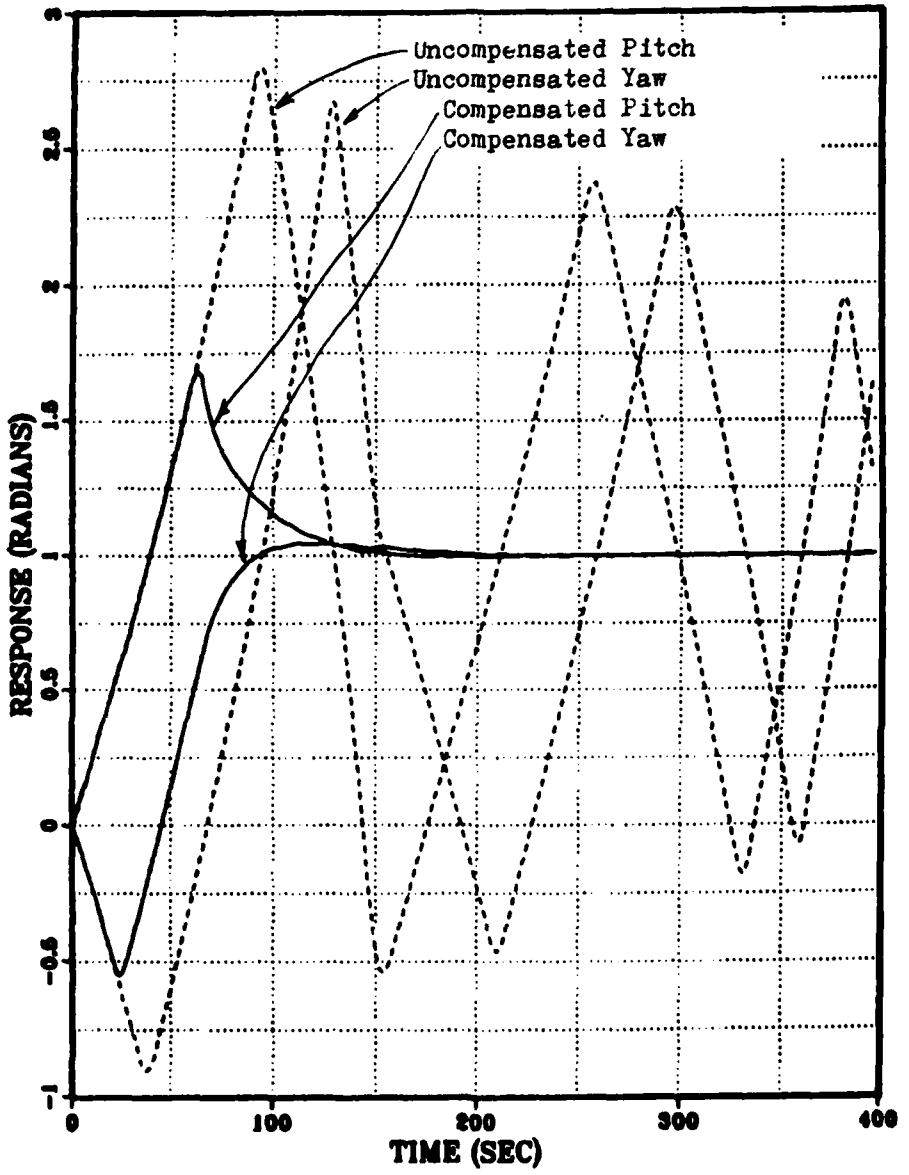

Fig. 4-13 Pitch- & Yaw-Step Response Roll Rate 5.0 rad/sec

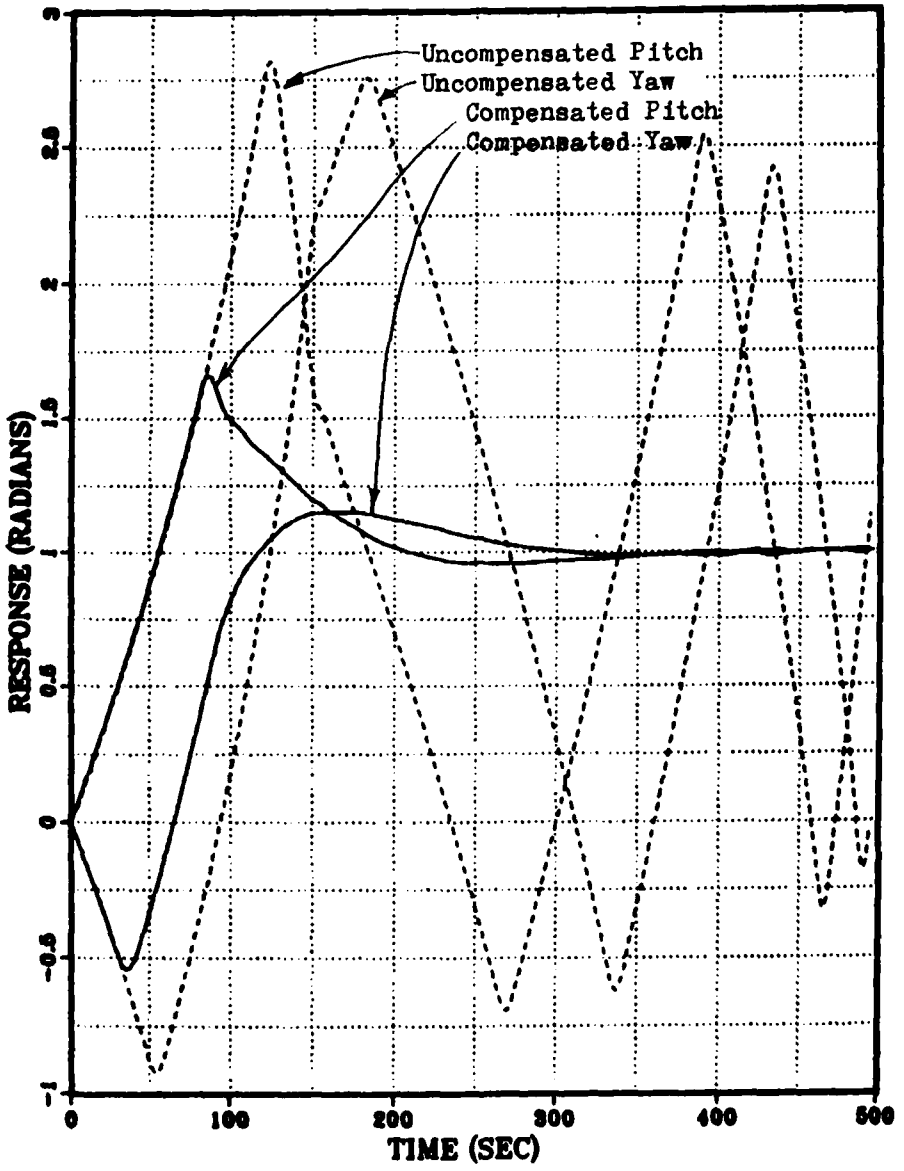

Fig 4-14 Pitch- & Yaw-Step Response Roll Rate 7.5 rad/sec

The simulations indicate that substantial performance restoration is possible with the proposed compensation schemes. However, the restoration is not complete and is still much worse, in terms of overshoot and settling time, than the non-rolling missile.

V. CONCLUSIONS

The compensation scheme proposed partially restores the pre-roll performance of the missile. Table 5-1 summarizes the level of perfcrmance degradation caused by roll and the restoration which was obtained with this compensation scheme under pitch- and yaw-step inputs and a roll rate of 2.5 rad/sec. As indicated, the degradation is significant even at this relatively low (and stable) roll rate. The compensated system's performance is still far worse than that of the non-rolling system.

The compensation scheme relies primarily on the nonlinear damping effect of the variable velocity feedback gains which "anticipate" the approach of the commanded position. Since the cross-coupling terms introduced by roll are not directly cancelled by the proposed modification, the region of stable operation and the degree to which the system's performance can be restored is directly controlled by the roll rate. Furthermore, the saturation caused by the nozzle deflection will prevent any compensation scheme, which only modifies the control input, from fully restoring the system's performance. To completely restore the system to its pre-roll performance at any roll rate, additional control inputs to the system plant dynamics (such as, side thrusters or additional vectoring of the main rocket motor) are necessary.

TABLE 5-1

PERFORMANCE COMPARISON

	Non-Rolling System	Uncompensated Rolling System (p = 2.5 rad/sec)	Compensated System
Settling Time	9 sec	140 sec	80 sec
Peak Overshoot	8.5%	170%	70%

APPENDIX A
NON-ROLLING MISSILE SIMULATION

The DSL/360 program used to simulate the non-rolling missile is shown below. The program consists of three stages, initial, derivative and terminal. The initial segment is used to define constants and calculate functions of the constants which will not change throughout the simulation run. The derivative section is where the actual integrations required to perform the simulations are conducted. This program is constructed to follow the block diagram of Fig. 2-1 directly. Note that the nozzle actuator transfer function was broken down into a three-step integration. The terminal stage determines the end condition of the simulation run and the output data. This data was formed into a data file and a packaged graphics program (DISSPLA) was used to construct the figures shown in the text. The parameter values listed in this example program are those during stage one.

```
* INITIALIZE CONSTANTS
CONST TST=7496000,L=363,J1=11048.8,KTH=1.0,KBTH=1.75,...
      WA=150,WB=15,PB=0.9,RATE=930.0,M1=189140
*
* COMPUTE SET VALUES
INITIAL
       ONE=WA*(WB**2)
       TWO=WA + 2*PB*WB
       THREE=2*PB*WB*WA + WB**2
*
* BEGIN SIMULATION
DERIVATIVE
       MASS=M1-RATE*TIME
       PCOM=STEP(0)
* ERROR SIGNAL
       E=PCOM-P
       EI=E-(KBTH*P1DOT)
       CM=KTH*EI
* SERVO TRANSFER FUNCTION
       SVO=INTGRL(0,SV1DOT)
       SV1DOT=INTGRL(0,SV2DOT)
       SV2DOT=INTGRL(0,SV3DOT)
       SV3DOT=ONE*(CM-SVO) - TWO*SV2DOT - THREE*SV1DOT
```

```
* LIMIT OF NOZZLE DEFLECTION
      DEFL=LIMIT(-0.0873,0.0873,SVO)
* MOMENT OF INERTIA
      B=J1*MASS
      Z=TST*L/B
* ANGULAR ACCELERATION
      P2DOT=Z*DEFL
* ANGULAR VELOCITY
      P1DOT=INTGRL(0,P2DOT)
      P=INTGRL(0,P1DOT)
*
* OUTPUT AND CONTROL STATEMENTS
TERMINAL
CONTRL FINTIM=15.0, DELT = 0.001
SAVE  0.015,P
PRINT 0.015,P
END
STOP
```

APPENDIX B
ROLLING MISSILE SIMULATION

Unlike the non-rolling system simulations, the rolling missile simulations were required to run over several consecutive booster stages. This required the addition of a 'dynamic' segment of simulation. The 'IF' statements, shown in the example simulation below, are used to switch from one set of parameters to another as one stage burns off and another starts. The switching is controlled by the elapsed time of the simulation run compared to the burn time of each stage.

```
* SET CONSTANTS
CONST KTB=1.0,KRTH=1.5,WA=150,WB=15,PB=0.9,ROLL=7.5
*
* INITIALIZE SET VALUES
INITIAL
      A = WA*(WB**2)
      B = WA + 2*PB*WB
      C = 2*PB*WB*WA + WB**2
      RESET=0.0
*INITIALIZE FIRST STAGE VALUES
      TST=7496000
      L=363
      J1=11048.8
      J2=136.1
      RATE=930.0
      M1=189140
*
* DECIDE WHICH STAGE OF FLIGHT
DYNAMIC
* ENTER STAGE TWO
      IF (TIME.LT.150) GO TO 10
          TST=1125000
          L = 230
          J1=4476.4
          RATE=81.49
          M1=40340
          RESET=150
* ENTER STAGE THREE
      IF (TIME.LT.509) GO TO 10
          TST=224900
          L=100
          J1=858.3
          J2=50.0
          RATE=14.75
          M1=8140
          RESET=509
10    CONTINUE
```

```
*
* SIMULATION RUN
DERIVATIVE
      SET=TIME-RESET
      MASS = M1 - (RATE*SET)
      PCOM = STEP(0)
      YCOM = STEP(0)
* ERROR SIGNALS POSITION FEEDBACK
      EP = PCOM-P
      EY = YCOM-Y
* ERROR SIGNALS VELOCITY FEEDBACK
      EIP = EP-(KRTH*P1DOT)
      EIY = EY-(KRTH*Y1DOT)
      CMP = KTH*EIP
      CMY = KTH*EIY
* SERVO TRANSFER FUNCTION IN PITCH PATH
      SVP = INTGRL(0,SVPDOT)
      SVPDOT = INTGRL(0,SVP2DT)
      SVP2DT = INTGRL(0,SVP3DT)
      SVP3DT = A*(CMP-SVP) - B*SVP2DT - C*SVPDOT
* PITCH DEFLECTION
      PDEFL = LIMIT(-0.0873,0.0873,SVP)
* SERVO TRANSFER FUNCTION IN YAW PATH
      SVY = INTGRL(0,SVYDOT)
      SVYDOT = INTGRL(0,SVY2DT)
      SVY2DT = INTGRL(0,SVY3DT)
      SVY3DT = A*(CMY-SVY) - B*SVY2DT - C*SVYDOT
* YAW DEFLECTION
      YDEFL = LIMIT(-0.0873,0.0873,SVY)
      JY = J1*MASS
      JZ = JY
      JX = J2*MASS
      ZP = TST*L/JY
      ZY = TST*L/JZ
* CROSS COUPLE MULTIPLIERS
      ALPHA = (JZ-JX)*ROLL/JY
      BETA = (JX-JY)*ROLL/JZ
* CROSS COUPLE TERM YAW TO PITCH
      CCYP = ALPHA*Y1DOT
* CROSS COUPLE TERM PITCH TO YAW
      CCPY = BETA*P1DOT
* PITCH ANGULAR ACCELERATION
      P2DOT = (ZP*PDEFL) + CCYP
* YAW ANGULAR ACCELERATION
      Y2DOT = (ZY*YDEFL) + CCPY
* PITCH ANGULAR VELOCITY
      P1DOT = INTGRL(0,P2DOT)
      P = INTGRL(0,P1DOT)
* YAW ANGULAR VELOCITY
      Y1DOT = INTGRL(0,Y2DOT)
      Y = INTGRL(0,Y1DOT)
*
* OUTPUT AND CONTROL
TERMINAL
CONTRL FINTIM=500.0, DELT=0.01
PRINT  0.50,P,Y
END
STOP
```

LIST OF REFERENCES

1. Garnell, P. and East, D.J., Guilded Weapons Control Systems, Peragamon Press, 1977.

2. Freeman, B.D., Optimal Control of a Ballistic Missile Thrust Vector Control System, M.S.E.E. Thesis, Naval Postgraduate School, Monterey, California, June 1982.

3. Thayler, G.J., Design of Feedback Systems, Dowden, Hutchinson and Ross, Inc., 1973.

BIBLIOGRAPHY

Astrom, K.J. and Bjorn, W., Computer Controlled Systems, Prentice-Hall, Inc., 1984.

Kirk, D.E., Optimal Control Theory, An Introduction, Prentice-Hall. Inc., 1970.

Kuo, B.C., Automatic Control Systems, Prentice-Hall, Inc., 1982.

Strum, R.D. and Ward, J.R., Electrical Circuits and Networks, Quantum Publishers, Inc., 1973.

AD-A164 505 BOOST CONTROL DESIGN FOR SPINNING MISSILE(U) NAVAL POSTGRADUATE SCHOOL MONTEREY CA R L PARK DEC 85 2/2

UNCLASSIFIED F/G 16/4.2 NL

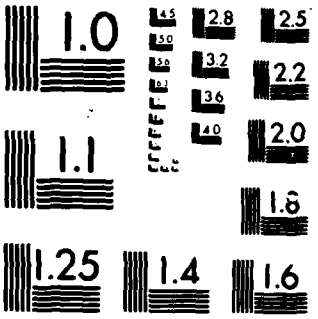

INITIAL DISTRIBUTION LIST

		No. Copies
1.	Defense Technical Information Center Cameron Station Alexandria, Virginia 22304-6145	2
2.	Library, Code 0142 Naval Postgraduate School Monterey, California 93943-5100	2
3.	Prof. R.D. Strum, Code 62St Dept. of Electrical and Computer Engineering Naval Postgraduate school Monterey, California 93943	2
4.	Prof. D.E. Kirk, Code 62Ki Dept. of Electrical and Computer Engineering Naval Postgraduate School Monterey, California 93943	1
5.	Capt. R.L. Park MCISSA Camp Pendleton, California 92055-0580	1

END

FILMED

3-86

DTIC